

Towards the Design and Manufacturing of Products Using Large-Scale FFF Printers

by

DEVIN ALBERTI

A thesis submitted in partial fulfillment of the requirements for the degree of

Master of Science

Department of Mechanical Engineering  
University of Alberta

© DEVIN ALBERTI, 2020

## **Abstract**

In this thesis, the challenges involved with large-scale Fused Filament Fabrication (FFF) 3-dimensional (3D) printing is explored through an industrial application in which a cantilever chair is produced as a case study. The chair is designed in SOLIDWORKS® in which easy variability and complex geometry are emphasized to take advantage of 3D printing's ability for mass customization and economic complexity. The ability to move the process towards creating fully sustainable, recyclable, and biodegradable products is also demonstrated through the use of PLA filament as the 3D print material. The cantilever chair's mass is reduced using SOLIDWORKS' finite element analysis tool in which the inclusion of a brace addition was chosen for production due to its reduced material consumption and avoidance of fatigue failure complications. The characteristics of large-scale FFF 3D printers and their connection with slicer settings are also discussed. The poor adhesion performance caused by thermal gradients on the large glass build surface are improved through forced cooling fan profiles and adhesion additions. Significant oozing and diminished feed rate to flow rate responsiveness caused by large heat chambers within large-scale hotends are improved through retraction, travel movement, flow rate, and acceleration settings. Dimensional inaccuracies caused by large translating masses are considered with respect to accelerations, print speed, frame rigidity, and mechanical clearances. After these slicer settings were refined within Simplify3D for a 3DP 300 printer equipped with HFE 300 hotends, the chair was successfully produced. During production, several issues arise including inadequate adhesion, significant warping, and filament degradation. Economic and easily applicable solutions are tested to determine an adhesive substance that would both increase PLA-glass adhesion while at operating print temperatures and reduce adhesion when cooled to ambient room temperature. Of the substances tested, a sugar/ water solution is determined superior

in both circumstances compared to a salt/water solution, hairspray, and bare glass. An enclosure is then designed and built to reduce warping by increasing ambient print temperatures and reducing thermal gradients caused by drafts and ambient room temperature fluctuations. Considerations such as future modification, build surface access, and printer access are implemented into its design. Lastly, a filament storage solution is presented to halt filament degradation through the use of desiccant and an airtight pet food container to provide a steady low-humid environment. Complications arouse during the COVID-19 pandemic in which testing of the enclosure and filament storage were not completed. Furthermore, the effects print scale, print parameters, and print material have on mechanical, visual, and economic-based optimization are reviewed from sources using desktop-scale FFF printers. The flow rate limitations of hotends and nozzle diameters, and the relationship between nozzle diameters, extrusion widths, and layer heights are discussed. The geometrical effects of the extrusion width to nozzle diameter and extrusion width to layer height ratios are illustrated and the effect the extrusion width to layer height ratio has on a print's mechanical properties are reviewed. An equation relating volumetric flow rate to nozzle diameter, print speed, extrusion width to nozzle diameter ratio, and extrusion width to layer height ratio is then created and used to present optimal volumetric flow rate combinations of varying nozzle diameters, extrusion width to layer height ratios, and print speeds for 3D Platform's HFE 300 hotend. These combinations are then applied to the braced-cantilever chair case study by observing Simplify3D's estimated print time and material consumption. From this, it is discovered that larger nozzle sizes could result in significant increases in material consumption and print time due to print parameter settings and print geometry. The affect print parameters have on the mechanical properties of FFF objects are further reviewed with regards to infill density, infill geometry, nozzle temperature, and cooling parameters. From this review, it is revealed that forced

cooling and low nozzle temperatures typically effects the mechanical properties of prints negatively through diminished layer bonding. Lastly, the effect of print material color, print post-processing treatments, and wood-based inclusions are reviewed. Significant discoveries include the superior bonding ability of natural PLA, the post-processing radiation treatment to reduce anisotropic tensile strength behavior, and the use of cellulose nanofibers to increase PLA's tensile strength and elastic modulus.

## Acknowledgments

I would like to thank all who have supported and/or guided me through the completion of my research and general requirements in obtaining my MSc. in Mechanical Engineering through the University of Alberta. Most influential are my supervisors, Dr. Cagri Ayranci and Dr. David Nobes, for providing and accepting me with the opportunity to further my academic education, exercise engineering design, and learn and operate the mechatronic systems of 3D printing technologies. I also greatly appreciate their patience, affability, enthusiasm, and willingness to share their knowledge and experience.

I would also like to thank my parents Marianne and Michael Alberti, my fiancée Katrina Neill, and my dear friend Trystin Stobbart for their constant social support and comfort. It is thanks to their compassion and reassurance that I have maintained motivation and diligence throughout my academic education.

Additionally, I would like to thank the many U of A graduate students I have had the pleasure to meet and work with for their affability and willingness to help throughout my research struggles. Special thanks to Linda Hasanovich, Yu Chen, and Eyup Demir.

Finally, I would like to thank Alberta Innovates for funding my study through ABF grants title: “Towards assembling nature back together: additive manufacturing of large-scale CNC-reinforced lignin composites for green composites”.

## Table of Contents

CHAPTER 1.	Introduction .....	1
CHAPTER 2.	Product Design .....	5
2.1	Chair Style Considerations.....	5
2.1.1	Ladder-Back Chair.....	5
2.1.2	Voronoi Chair .....	6
2.1.3	Cantilever Chair .....	7
2.2	Chair Design and CAD Modeling.....	8
2.2.1	General Parameters .....	9
2.2.2	Load Bearing Parameters .....	10
2.2.3	Sketch Assembly and CAD Creation.....	12
2.2.4	Additions.....	15
2.3	FEA Analysis .....	16
2.3.1	FFF Defined Strength Parameters.....	17
2.3.2	Simulation Parameters .....	18
2.3.3	Material Choice.....	20
2.3.4	Simulation Results .....	22
CHAPTER 3.	Print Preparation .....	27
3.1	Slicing Software .....	27
3.2	Print Parameters .....	28
3.2.1	Build Surface .....	29
3.2.2	Hotend.....	30
3.2.3	Overall Mass .....	33
CHAPTER 4.	Product Creation .....	36
4.1	Adhesion.....	37

4.1.1	Adhesion Considerations .....	38
4.1.2	Adhesion Experimental Design .....	40
4.1.3	Adhesion Experimental Procedure .....	41
4.1.4	Adhesion Results .....	42
4.1.5	Adhesion Implementation.....	44
4.2	Warping.....	47
4.2.1	Enclosure Adaptability.....	48
4.2.2	Enclosure Accessibility.....	49
4.2.3	Enclosure Implementation .....	52
4.3	Filament Storage .....	53
4.3.1	Filament Storage .....	55
4.3.2	Filament Drying Options .....	56
CHAPTER 5.	Product Optimization.....	59
5.1	Effects of Printer Scale.....	60
5.2	Effects of Print Parameters.....	67
5.3	Effects of Print Material.....	68
CHAPTER 6.	Conclusion .....	71

## Table of Tables

Table 2.1: Chair dimension guidelines for a casual easy chair adapted from [33]. .....	9
Table 2.2: Mechanical properties of PLA adapted from [56]. .....	22
Table 3.1: General print parameters assigned within Simplify3D for the 3DP 300 printer equipped with HFE 300 hotends. ....	29
Table 4.1: Bed adhesion test results for glass, hairspray, sugar water, and salt water at 60 °C and 25 °C print bed temperatures. ....	43
Table 5.1: Comparing print speeds (V), layer heights (H), and Simplify3D's estimated print times (T) and PLA mass consumptions (M) for printing the braced-cantilever chair at various nozzle diameters (D) and extrusion width to layer height ratios (W/H) with a volumetric flow rate (Q) of 68.38 mm <sup>3</sup> /s, extrusion width to nozzle diameter ratio (W/D) of 1.2, and no brim. ....	65



## Table of Figures

Figure 2.1: Annotated images of a ladder-back chair adapted from [26] showing the features that define it (a) and the possible combination of 3D printed members that could create it (b).....	6
Figure 2.2: Annotated image of a Voronoi chair sourced with permission from [28] showing the feature that defines it.....	7
Figure 2.3: Annotated images of cantilever chairs with (a) being of the typical tubular design sourced from [30] and (b) being a solid plastic design commonly known as a Panton chair sourced from [31]. .....	8
Figure 2.4: Orthogonal images of the 3-dimensional Preliminary Plan SOLIDWORKS sketch.	10
Figure 2.5: Images of the Final Plan (Rail) (a) and Final Plan (Center) (b) SOLIDWORKS sketches with the Preliminary Plan shown in gray. ....	11
Figure 2.6: Image of the Surface SOLIDWORKS sketch. ....	12
Figure 2.7: Annotated illustrations of the SOLIDWORKS sketches used within the loft extrusion feature to virtually create the chair in which (a) is the guide curves, (b) is the repeated profile, (c) is the assembled wireframe and (d) is the resulting CAD model. ....	14
Figure 2.8: Annotated illustration of the SOLIDWORKS sketches (a) and resulting CAD model (b) of the cantilever chair's brace addition. ....	16
Figure 2.9: Annotated illustration displaying the implementation of the Rail Fill Width, Center Fill Width, and Shell Width parameters into the cantilever chair's FEA CAD model. ....	18
Figure 2.10: Annotated illustrations displaying the applied external loads (a) and fixtures (b) in the SOLIDWORKS static simulations. ....	19
Figure 2.11: Mesh convergence graph displaying the logarithmic behavior of simulated stress with decreasing mesh element size. ....	20
Figure 2.12: Line graph displaying the iterative FEA progression performed on the cantilever chair to reduce volume and keep a minimum factor of safety of 2.0.....	23
Figure 2.13: Line graph displaying the iterative FEA progression performed on the braced-cantilever chair to reduce volume and keep a minimum factor of safety of 2.0.....	23
Figure 2.14: Images displaying the stress distribution (a) and displacement distribution (b) of the cantilever chair design at its final FEA iteration. ....	24
Figure 2.15: Images displaying the stress distribution (a) and displacement distribution (b) of the braced-cantilever chair design at its final FEA iteration. ....	25

Figure 2.16: Annotated illustration comparing the simulated braced-cantilever chair deflection with a 10 mm brace width (a) and a 15 mm brace width (b) with the initial unloaded orientation represented in translucent gray. ....	26
Figure 3.1: Annotated images comparing the approximate lengths of the heat chambers within E3D's V6 (a), E3D's Volcano (b), and 3D Platform's HFE 300 (c) hotends. Images of the V6 and Volcano hotends were sourced from [70] and [71] respectively with permission. ....	31
Figure 4.1: Images displaying Simplify3D's visual G-code print representation and estimated print time and material requirements for the cantilever chair (a) and the braced-cantilever chair (b) designs.....	36
Figure 4.2: Image displaying sugar water application tests using 200 g/L and 100 g/L concentrations. ....	39
Figure 4.3: Image displaying saltwater application tests using 200 g/L, 100 g/L, 60 g/L, 20 g/L, and 10 g/L concentrations. ....	40
Figure 4.4: Annotated illustrations displaying the adhesion test tower dimensions and features. ....	41
Figure 4.5: Images displaying the completed 6 adhesion test tower print (a) and an adhesion test tower undergoing the adhesion test procedure (b) for clean glass. ....	42
Figure 4.6: Bar graph displaying the adhesion test results for glass, hairspray, sugar water, and salt water at 60 °C and 25 °C print bed temperatures. ....	44
Figure 4.7: Annotated images of the braced-cantilever chair's adhesion performance with the use of sugar water and a large brim width with (a) displaying the front seating radius and (b) showing the rear floor lip. ....	45
Figure 4.8: Annotated images of the blobbing effect caused by having the secondary hotend at 230 °C during printing of the braced-cantilever chair in which (a) is at the outer upper brace surface and (b) is at the inner lower brace surface. ....	46
Figure 4.9: Annotated image of the ringing effect occurring on the front surface of the back rest during printing of the braced-cantilever chair. ....	47
Figure 4.10: Annotated illustration of the custom designed 3DP 300 enclosure's SOLIDWORKS CAD model. ....	50
Figure 4.11: Annotated illustrations of the 3DP 300 printer's custom enclosure's build surface access door design.....	51

Figure 4.12: Annotated illustrations of the 3DP 300's custom enclosure's printer access design.	52
Figure 4.13: Annotated image of the custom built 3DP 300 enclosure.	53
Figure 5.1: Images of the successfully printed PLA braced-cantilever chair alongside a visually similar tube style chair.	59
Figure 5.2: Annotated illustration displaying the approximate flow distribution of extruded filament when the extrusion width is equal to (a), larger than (b), and excessively larger than (c), the nozzle diameter.	61
Figure 5.3: Annotated illustration displaying the effect extrusion width to layer height ratios (W/H) have on bonding surfaces.	62
Figure 5.4: Line graph displaying the relationship between nozzle diameter (D), extrusion width to layer height ratio (W/H), and print velocity (V) when the volumetric flow rate (Q) and extrusion width to nozzle diameter ratio (W/D) is kept constant at 68.38 mm <sup>3</sup> /s and 1.2 respectively.	64
Figure 5.5: Annotated images comparing Simplify3D's 10% rectilinear infill and 2.0 mm shell when a nozzle size of 1.0 mm (a), 2 mm (b), and 3 mm (c) is defined with a (W/H) ratio of 4 at a braced-cantilever chair print layer 27 mm from the build surface.	66

# CHAPTER 1. INTRODUCTION

Additive manufacturing (AM) was first realized by Charles Hall in 1986 with the technology Stereolithography (SLA) in which photopolymer resin is cured in successive layers by a UV laser to create an object [1], [2]. Since then, there have been many AM technologies developed that use similar layer-by-layer processing but with different materials and fusing methods. These technologies are commonly labeled under the umbrella term 3D printing, and include fused deposition modeling (FDM), selective laser sintering (SLS), selective laser melting (SLM), binder jetting, inkjet printing, contour crafting, laminated object manufacturing (LOM), direct energy deposition (DED), and more [1], [3]. The primary use of AM was rapid prototyping due to their ability to create physical representations of products quickly and economically with negligible setup time between iterations. This helped accelerate design and allowed investors to analyze products visually and physically [3]–[5]. While still heavily utilized for prototyping, AM has been increasingly used for final products and functional parts thanks to advancements in precision, repeatability, and material selection [3], [6]. The percentage of total 3D printed objects utilized as functional parts or final products was estimated at 20% in 2010. This was further estimated to increase to 50% by the end of 2020 [1], [4]. The 3D printing industry's worth is also expected to raise from \$7 billion to \$17.2 billion between 2016 and 2020. This raise in popularity is due to the advantages AM provides over traditional manufacturing methods like injection molding and subtractive manufacturing (SM) [7].

One substantial advantage is its ability to produce increasingly complex geometries without requiring additional costs or time. While SM processes may require longer toolpaths, custom tooling, and/or additional labor to achieve higher levels of geometric complexity, the 3D printing approach of adding material layer-by-layer only relies on the code delivered to the machine [6]. This level of near unlimited geometric freedom grants the ability to produce single part objects which would otherwise be impossible with injection molding or SM [3]. Aerospace and auto industries are currently utilizing AM for this reason as it provides the ability to create specialized lightweight parts through efficient material placement [1], [3], [6].

Another considerable advantage AM has over traditional manufacturing processes is its ability to easily achieve mass customization. Injection molding and SM processes require large setup times between product alterations in the form of mold manufacturing and toolpath generation

respectively [3], [5]. For traditional manufacturing processes to achieve mass customization, various modules are typically manufactured and stored in which labor is required to build the customized product [4]. AM technologies rely on code to produce the desired geometry. This code is automatically generated from computer-aided design (CAD) models which can be easily adjusted in software thereby producing negligible setup times between product alterations. The ability of AM to produce varying products quickly and economically is proving to impact the medical industry with customized products such as soles, hearing aids, medical implants, and braces [2], [3], [6], [7]. Other industries such as jewelry and toys also benefit from the ability to provide mass customization [2], [6]. With consumers typically willing to pay more for a customized product [5], the number of industries introducing mass customization into their products with AM technology is likely to increase.

The ability to produce varying products with negligible setup time also reduces the need for inventory space. 3D printers can be used to create products on demand rather than mass producing a product using traditional methods and storing them in inventories [4]. They can also be left running overnight without human supervision and produce multiple products at a time to meet current demand [3], [6]. This transforms the traditional approach of transporting products from a centralized factory to transporting digital files over the internet in which local 3D printers can use to create the demanded product [3]. This would reduce transportation costs and lead time which could prove beneficial for spare parts in military applications and remote locations [3]. The ability to instantaneously produce products globally has already proved useful in reducing medical equipment shortages during the COVID-19 pandemic. Companies around the world utilized their 3D printers to produce 3D printed valve, respirator, and face shield components to meet demands thereby saving lives and protecting healthcare workers [8].

Of the 3D printing technologies mentioned, FDM invented and commercialized by Scott Crump in 1988 is considered the simplest, most economical, and fastest currently available [1], [2]. This technology involves extruding thermoplastic filament through a heated nozzle that moves in relation to the build surface to selectively deposit material for each successive layer [1]–[3], [7]. The FDM process is commonly represented under other terms to avoid trademark disputes such as plastic jet printing, thermoplastic extrusion, fused filament method, and more commonly, fused filament fabrication (FFF) [2]. These FFF printers were made popular amongst the public thanks

largely to the open source RepRap project. RepRap, short for replicating rapid prototype, was founded in 2005 by Adrian Bowyer with the goal to create a 3D printer in which can self-replicate [2]. This project is responsible for the majority of consumer grade desktop 3D printers used today [7], including some industrial scale FFF printers in which operate on the RepRap firmware. Currently, FFF printers frequently appear in schools, universities, and libraries [9]. Hobbyists have also formed around FFF printing and share their experiences and knowledge on online forums, many of which are sourced in this thesis. Additionally, companies like UPS and Lowe's have brought these 3D printing services to the public allowing individuals to create their own objects [7]. As RepRap and other open source projects continue to drive down the price of 3D printers, we can expect a future where individuals digitally purchase toys, replacement parts, customized objects, etc. before printing them on their own household desktop FFF printer [2].

While common, economic, and fast, FFF printers are typically not used for functional parts or commercial products due to their relatively poor strength and layered appearance [1], [9]. With 3D printing generally having slower production rates compared to traditional manufacturing means [3], [4], [6]; the increased time required for processes such as SLA and SLS are generally preferred for their increased product strength and appearance. Instead, FFF printers are commonly used alongside traditional manufacturing means such as the creation of molds and cores for metal castings [6] or in areas where strength and appearance is insignificant such as specialized handheld tools [2]. However, unlike most 3D printing technologies, FFF technology is feasible for large-scale production. The big area additive manufacturing (BAAM) machine is fundamentally a FFF 3D printing technology that utilizes thermoplastic in pellet form and is capable of producing a full size car frame in a single print [10], [11]. Using large-scale FFF printers provide the opportunity to utilize the advantages AM 3D printers provide while obtaining products of scale that are otherwise limited to traditional manufacturing processes.

In this thesis, FFF printers with a build volume of 0.5 m<sup>3</sup> or more are considered large-scale. These large-scale FFF printers are becoming increasingly available with BigRep [12], Modix [13], Cosine Additive [14], BLB Industries [15], and 3D Platform [16] being some of the providers currently available in 2020. The availability of these printers has enabled larger consumer based 3D printed products with advancements emerging within the automotive, furniture, and medical industries [17]–[19]. While the utilization of large-scale FFF printers for

consumer products are slowly growing, no literature could be found which discuss the challenges that exist when using a large-scale FFF printer.

In this thesis, the utilization of a large-scale FFF printer is explored for an industrial application in which a commercial product is created as a case study. CHAPTER 2 covers product design. The thought process involved with choosing an appropriate product to display the feasibility of 3D printing in an industrial setting is presented. This product is then designed and modeled with emphasis on aiding 3D printing advantages such as complex geometry and mass customization. Lastly, a simulation is created and subjected to the product's model which is then iteratively adjusted to optimize material placement and reduce print time. CHAPTER 3 covers print preparation. The 3D printing process is explained along with the software required. Various issues that are related to printer scale are discussed along with the software's print parameters that are adjusted to reduce these issues. CHAPTER 4 covers product creation in which the product designed in CHAPTER 2 is printed on a large-scale FFF printer using the print parameters assigned in CHAPTER 3. Several additional issues experienced during the product's creation involving adhesion, warping, and filament storage are discussed along with the design, creation, and implementation of solutions to these issues. While the solution to each issue is discussed, some were unable to be implemented and/or verified due to the university lockdown procedure initiated for safety regarding the COVID-19 pandemic. Lastly, CHAPTER 5 discusses options that could be pursued to further optimize FFF printed products including printer scale, print parameters, and print material.

## CHAPTER 2. PRODUCT DESIGN

Several aspects were considered when determining an appropriate object that would best demonstrate the industrial application of large-scale FFF. The object had to be of large-scale, require some degree of structural integrity, and demonstrate the ability to be easily modified. The largest 3D printer available for this demonstration was a 3DP 300 which utilizes a  $1.0\text{ m} \times 1.0\text{ m} \times 0.7\text{ m}$  build area [20], [21]. With the available build surface in mind, a chair was determined to fit the criteria. A chair is relatively large when considering most 3D printers available, required to be structurally stable when the load of an individual's weight is applied, and can be modified to suit different sizes, weight accommodations, and features.

### 2.1 Chair Style Considerations

Three plausible chair styles were considered in determining the appropriate style for this project: the ladder-back chair [22], Voronoi chair [23], and cantilever chair [24], [25]. Of these three, the cantilever chair was chosen due to its ability to be easily modeled, modified, simulated, and 3D printed as one piece while also utilizing AM advantages. Descriptions of the chair types considered along with their respective advantages and disadvantages can be found in the following subheadings.

#### 2.1.1 *Ladder-Back Chair*

The ladder-back chair is a popular style from the Middle Ages [22]. As illustrated in Figure 2.1a, the ladder-back chair is described as a chair having two uprights connected with horizontal members [22].

In modern times, this chair is commonly used in a dining setting. Due to its simplistic design, the chair could be easily printed in 6 separate pieces as illustrated in Figure 2.1b. The members highlighted in red could be printed on its side as a single piece, members highlighted in blue printed upside down, and the braces highlighted in green printed individually. Also, since the members are simple rectangular members, higher print speeds could be utilized with little effect on the resulting print quality. Another benefit of this style is the ability to provide additional strength by fastening the members together with supporting rods or wires running through the horizontal members. Lastly, modification of the chair's parameters would be easily achieved by changing the lengths, widths, and thicknesses of the various members.



Since the chair contains multiple parts, labor for assembly and a larger total print surface would be required thereby reducing the feasibility of utilizing 3D printing for its production. Furthermore, the act of producing a modular chair with member of varying lengths and thicknesses is a technique commonly used with traditional manufacturing methods to provide mass customization [4]. These issues therefore negate the ability of this chair style to effectively demonstrate the industrial application of FFF.

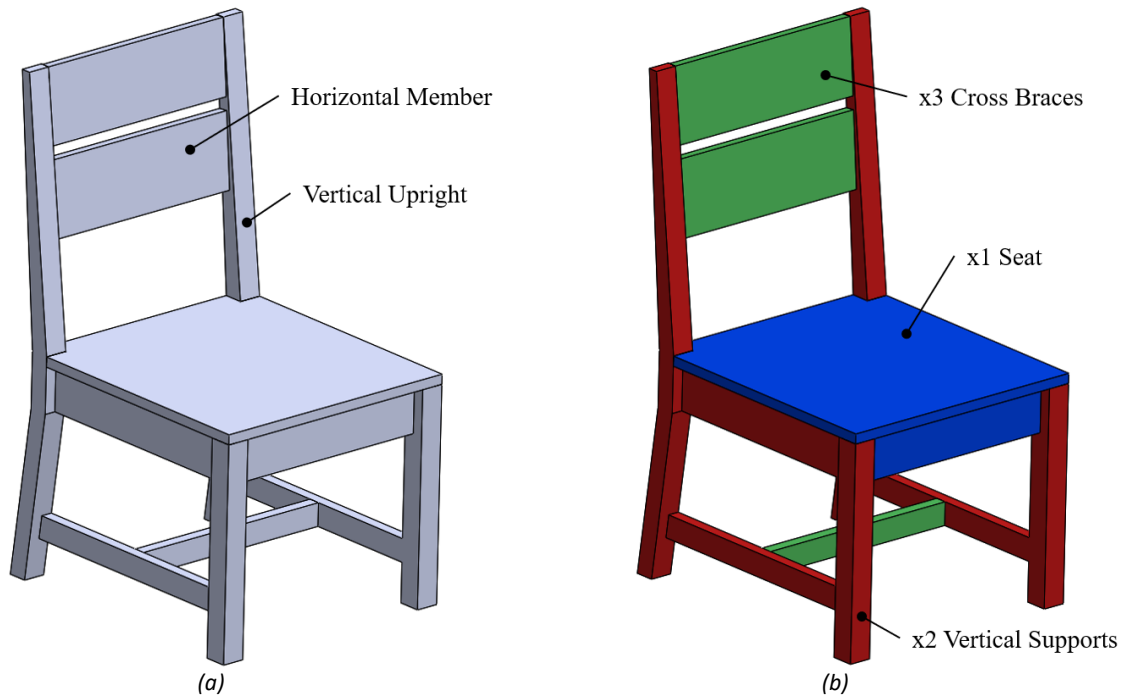


Figure 2.1: Annotated images of a ladder-back chair adapted from [26] showing the features that define it (a) and the possible combination of 3D printed members that could create it (b).

### 2.1.2 Voronoi Chair

The Voronoi chair is a relatively new style inspired from the Voronoi cell structure [23]; an example of which can be seen in Figure 2.2. The Voronoi cell structure can be seen in natural phenomena such as cell walls, desert crust, and atom arrangement. Since it was realized by Georgy Voronoi in 1907, it has been utilized in various computer aided calculations [27] which is why the chair may appear similar to components created using artificial intelligence.

The primary benefit of this design is the potential efficiency in which it could place material in areas that would most effectively withstand stresses created when under load. This would result

in a functional chair with the least amount of material. It also benefits from the capability of being created in a single print, therefore reducing any need for assembly.

Although it is possible to print this style, it would be exceedingly difficult to do so successfully or in a way that would result in a quality print due to all print orientations resulting in areas where material would be deposited without foundational support. While supports could be printed, this would greatly increase the material needed, require expensive water-soluble filament to maintain a desirable surface, and require additional labor to separate the supports from the chair. Lastly, adjusting the model would be exceedingly difficult; however, a company may find this worth attempting due to the possibility of the unique modern design being desirable among consumers.

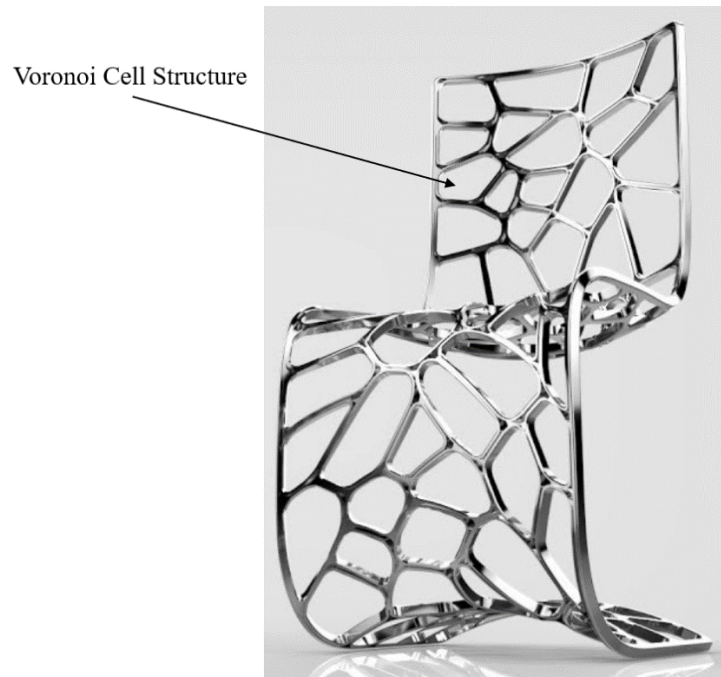


*Figure 2.2: Annotated image of a Voronoi chair sourced with permission from [28] showing the feature that defines it.*

### **2.1.3 Cantilever Chair**

The cantilever chair first became popular in the late 1920's and typically appeared as a simplistic tubular steel chair with no rear legs [24], as illustrated in Figure 2.3a. More generically, a cantilever chair is any chair which is supported by a single leg or legs which extrude from one side of the seat in the shape of an L to create a supporting platform [25]. With this more generalized definition, the Panton chair is also considered a cantilever chair. Panton chairs, an example of

which is seen in Figure 2.3b, are supported in the same manner but is built from a single piece of injection molded plastic [29].

This style can be printed as a single piece and has the potential to be printed well without including printed supports. This is possible by printing the chair on its side and ensuring the curvature does not become excessively steep such that successive extrusions will have adequate foundational support from the previous print layer. The style can also be easily modified by varying the cross-sectional thickness along its curvature to strengthen areas that would experience the most stress. Lastly, this style enables installation of support rods or wires along its outer rails or perpendicularly through its cross section for situations where additional strength is required.

The primary disadvantage of the solid cantilever chair style is its greater relative mass compared to the previously mentioned types. This results in additional print time and print material, both of which increase overall cost.



*Figure 2.3: Annotated images of cantilever chairs with (a) being of the typical tubular design sourced from [30] and (b) being a solid plastic design commonly known as a Panton chair sourced from [31].*

## 2.2 Chair Design and CAD Modeling

The cantilever chair was modeled in SOLIDWORKS® 2018 SP3.0 [32] with inspiration from Figure 2.3b. Two SOLIDWORKS features were used extensively, that being the loft

extrusion and the equations table. The loft extrusion involves at least two profile sketches and optional guide curve sketches. Once the necessary sketches are defined, SOLIDWORKS will create a body that morphs seamlessly between each profile sketch while following along any included guide curve sketches. Utilizing this feature allows chair geometry containing variable profiles in which material could be optimally placed to withstand the desired load. To easily adjust the loft extrusion geometry, various sketch dimensions were stored as variables in the equations table. This allows the chair's geometry to be modified by simply adjusting the variables of interest within the table and refreshing the model. The following subheadings provide a detailed explanation on how the chair's CAD model was created.

### 2.2.1 General Parameters

The chair's geometry is controlled by four SOLIDWORKS sketches hereby known as the chair's essential sketches. The first essential sketch is called the Preliminary Plan. This sketch contains the overall chair dimensions which were adapted from Brezlin's recommended dimensions for an easy chair [33]. These dimensions, and the dimensions chosen for the Preliminary Plan, are shown in Table 2.1. The Seat Inclination and Seat Back Inclination were taken smaller than would otherwise seem appropriate due to the expected deflection caused by the cantilever chair style under load,.

*Table 2.1: Chair dimension guidelines for a casual easy chair adapted from [33].*

Parameter	Guidelines	Incorporated
Seat Width	16" – 20"	45 cm (17.72")
Seat Depth	15" – 18"	40 cm (15.75")
Seat Height	16"	41 cm (16.14")
Seat Inclination	10°	2°
Seat Back Length	14" – 16"	36 cm (14.17")
Seat Back Inclination	5° – 30°	7°

The Preliminary Plan can be seen in Figure 2.4. The overall dimensions were entered into the equations table and placed into the sketch as variables. This is evident by the red uppercase sigma beside each variable dimension. The Preliminary Plan can be considered the backbone of the model in that any changes to these variables will refresh all proceeding sketches causing the chair to update to the desired size.

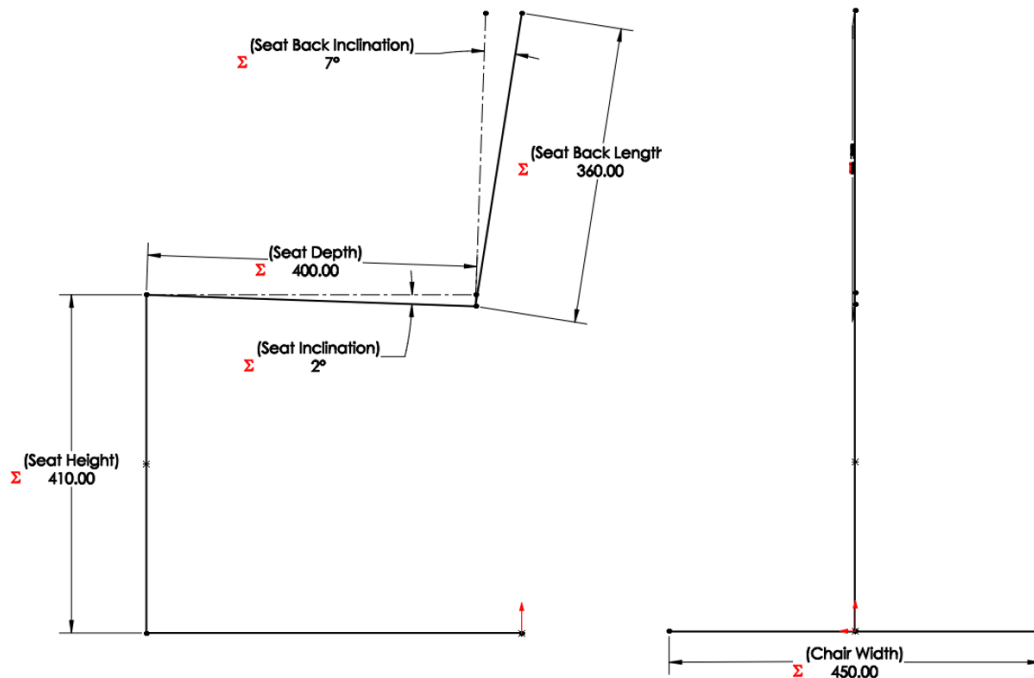


Figure 2.4: Orthogonal images of the 3-dimensional Preliminary Plan SOLIDWORKS sketch.  
(Dimensions in mm unless stated otherwise)

### 2.2.2 Load Bearing Parameters

The next two essential sketches are called the Final Plan (Center) and Final Plan (Rail), seen in Figure 2.5a and Figure 2.5b respectively. These sketches can be considered the ribs of the chair in that they provide the framework for proceeding sketches while being initially defined off the Preliminary Plan. These Final Plan sketches define the vertical cross sections of the chair model at the center and the rail, respectively, with the rail being the chair's planar face on either side.

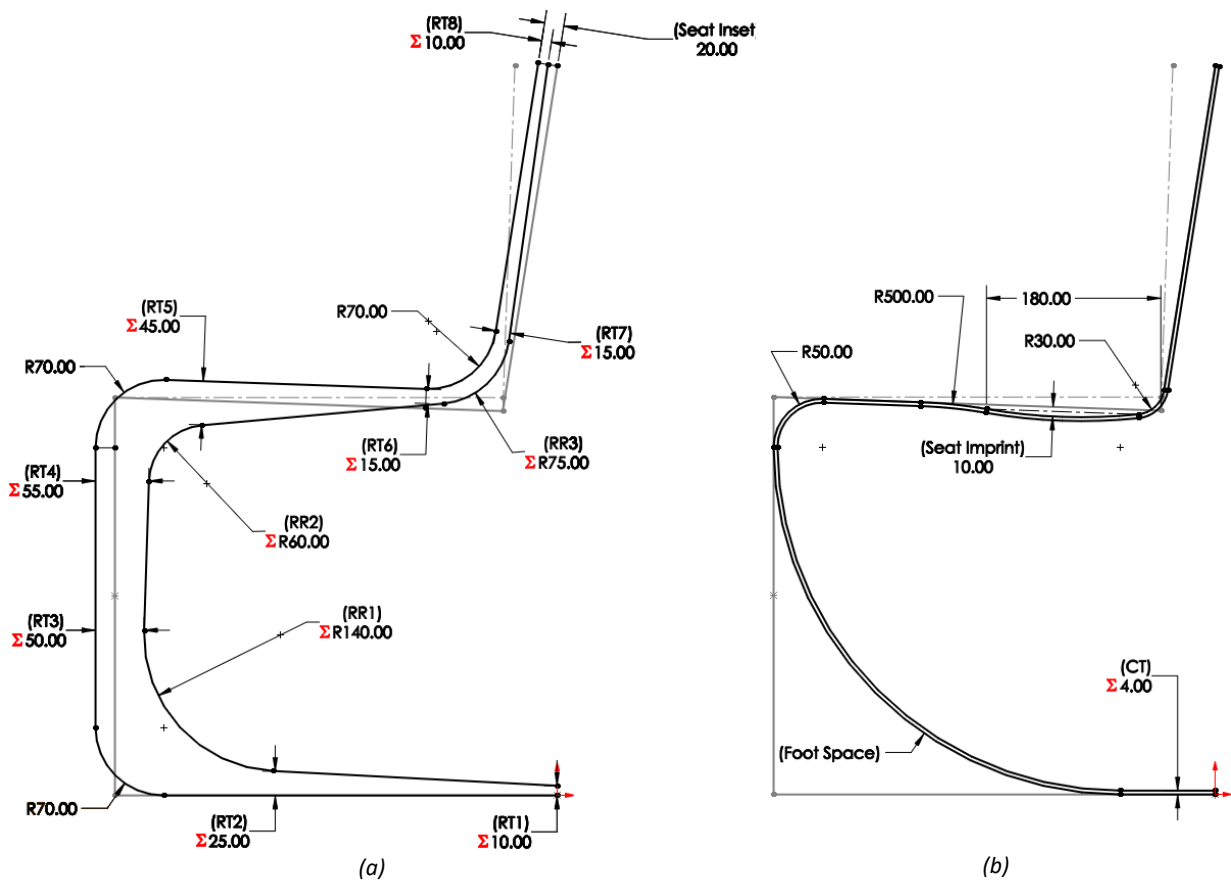


Figure 2.5: Images of the Final Plan (Rail) (a) and Final Plan (Center) (b) SOLIDWORKS sketches with the Preliminary Plan shown in gray.  
(Dimensions in mm)

Although the primary objective was to show the general feasibility of FFF in the industry, an effort was made to make the chair comfortable. This was done by implementing a Seat Inset, Seat Imprint, and Foot Space. The Seat Inset is seen in the Final Plan (Rail) as 20 mm and defines the distance in which the rails of the chair protrude forward and upward from its center. This feature acts to envelope the user slightly to prevent sliding. The Seat Imprint is seen in the Final Plane (Center) as 10 mm and helps to further center the user and prevent slipping by providing a crater at the rear. Lastly, the Foot Space allows space for an individual to tuck their feet a short way under the chair. This feature is seen in Final Plan (Center) and provides the additional function of strengthening the lower chair radii by acting as a brace. These features, along with a few others, were not defined as variables to reduce any unnecessary complexity in the model, though they could easily be varied if so desired.

The dimensions in the Final Plans which were defined as variables where those which would affect the chairs strength. These dimensions are scattered throughout Figure 2.5 and are evident by their respective red uppercase sigma. In Final Plan (Rail), these variables are the Rail Thickness' and Rail Radii abbreviated as RT1 to RT8 and RR1 to RR3, respectively. These dimensions allow the rail thickness to vary along its length as to provide the ability to optimize material for the desired load. In Final Plan (Center), variation in thickness is not necessary as its primary role is to transfer the load to the rails on either side. Therefore, the Final Plan (Center) contains a single variable called the Center Thickness seen abbreviated as CT.

The final essential sketch is the Surface sketch illustrated in Figure 2.6. This sketch acts as the skin of the model in that it is defined primarily off the Final Plane sketches. This allows the profile to stretch and conform its shape depending on where the profile is placed relative to the Final Plan sketches. The Surface sketch contains the final strength variable labeled Rail Width. This variable defines the distance in which the Final Plane (Rail) vertical cross section is held constant before transitioning to the Final Plane (Center) cross section. The Surface sketch also contains two other variables labeled TSC and TSR for Tangent Strength Center and Tangent Strength Rail, respectively. These variables were only added into the equations table due to the repetition in which they exist throughout the model. Other than a slight adjustment after the loft extrusion was created, the magnitudes shown were considered constants along with the other comfort features stated earlier.

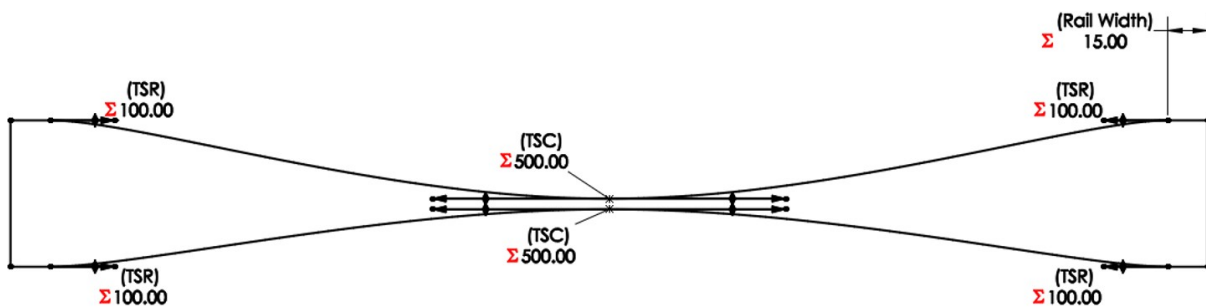


Figure 2.6: Image of the Surface SOLIDWORKS sketch.  
(Dimensions in mm)

### 2.2.3 Sketch Assembly and CAD Creation

The loft extrusion within SOLIDWORKS was used to create the chair model. The guide curve sketches required for the chair were created by simply projecting the Final Plan sketch curves onto planes positioned with respect to the Chair Width defined in the Preliminary Plan. This

resulted in a total of 6 guide curves as illustrated in Figure 2.7a. The Surface sketch discussed previously was created 10 times and spaced relatively evenly along the guide curve sketches to be used as profile sketches. While the loft extrusion only requires a profile sketch at the beginning and end, additional profiles were deemed necessary to prevent the model from shifting in unexpected ways. The Surface sketches vary independently from each other as the four corners and the two central points highlighted in Figure 2.7b were defined to align on their respective guide curve sketches. Combining the guide curves and profiles together results in the wireframe structure seen in Figure 2.7c which SOLIDWORKS then uses within its loft extrusion feature to create the chair geometry seen in Figure 2.7d. Since the sketches were layered such that each sketch provides the framework for proceeding sketches; any change in variables contained in the Preliminary Plan, Final Plans, or Surface sketch will update and reshape the model to the desired specifications.



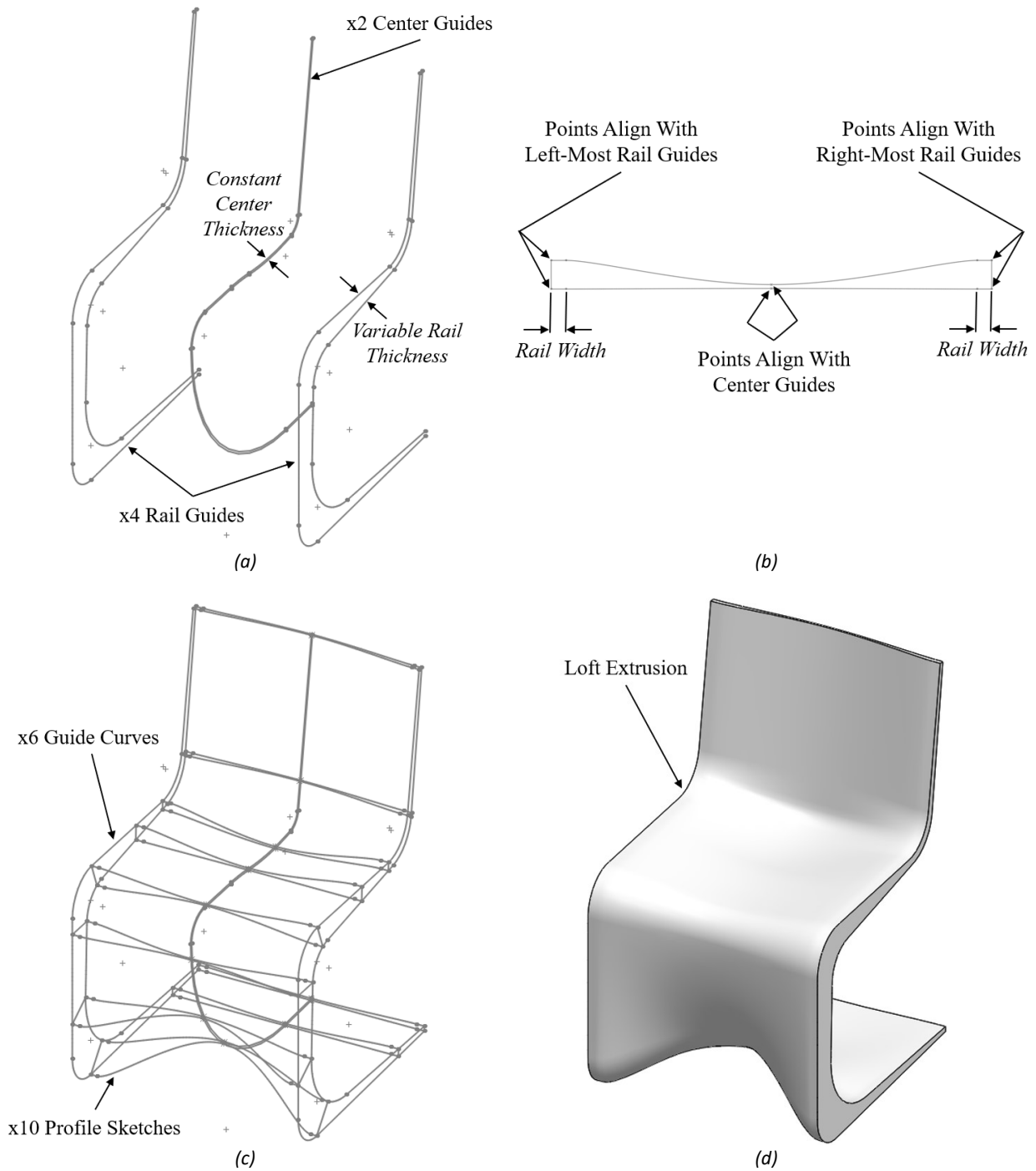


Figure 2.7: Annotated illustrations of the SOLIDWORKS sketches used within the loft extrusion feature to virtually create the chair in which (a) is the guide curves, (b) is the repeated profile, (c) is the assembled wireframe and (d) is the resulting CAD model.

#### **2.2.4 Additions**

To further customize the chair, togglable additions can be included such as luxury features, ergonomic advancements, and structural adjustments. These additions can be defined directly off the geometry created earlier and be suppressed when they are not desired. Further simplifying the process, SOLIDWORKS configurations can be created and toggled in which the desired additions are included.

In the case of this demonstration, a brace addition was created due to concerns regarding fatigue. Print parameters have a significant effect on the fatigue properties of 3D printed parts. While larger layer heights have been shown to increase fatigue resistance of 3D printed PLA [34], no experimentation was found that could directly relate to the large-scale prints that the 3DP 300 is capable of. Other than reducing structural complexity, the brace addition could also result in reduced print material and print time compared to the pure cantilever chair design. This was hypothesized from the ability to define considerably thinner rails due to the effective stress transfer that the brace could provide.

The brace addition significantly reduces elastic deformation by placing a vertical member at the rear of the chair. This vertical member is created using a positional sketch and a profile sketch as shown in Figure 2.8a, in which the profile thickness was defined as the variable Brace Width. After extruding the profile sketch between the two impeding surfaces, large radii were added resulting in the solid model shown in Figure 2.8b. Due to the design's negligible elastic deformation, the Seat Slope and Seat Back Incline Angle were reverted to 10° and 15° respectively.

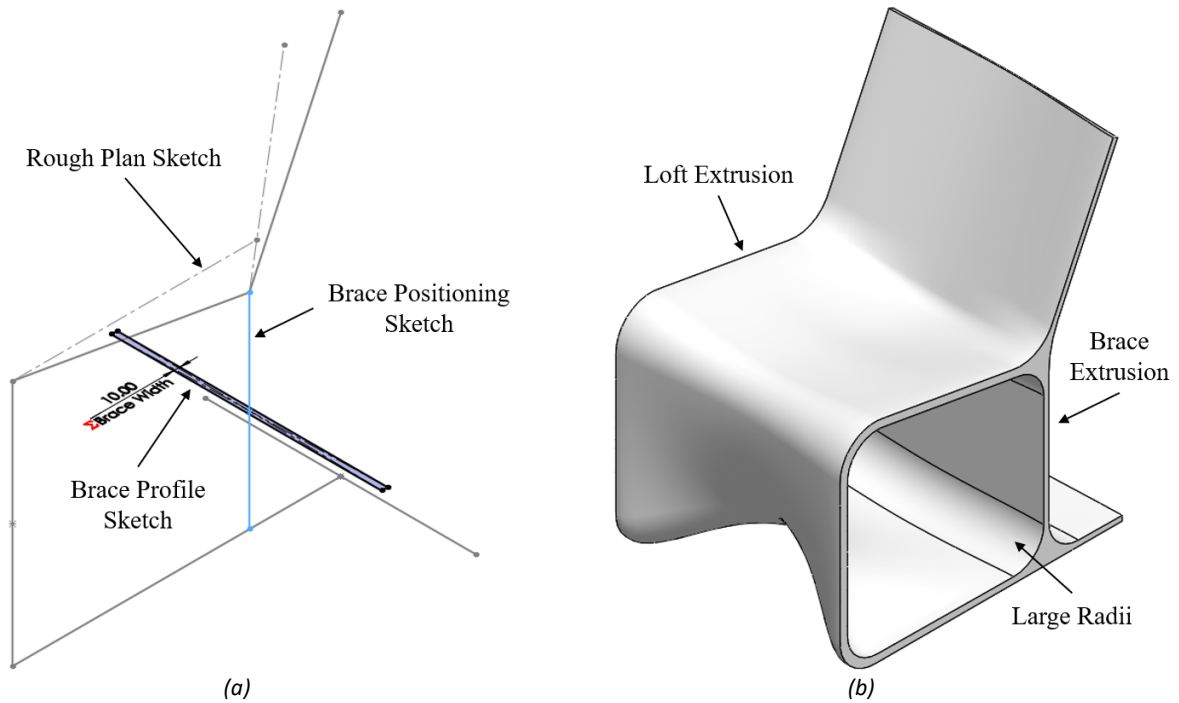


Figure 2.8: Annotated illustration of the SOLIDWORKS sketches (a) and resulting CAD model (b) of the cantilever chair's brace addition.  
(Dimensions in mm)

## 2.3 FEA Analysis

SOLIDWORKS was also used to compute finite element analysis (FEA) iteratively on both the cantilever and braced-cantilever chair designs. The purpose of FEA was to determine the appropriate variable magnitudes such that each chair design would be capable of withstanding the forces involved during use while consuming the least amount of material. To avoid complexity and stay within the computing capabilities of SOLIDWORKS, the chair was assumed isotropic. While this is acceptable for the modulus of elasticity, the tensile strength of FFF objects represents an anisotropic material with decreasing strength through the longitudinal (in line with extrusion), transverse (across extrusions of the same layer), and normal (across print layers) directions, respectively [35], [36]. The normal tensile strength has been shown by [37] to be as low as 47.71%. FEA was therefore completed with the goal to approach but not drop below a Factor of Safety of 2, with several choices being made to obtain conservative results. The following subheadings go in depth on how the simulations were created and their results.

### **2.3.1 FFF Defined Strength Parameters**

To further allow the optimization of material, FFF's capability of producing hollow geometry was utilized. This was achieved by varying the infill percentage of select print layers. Specifically, the infill percentage was assigned to 100% for a distance from either side and for a central distance. These distances were called the Rail Fill Width and Center Fill Width, respectively. These sections would provide the structural strength of the chair while the area between them was assigned to 10% infill for internal print support. An additional parameter is the Shell Width which defines the perimeter thickness that surrounds all sections.

For FEA to be completed, the CAD model had to be further adjusted to reflect the chair's physical geometry. The strength parameters can be seen incorporated into the chair's model in Figure 2.9. As before, the Rail Fill Width, Center Fill Width, and Shell Width were defined as variables within the equations table such that they could be easily adjusted for FEA iterations. The implementation of these parameters into the CAD model were done by utilizing the split, shell and combine features within SOLIDWORKS. First, the split feature was used to slice the model along the Rail Fill Width and Center Fill Width boundaries, thereby creating multiple bodies. The 10% infill section bodies were then hollowed out to the specified Shell Width parameter using the shell feature. Lastly, the combine feature was used to merge all bodies back together. The 10% infill sections were kept hollow to avoid complexity and provide a conservative simulation result. Since the primary function of the infill was to provide internal print support, a rectilinear infill pattern was chosen for its superior areal coverage to mass ratio. Not only is this infill pattern known to provide inferior tensile strength compared to other patterns, but the strength to mass ratio is also expected to be lower [38], therefore it would not have any significant structural contribution.

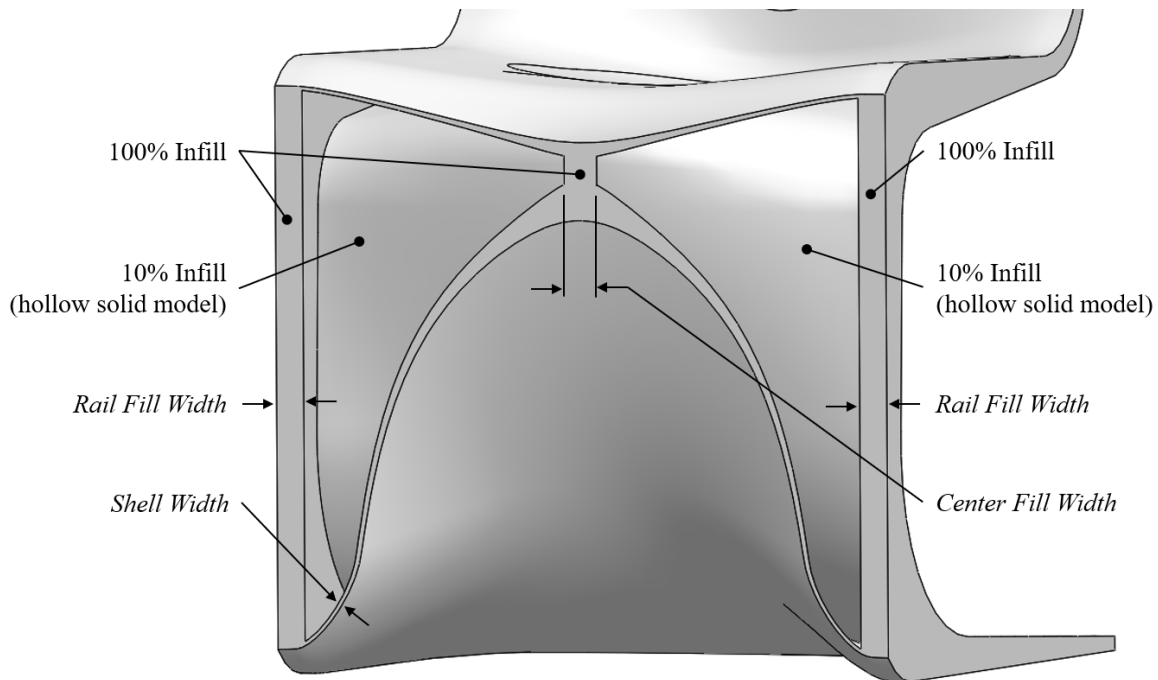


Figure 2.9: Annotated illustration displaying the implementation of the Rail Fill Width, Center Fill Width, and Shell Width parameters into the cantilever chair's FEA CAD model.

### 2.3.2 Simulation Parameters

FEA was completed within SOLIDWORKS as a static simulation. Static simulations require external loads, fixtures, and mesh parameters. External loads simulate the forces exerted directly on the object during use while fixtures simulate the forces exerted indirectly to keep the object in static equilibrium. Lastly, mesh parameters define the element structure implemented on the chair.

Two external loads were defined to the chair as illustrated in Figure 2.10a. The primary external load was a force distributed over a 30 cm by 20 cm oval projected approximately to where one would be sitting. This external load was implemented to simulate the weight of the user. The force was defined as 275 lb., approximately 124.74 kg, as this was recorded to be the 95<sup>th</sup> percentile US male weight given by ANSI/BIFMA X5.1 [39]. The secondary external load was a force distributed over a semi-ovular area, defined by projecting a horizontal line downward across the back rest. This external load was implemented to simulate the pressure exerted when the user leaned against the back rest. The force was intuitively defined as 9.07 kg (20 lb.) which was deemed acceptable. To retain simulation accuracy in the event of large deflections, the weight force was defined to be in the vertical direction while the lean force was defined to be perpendicular to the back rest's surface.

There were two fixtures defined to the chair as illustrated in Figure 2.10b. The primary fixture was a roller/slider type which applies a force normal to the selected surface such that the object does not drop below the surface in which it was initially defined. This fixture served to simulate the normal force exerted by the floor. The surface in which the roller/slider type fixture was defined to was created by using the extruded cut feature to shave a negligibly thin 0.1 mm portion off the bottom of the chair model. The secondary fixture was a fixed type which applies forces such that the geometry it is applied to remains spatially fixed. This fixture served to satisfy the simulation requirements and is applied to the rear bottom cross-sectional surface of the chair.

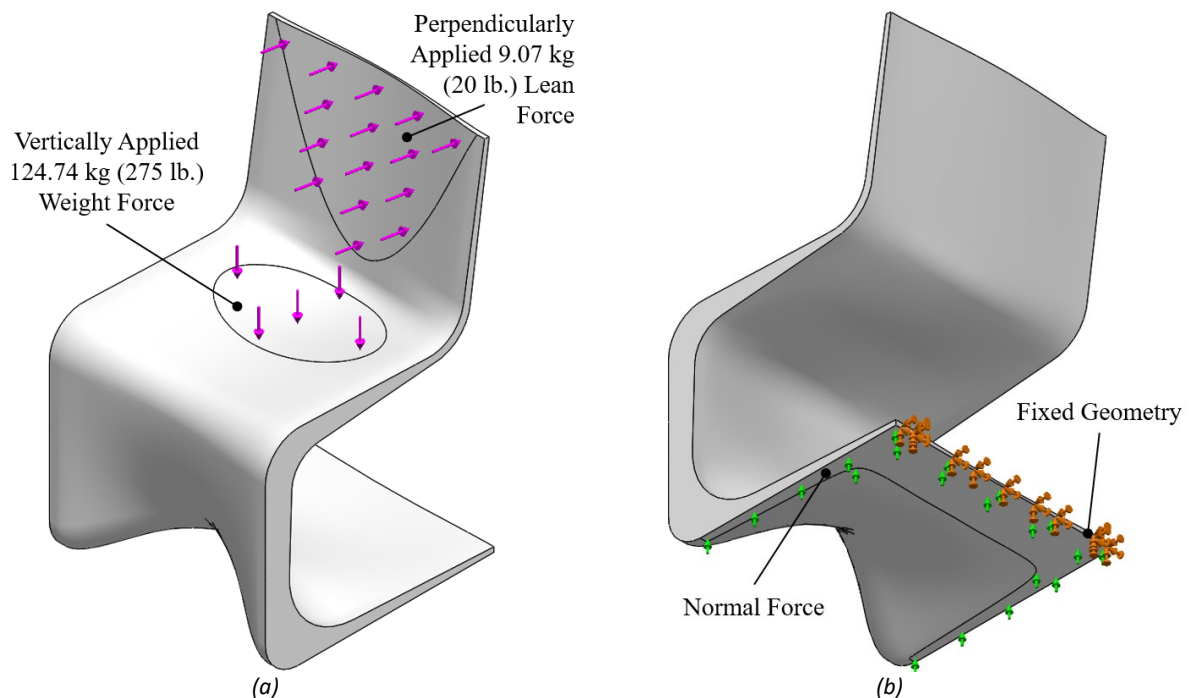


Figure 2.10: Annotated illustrations displaying the applied external loads (a) and fixtures (b) in the SOLIDWORKS static simulations.

The mesh parameters consist of a few definitions, though only two of them were directly modified. The first parameter was the type of mesh used. SOLIDWORKS static simulations offer three different mesh types: standard mesh, curve-based mesh, and blended curve-based mesh. Of these options, the blended curve-based mesh was chosen due to its ability to successfully mesh the chair when different variable dimensions were selected. This mesh type also worked well to avoid skewing the maximum stress result from falsely calculating large stress concentrations at the normal force boundary. The other mesh parameter was the maximum mesh size. This is an important property as a mesh size too large will give inaccurate results, while too small will cause

excessive simulation computing times. To determine the appropriate magnitude, a mesh convergence graph was created as displayed in Figure 2.11. This involves progressively reducing the maximum mesh size until the resulting max stress converges. As evident in the graph, the initial cell size was taken as 40 mm and was progressively halved until 5 mm where it was deemed to be of reasonable accuracy. Reducing the mesh size any further not only increases the simulation time, but also negatively effects the stress results around the normal force boundary causing inaccurate max stress results. This mesh convergence was only completed once with 5 mm taken as adequate for all proceeding simulations. Since the hollow sections would contain 10% infill, any small inaccuracies were assumed negligible due to all results being conservative.

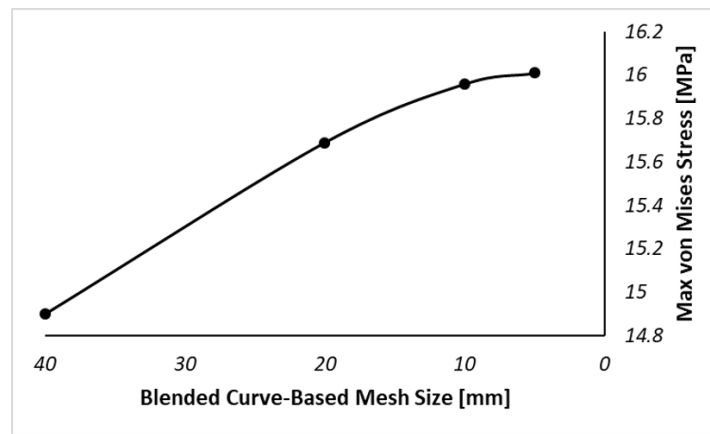


Figure 2.11: Mesh convergence graph displaying the logarithmic behavior of simulated stress with decreasing mesh element size.

### 2.3.3 Material Choice

Polylactic Acid (PLA) is one of the more popular FFF 3D printing filament materials used throughout the 3D printing community. Its popularity and abundant use in filament composites [1] has accelerated PLA-based polymer technology growth to the point where PLA options either rival or benefit over other polymer options in situations where specific properties are desired [40]. Other than PLA being relatively easy to print thanks to its lower melting point of 130-180 °C [41], its popularity is significantly influenced by its environmentally friendly characteristics. Specifically, its sustainability [42], recyclability [43], and biodegradability [40]. For these reasons, PLA was chosen to be used for printing of the chair.

The source of PLA's sustainability derives from its ability to be created solely from renewable matter. Unlike many other thermoplastic filaments available, PLA is made from starch extracted from rice, sugar beets, sugarcane or corn with the later of the three commonly used [40],

[42]. Thanks to the exclusion of petroleum, PLA consumes less fossil energy compared to petroleum-based thermoplastics. PLA was estimated to consume 25-55% less fossil energy in 2003 than its petroleum-based counterparts, and is believed to consume up to 90% less when the manufacturing process becomes more efficient and relies on renewable energy sources [42].

PLA has also been shown to be recyclable in that PLA can be melted down and re-formed with little reduction in its mechanical properties. PLA had been recycled and injection molded 20 times by [43] with no significant changes in properties other than a reduction in viscosity. 3D printed PLA has also been shown to sustain multiple extrusions with minimal mechanical property degradation with [44] obtaining identical surface quality and 2-11% reduction in mechanical properties and [45] obtaining no significant reductions in mechanical properties until the third recycling attempt. Additionally, polydiacetylenes (PDA) coating recycled PLA pellets has been shown to reduce mechanical property degradation of 3D printed parts by [46], in which the tensile strength had increased by 14.9% and elongation at break by 3.74%. While current recycling methods fail to recycle PLA due to identification difficulties [47], recycling could be beneficial in the future or for large-scale business that utilize PLA processing.

Additionally, PLA has been shown to be biodegradable through hydrolysis. Hydrolysis is the process of compounds being broken down through the absorption of water molecules. In the case of PLA, water molecules are known to break its ester chains thereby reducing its molecular weight [40], [41], [48]. The rate of PLA degradation is dependent on many parameters such as initial molecular weight, crystallinity, geometry, PLA purity, humidity, and temperature [40], [48]. Additionally, the degradation rate of PLA is autocatalytic, meaning the rate of hydrolysis increases the further it degrades [49]. PLA is stable under typical conditions in which its mechanical properties remain undeteriorated for years [40]; however, [50] has shown PLA's molecular weight reduce by 41.6% over 5.5 months when submerged in water. Furthermore, results obtained by [48] led to their assumption that PLA objects a few millimeters thick would fully degrade within 2-3 years when subjected to a high humidity environment. The temperature of the high humidity environment also has a significant effect on PLA's degradation rate. While temperatures below room temperature can result in PLA lasting over 4 years, PLA will degrade to the point of being consumed by micro-organisms within a month when subjected to temperatures of 60 °C or more [41]. Though PLA is considered compostable [42], few composting facilities accept PLA due to



the requirement of high temperatures for reasonable degradation rates. Along with other complications such as PLA being incompatible with compost material certifications or dense PLAs not fully degrading within set timeframes, most PLA materials are instead sent to landfills [47].

With the material determined, the simulation's mechanical properties could then be defined. Filament.ca's EcoTough white PLA was used to print the chair. The only mechanical property stated for this filament is its minimum tensile strength of 89 MPa [51]. This tensile strength is likely inaccurate for 3D printed objects due to the vast number of variables involved during the 3D printing process. Instead, the mechanical properties were taken from MakeItFrom.com. These values are displayed in Table 2.2 with Poisson's ratio assumed as 0.3. These values seem appropriate when considering results from the many studies completed on the mechanical properties of 3D printed PLA [35]–[38], [44], [52]–[54]. While sources show the elastic modulus of 3D printed objects behaving isotropically, the tensile strength behaves anisotropically in which the tensile strength in the normal direction is approximately 50% of that of the longitudinal direction [35]–[37], [53], [55]. This reduction in tensile strength was adapted into the SOLIDWORKS FEA simulations by ensuring the factor of safety did not drop below 2.

*Table 2.2: Mechanical properties of PLA adapted from [56].*

<b>Mechanical Property</b>	<b>Value</b>
Density	1.3 g/cm <sup>3</sup>
Elastic Modulus	3.5 GPa
Shear Modulus	2.4 GPa
Ultimate Tensile Strength	50 MPa

#### **2.3.4 Simulation Results**

Each static simulation was created and ran manually for both the cantilever and braced-cantilever chair models. After each iteration, the stress distribution was observed, and specific variable magnitudes were adjusted. The goal was to minimize mass while keeping a factor of safety of 2 or more. The iterative FEA progression for the cantilever and braced-cantilever chairs are shown in Figure 2.12 and Figure 2.13 respectively. A detailed list of variable magnitudes used for each iteration along with a description of each max stress location can be seen in Appendix A. Orthogonal drawings displaying the overall dimensions of the cantilever and braced-cantilever's final iteration can be seen in Appendix B. The final iteration's stress and displacement distributions

are illustrated in Figure 2.14 for the cantilever chair and Figure 2.15 for the braced-cantilever chair. In these figures, von Mises and URES refers to the combined stress and displacement across 3-dimensional space respectively.

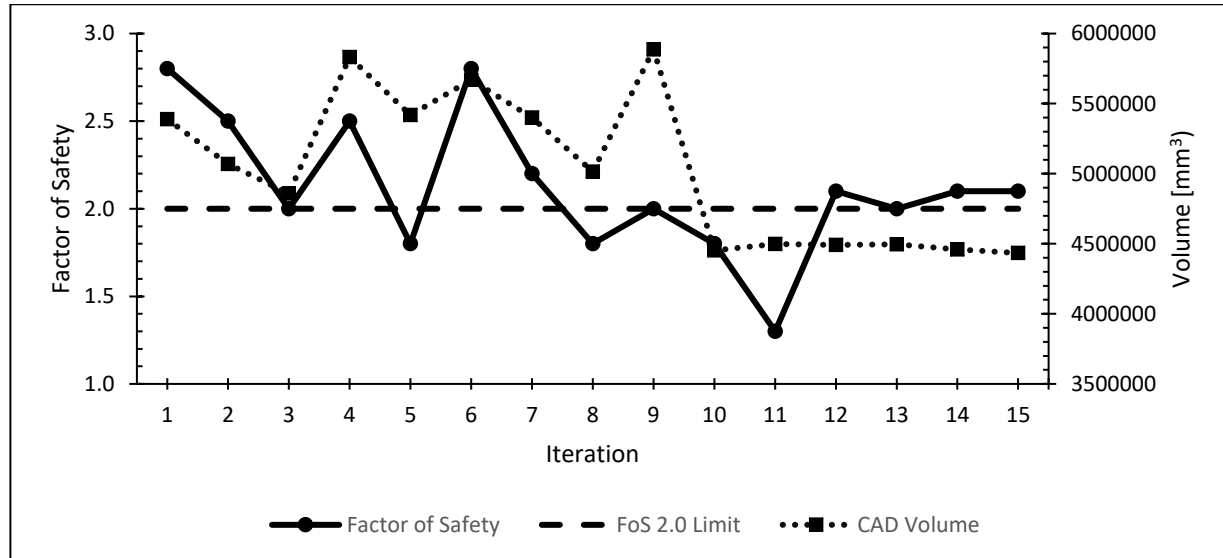


Figure 2.12: Line graph displaying the iterative FEA progression performed on the cantilever chair to reduce volume and keep a minimum factor of safety of 2.0.

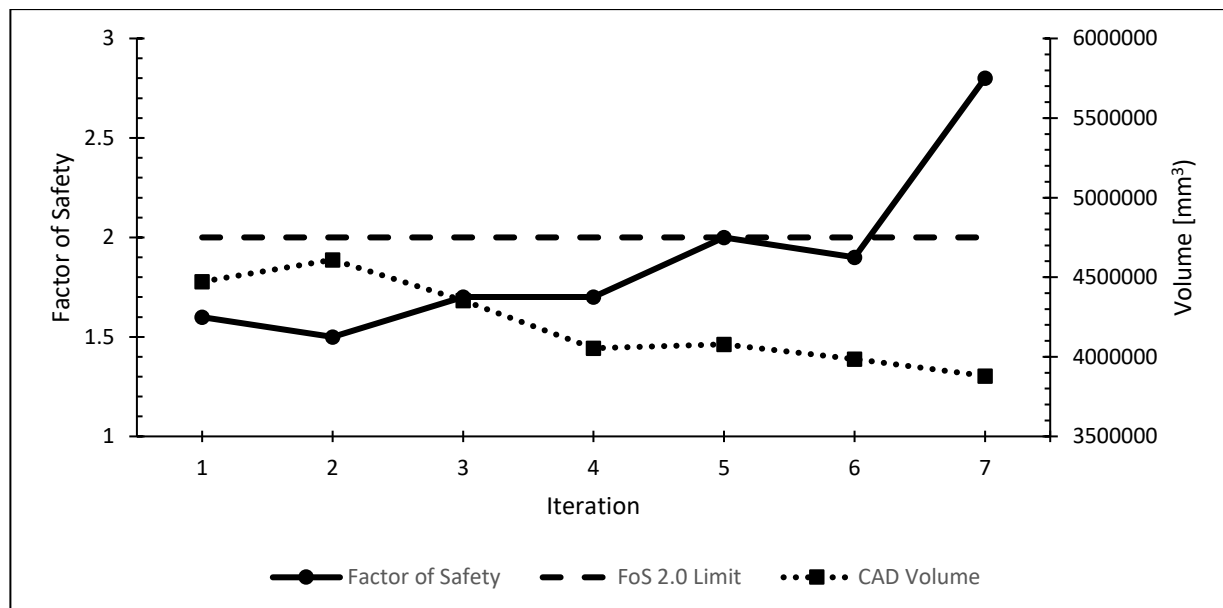


Figure 2.13: Line graph displaying the iterative FEA progression performed on the braced-cantilever chair to reduce volume and keep a minimum factor of safety of 2.0.

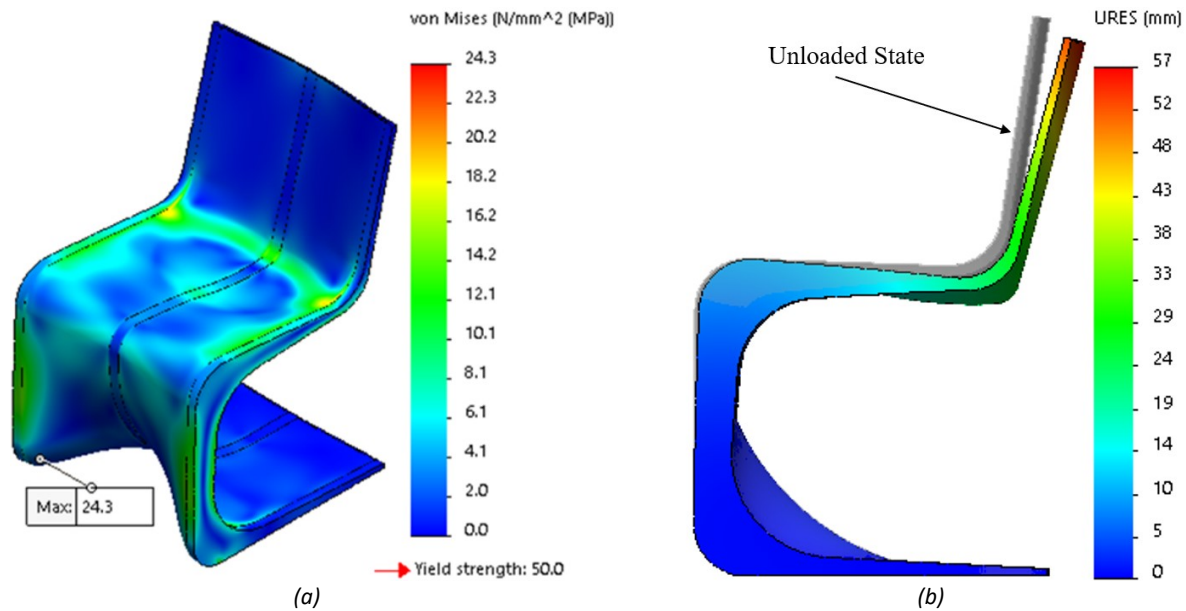


Figure 2.14: Images displaying the stress distribution (a) and displacement distribution (b) of the cantilever chair design at its final FEA iteration.

As seen in Figure 2.14a, the stress distribution for the cantilever chair design is relatively well dispersed along the seating and frontal areas. The peak stress can be observed at the normal force Fixture boundary, which results in a factor of safety of 2.1. This stress concentration appears due to the singularity point existing at the Fixture boundary. In reality, this stress is expected to be much lower. The true factor of safety was estimated at 2.2 with the peak stress located on the internal edge at the rail radius closest to the back rest. As expected, the displacement distribution illustrated in Figure 2.14b shows the chair having an increased seat and back rest inclination angle. This increased inclination appears to lie around the recommended easy chair dimensions listed in Table 2.1; therefore, no model adjustments were computed.

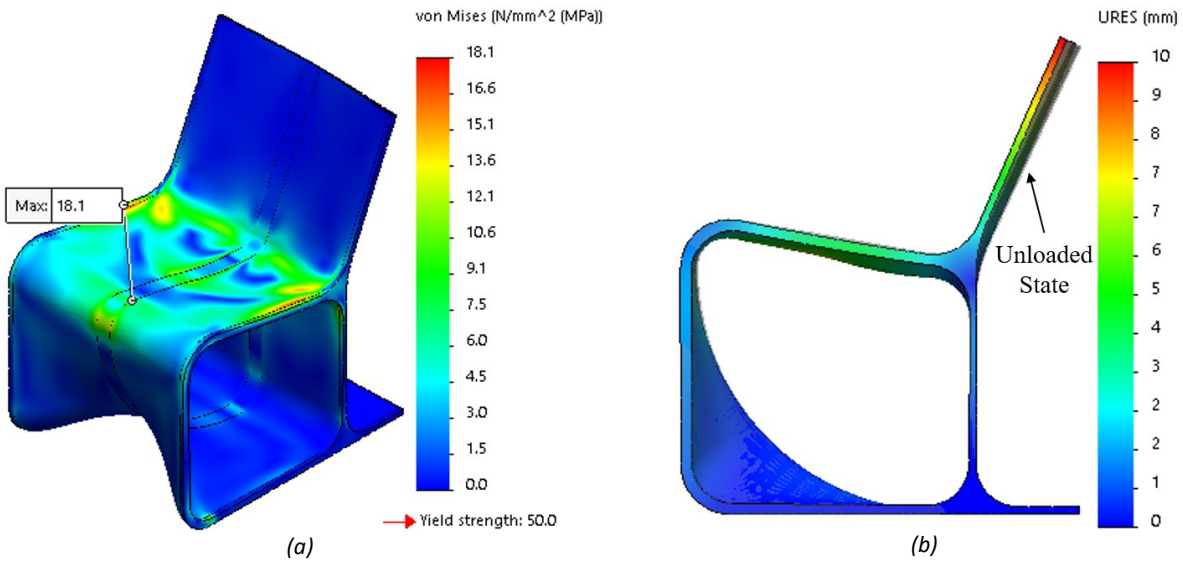


Figure 2.15: Images displaying the stress distribution (a) and displacement distribution (b) of the braced-cantilever chair design at its final FEA iteration.

The stress distribution for the braced-cantilever chair design is relatively well dispersed at the seating area as seen in Figure 2.15a. The peak stress can be observed at the center of the front seating radius; specifically, at the internal edge beside the center fill width. This peak stress results in a factor of safety of 2.8, significantly larger than the 2.0 goal. This was not further lowered due to the drastic effect further thinning of the rails had on the structural integrity of the chair. A small change would result in large increases in stress with little improvement in overall mass. Another issue was the unpredictability of the chair's structural integrity. When the brace width was reduced from 15 mm to 10 mm, the factor of safety increased from 1.9 to 2.8 as seen in Figure 2.13 between iterations 6 and 7. When this behaviour was analyzed further, it was found that the thinner brace width allowed the upper brace node to deflect much more than it could originally as observed in Figure 2.16. This deflection allowed the stresses to spread out more evenly and therefore greatly reduced the stress concentrations around the area. Additional simulations were completed by gradually increasing the lean force to 36.29 kg (80 lb.) and the seat weight force to 192.78 kg (425 lb.) to ensure the chair was stable. Despite the seemingly sensitive simulation results completed previously, the chair did not fail in any of these additional tests. When comparing the deformation distribution from the cantilever chair design in Figure 2.14b, and the braced-cantilever chair design in Figure 2.15b, it can be seen that the brace performs well in reducing elastic deformation and therefore allows for much thinner rails.

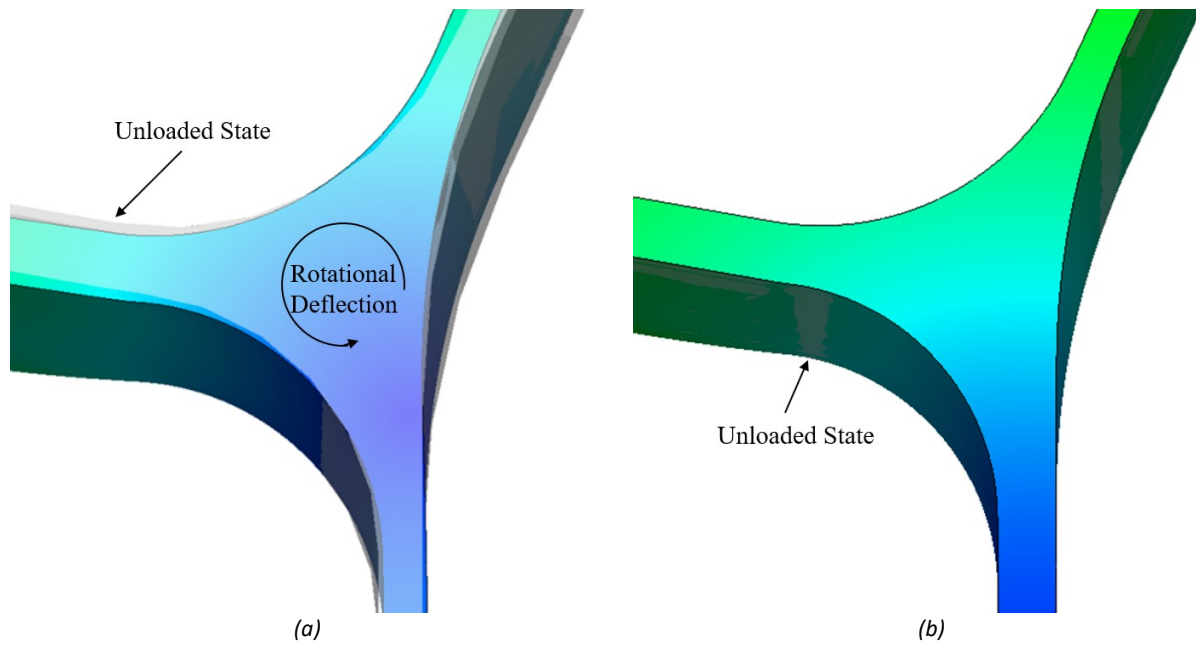


Figure 2.16: Annotated illustration comparing the simulated braced-cantilever chair deflection with a 10 mm brace width (a) and a 15 mm brace width (b) with the initial unloaded orientation represented in translucent gray.

## CHAPTER 3. PRINT PREPARATION

The 3DP 300 printer was used to print the chair. These series of printers by 3D Platform are controlled by the open source firmware RepRap on a Duet board, and therefore have no restriction on the material or slicer used [20]. While the material chosen was stated in chapter 2.3.3, the slicing software has yet to be discussed. The slicer is a critical step in the 3D printing workflow as it translates the CAD mesh file into a file type the printer can read. The slicer also implements user defined print parameters into the exported file which significantly effects the print result both visually and mechanically.

### 3.1 Slicing Software

Aside from select closed-source variants, 3D printers require G-code files to perform prints. These files are created by slicing software and contain step-by-step instructions that the 3D printer's firmware can read and execute. Slicers function by slicing an imported mesh CAD model, commonly represented in the .stl format, into cross-sectional layers and generating a series of printer actions that recreate the model layer-by-layer [7], [57]. During this generation, the slicer software refers to user selected print parameters to create the print to the desired specifications. These print parameters include extrusion parameters such as extrusion width, height, speed, temperature along with physical parameters such as print wall thickness, infill percentage, solid top/bottom layers, etc.

There are many different slicers available to choose from; however, the two most popular options amongst the 3D printing community appear to be Simplify3D [58] and Ultimaker Cura [59]. Simplify3D is commonly viewed as the best slicer you can buy with its robust features and quick processing speeds, while Cura is viewed as the best free slicer available with it being open source, easy to use, and feature abundant [60]. Typically, Simplify3D is popular amongst professionals and enthusiasts for its superior speed and robust features while Cura is popular amongst hobbyists due to its feature abundance and free utilization.

At first, Cura was used for all prints completed on the 3DP 300 printer. This was quickly changed to Simplify3D for a few reasons. First, Cura did not generate the desired toolpaths in certain situations where a single wall extrusion thickness was desired. The slicer would extrude the perimeter as expected, then retrace its path backwards instead of immediately continuing with

the print. This has little effect on a smaller desktop printer; however, this resulted in extrusion issues with the large-scale printer due to oozing. This and other large-scale printer characteristics are discussed in the proceeding subchapters. Another issue was that some print parameter settings available within Cura did not register correctly in the 3DP 300's RepRap firmware, causing it to display errors on the command window. While the only parameters found to cause errors were those which changed acceleration settings, it made the slicer feel incompatible with the 3DP 300. Lastly, 3DP recommended Simplify3D due to its use internally for their own testing and troubleshooting [61]. After using Simplify3D for some time, it proved to provide a more professional feel over Cura with robust features, fast processing speeds, informative visuals, and a UI that is easily navigated.

## **3.2 Print Parameters**

The specific 3D Platform printer used was the 3DP 300-2E7C2-A3300-100. This printer's 1 m × 1 m build surface consists of a heated borosilicate glass sheet, in which heat is applied directly by a silicon heat pad located underneath. The printer deposits thermoplastic through dual water cooled HFE 300 extruders equipped with 1 mm nozzles which translate on aluminum extrusion rails powered by closed loop servo SurePrint™ motors with lead screws [20], [21]. Synonymous to most complex machines, each 3D printer behaves differently. Many factors such as the environment, print material, drive system, computing system, and more all effect how a printer performs. These factors result in unrepeatable print results between similar printers with identical print parameters [3].

To determine the appropriate print parameters for the 3DP 300 printer, various experimental, functional, and collaborative prints were completed using a print profile provided by 3DP. Throughout this process, multiple parameters were modified to obtain better results. It soon became obvious that, while the 3DP 300 printer is an impressive piece of machinery, the general use of large-scale FFF 3D printers comes with its own drawbacks compared to their desktop sized variants. These disadvantages present limitations in which object geometry and print parameters need to be considered to achieve a desirable print. The key points of consideration include its build surface, print head, and overall mass. These are discussed in detail in the following subheadings. The final print parameters can be seen in Appendix C with the general parameters shown in Table 3.1.

Table 3.1: General print parameters assigned within Simplify3D for the 3DP 300 printer equipped with HFE 300 hotends.

<b>Nozzle Diameter:</b> 1.00 mm	<b>Nozzle Temperature:</b> 205 °C
<b>Extrusion Multiplier:</b> 1.00	<b>Bed Temperature:</b> 60 °C
<b>Extrusion Width:</b> Auto (1.20 mm)	<b>Infill Pattern:</b> Rectilinear
<b>Primary Layer Height:</b> 0.5 mm	<b>Infill Angle Offsets:</b> 45°/-45°
<b>Print Speed:</b> 100 mm/s	<b>Outline Overlap:</b> 8%

### 3.2.1 Build Surface

Most desktop FFF 3D printers have a build surface or print bed consisting of glass, aluminum, or both. Glass provides a smooth flat surface that resists scratches and thermal expansion while aluminum provides great heat conduction and capacity which can be important for heated build surfaces [57], [62]. Providing a heated build surface becomes important in being able to successfully print with minimal warping. By having the build plate temperature just below the glass transition temperature of the print material, the adhesive capabilities are greatly increased [63]–[65]. This is likely due to the reduction of shear stress between the print material and print surface. While cooling down from its extrudate’s exit temperature, thermoplastics will shrink relative to its thermal expansion coefficient. This extruded plastic will stay in a molten like state up until it reaches its glass transition temperature in which the plastic will harden. Any shrinkage before the glass transition point will cause minimal if any stress due to its inability to hold a physical form. However, once the thermoplastic hardens, shear stress forms at the print surface interface due to differences in thermal expansion. If the first few layers are not held at temperatures just after their glass transition point, this shear force will greatly reduce or eliminate adhesion strength to the build surface.

While the 3DP 300 printer has a heated glass build surface, it lacks the aluminum plate that helps distribute and hold heat. This results in poor thermal distribution with an estimated thermal gradient of 15 °C between the build surface center and the sides when heated to 60 °C. Additionally, any air movement created by the cooling fans within proximity to the glass results in rapid cooling of its surface. These issues cause adhesion problems due to reasons explained earlier. When a 3D Platform distributor was asked why there was not an aluminum build plate option available, they stated that 3D Platform were experiencing build surface leveling issues in their tests [66]. Aluminum’s relatively large thermal expansion properties causes plates to bulge,



curve, and buckle from thermal gradients and/or internal stresses. This deformation is minimal in smaller scale printers mentioned earlier but can be very problematic in large-scale printers.

To allow successful prints, care was taken to obtain the highest initial adhesion possible. As agreed amongst the 3D printing community, the first print layer is the most important aspect of print bed adhesion [65], [67]. Adhesion is greatly compromised if the first layer does not have adequate “squish” or compression onto the build surface. A poor first layer will often lead to a failed print regardless of a heated print bed. To ensure good squish is achieved everywhere, every time, the automatic bed mesh leveling feature provided by the 3DP 300 printer was used before every print while the print bed was heated to print temperature. This mesh leveling feature measures the relative height of the print bed in a 21 x 21 grid to generate a height map of the build surface. The 3DP 300 printer then uses this height map to adjust its z-axis within a 50  $\mu\text{m}$  resolution to maintain a constant height from the build surface [21]. Additionally, the babystepping feature was used while the first layer was printed. This enables small resolution adjustments to the nozzle height in real time, therefore allowing the user to ensure an appropriate amount of squish is achieved [20].

Several print parameters were also modified to maximize adhesion. First, the cooling fan profile was adjusted such that it would exponentially ramp up from 0 to 60% power over the first 80 print layers. This helps prevent the fans from significantly cooling the print bed when they are in proximity to the surface. For large prints where there is adequate cooling time between layers, the cooling fans were disabled all together. A brim was also implemented for every print. A brim consists of extruding multiple first-layer outlines of the print’s perimeter, visually similar to the brim of a sun hat, which increases adhesion by resisting lifting forces at the print edges [65], [67]–[69]. This not only helps increase adhesion, but also reduces the ability for cooling fans and drafts to affect the glass temperature within proximity to the print.

### **3.2.2 Hotend**

The 3DP’s HFE 300 hotend is advertised to be capable of printing at a mass flow rate of 0.32 kg/hr [20], [21]. When considering PLA’s density shown in Table 2.2, that equates to a volumetric flow rate of 68.38  $\text{mm}^3/\text{s}$ . While the print parameters shown in Table 3.1 suggest a volumetric flow rate of 60  $\text{mm}^3/\text{s}$ , PLA prints have been successfully printed at upwards of 150 mm/s resulting in a flow rate of 90  $\text{mm}^3/\text{s}$  or 0.42 kg/hr. To put this in perspective, 3D Platform

provides a print time breakdown for a variety of prints comparing the HFE 300 hotend with popular high-quality desktop 3D printer hotends such as E3D's V6 and Volcano models. This data shows that the HFE 300 hotend can complete a print on average 702% faster than the V6 and 310% faster than the Volcano [21]. As illustrated in Figure 3.1, the size of a hotend's heat chamber significantly effects its flow rate capabilities. A larger heat chamber would allow faster filament feed rates while still maintaining the equivalent heat transfer time necessary to bring the thermoplastic up to extrude temperatures. While increasing the heat chamber of a hotend typically increases flow rates, it does so at the cost of increased oozing and reduced feed rate to flow rate responsiveness.

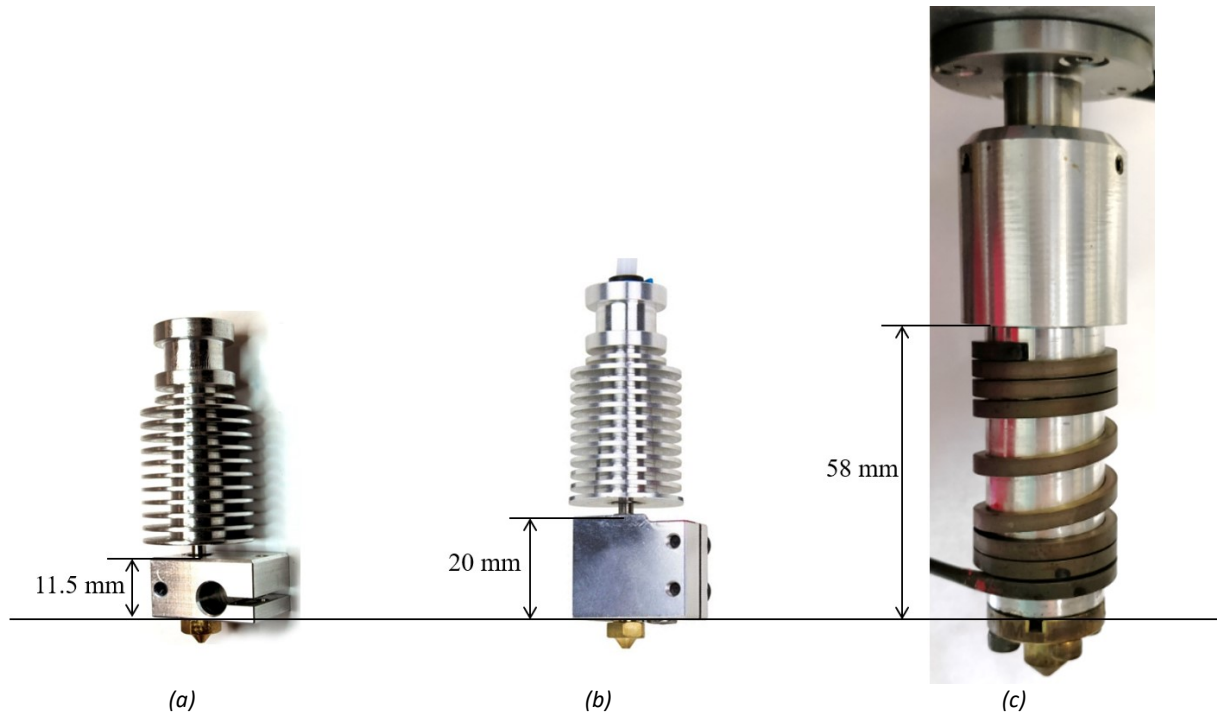


Figure 3.1: Annotated images comparing the approximate lengths of the heat chambers within E3D's V6 (a), E3D's Volcano (b), and 3D Platform's HFE 300 (c) hotends. Images of the V6 and Volcano hotends were sourced from [70] and [71] respectively with permission.

Oozing is the act of thermoplastic unintentionally flowing out of the hotend. This can create stringing and/or blobs on the surface of the print during travel movements where the hotend is moving to its next extrusion starting point. The act of oozing is inevitable; however, stringing, blobs, and other imperfections caused by oozing can typically be avoided by adjusting retraction settings within the print parameters of the slicer [72]–[74]. A Retraction is the act of reverse extruding a short distance before the start of a travel movement. The theory is that by pulling back the filament, negative pressure is formed in the heat chamber for a brief period. This then pulls back the molten thermoplastic just enough such that oozing does not exit the nozzle before the

hotend can reach the end of its travel movement. Ideally, the retraction distance and retraction speed are set large enough to avoid stringing or blobs but not too large as to cause separation between the solid and molten material contained within the heat chamber or introduce air pockets into the heat chamber.

Desktop FFF printers typically have nozzles between 0.35 mm and 0.5 mm in diameter [7], [57]. This, along with their relatively small heat chambers containing minimal molten plastic weight, result in larger ooze resistance than that of large-scale hotends such as the HFE 300. While retractions can typically solve oozing issues on desktop 3D printers, the large-scale of the HFE 300 hotend accelerates oozing to the point where additional print parameters must be considered. To avoid stringing, retractions were enabled with a distance of 2.00 mm and a speed of 2800 mm/min. This allows enough backflow as to break the thermoplastic connection at the print but is unable to prevent oozing from occurring during the travel movements. To prevent the ooze from leaving blobs on the sides of the print, the Simplify3D feature labeled ‘avoid crossing outline for travel movements’ was enabled with a detour factor of 3. This prevents the nozzle from crossing the part perimeter if a travel path exists that is less than 300% the length of the default linear travel movement. This does not stop oozing, but rather smears the leaking thermoplastic across print layer. This then leads to issues where the hotend under-extrudes for a short period after a travel movement due to the reduced volume of thermoplastic within the hotend. Due to the oozed volume being relative to the travel movement, a few print parameters were modified. First, the extra restart distance within the retraction settings was set to 0.10 mm. This will therefore result in 2.10 mm of extruded filament at the start of each extrusion that follows a retraction, with the extra 0.10 mm used to ensure the nozzle is primed. Additional print parameters include setting the start point to ‘optimize start points for fastest printing speeds’ to minimize travel movements and setting the ‘minimum travel for retraction’ to 4.00 mm to avoid excessive extrusions after short travels.

Feed rate to flow rate responsiveness was also found to be negatively affected with increasing heat chamber size. A 3D printer extrudes material by feeding filament into the hotend’s heat chamber using a stepper motor. This filament then melts and is forced out through the nozzle from the pressure created within the heat chamber. Due to this relationship between feed rate, pressure, and extrusion rate, there exists a delay between a change in feed rate and a change in

extrusion rate. This delay in response causes over and under extrusion for a short time whenever there is a change in feed rate such as during accelerations and changes in extrusion width. This effect is negligible for small hotends existing on desktop 3D printers but can be significant on large-scale hotends due to the larger heat chamber volume requiring a greater amount of material to raise or lower its pressure.

Reducing circumstances where feed rate is changed was found to significantly reduce issues caused by poor responsiveness. In terms of acceleration, that means setting the highest acceleration permissible to reduce slowdown time taken whenever the printer hotend changed directions. This is, and was, defined directly into the RepRap firmware of the 3DP 300 printer. For gap fills, that means setting the minimum and maximum printing widths under single extrusions to 100%. This will tell the slicer to dismiss filling in small gaps within 100% infills if any variation in extrusion width is required. Unlike Cura, Simplify3D did not have the option to adjust print speeds for changes in extrusion widths as of writing this thesis. This feature would be ideal as it allows fully printing a 100% infill layer without needing to change the feed rate. The only change in feed rates which were deemed necessary were those caused by reducing the first layer print speed to 50% to ensure good adhesion, perimeter speed to 50% to increase surface quality, and 100% infill print speed to 80% to reduce print disturbances caused by the nozzle-print impacts. All other pressure changes result from oozing travel movements. As discussed earlier, travel movement distances were minimized in the event where the print layer perimeter is not crossed. In the situations where travel distance is increased to keep within the layer perimeter, the retraction's extra restart distance of 0.10 mm help to recover the heat chamber's steady state extrusion pressure.

### **3.2.3 Overall Mass**

The last consideration in printing with the 3DP 300 printer is its overall mass. To get accurate clean print surfaces, it is best to keep the moving weight to a minimum. Some desktop printers with heavy moving components such as a linear actuated build surface can cause ringing. Ringing, also known as ghosting, is the ripple effect seen on print surfaces where a sudden change in direction occurs. This is typically caused by play within the mechanical system or induced vibrations on the frame caused by sudden accelerations. Fixes typically include reducing print speed, acceleration, and ensuring a sturdy frame [75], [76].

Obviously, the moving mass of a large-scale printer will weigh more than a typical desktop sized printer. When considering that the 3DP 300's overall weight is approximately 246 kg [20], [21], the mass being accelerated and decelerated during the printing process can be significantly large. Most desktop 3D printers use stepper motors to drive the printer's movement [57], which are capable of providing large amounts of torque at slow rotational speeds. However, 3D Platform uses their SurePrint servo motors [20], [21]. This technology improved over their previous stepper motor system by increasing print speed and accuracy through the use of StepServo<sup>TM</sup> closed loop stepper technology [77]. Benefits include 50% faster print times due to an 85% increase in torque, and 50% less heat and 67% less power consumption due to better power management from the closed-loop system [78]–[80]. Even with this superior technology, rippling still occurs regularly due to the large mass of the HFE 300 extruders and the long aluminum rails they translate on.

Ringling is likely created by a mixture of two sources. The first source is frame deflections. With the larger spans required in large-scale 3D printers, small material deflections or mechanical clearances are amplified considerably at the nozzle. This can include elastic deformation in the aluminum extrusions, clearances in various bearings, lead screw whip, etc. Under sharp accelerations, these deflections/clearances can jostle back and forth causing ringling. The other source is likely the SurePrint motors themselves. In addition to the greater torque, fast print speeds are permissible due to the increase screw lead of 25 mm [81]. When considering that a typical stepper motor has 200 steps per revolution, we can expect a resolution of 0.125 mm in the  $x$  and  $y$  axes. The stated layer resolution of the 3DP 300 printer is 50  $\mu\text{m}$  [20], [21], which can be explained through the use of half stepping. While half-stepping doubles the resolution, it comes at a cost of reduced holding torque. A 3DP manual for an earlier printer also having SurePrint motors stated that a resolution of 100  $\mu\text{m}$  was achievable with a finely tuned printer equipped with a smaller extruder and a 0.4 mm nozzle [82]. Considering that the HFE 300 hotend weighs significantly more than the Volcano, carries a water-cooled loop, and uses stock acceleration settings from 3DP; the resolution obtained on the 3DP 300 printer is likely significantly less. In this case, the resolution is limited by the SurePrint motor's ability to redirect the large mass during printing and not by the physical step limitation of the system. Sharp accelerations/decelerations would therefore result in dimensional inaccuracies in the form of ringling.

Little can be done in print parameters to minimize ringing other than reducing print speed and accelerations. As mentioned earlier, reducing accelerations result in other issues caused by oozing. Reducing speed could be considered with a larger nozzle to keep the benefits of large flow rates; however, the 1 mm nozzle was the largest available for this demonstration. While tinkering with the accelerations or any PID systems utilized by the closed-loop SurePrint steppers could be beneficial, it was not attempted due to lack of experience and knowledge on the subject.

## CHAPTER 4. PRODUCT CREATION

The chair's G-code was created using Simplify3D 4.1.2 [58] with the CAD model created in chapter 2.2 and print parameters discussed in chapter 3.2. The dimensional parameters involving the internal geometry discussed in chapter 2.3 were implemented using Simplify3D's processes feature. This feature provides the ability to divide the print layers into multiple processes in which the print parameters of each process can be individually assigned. Using this, 5 processes were created to represent the Rail Fill Widths, Center Fill Width, and 10% infill hollow sections. These processes are illustrated in Figure 4.1 using Simplify3D's G-code graphical interface. The processes labeled Right Rail Fill Width, Center Fill Width, and Left Rail Fill Width were defined with 100% infill and the processes labeled Right Hollow and Left Hollow were defined with 10% infill. Also included in Figure 4.1 is the estimated print time and material usage provided by Simplify3D.

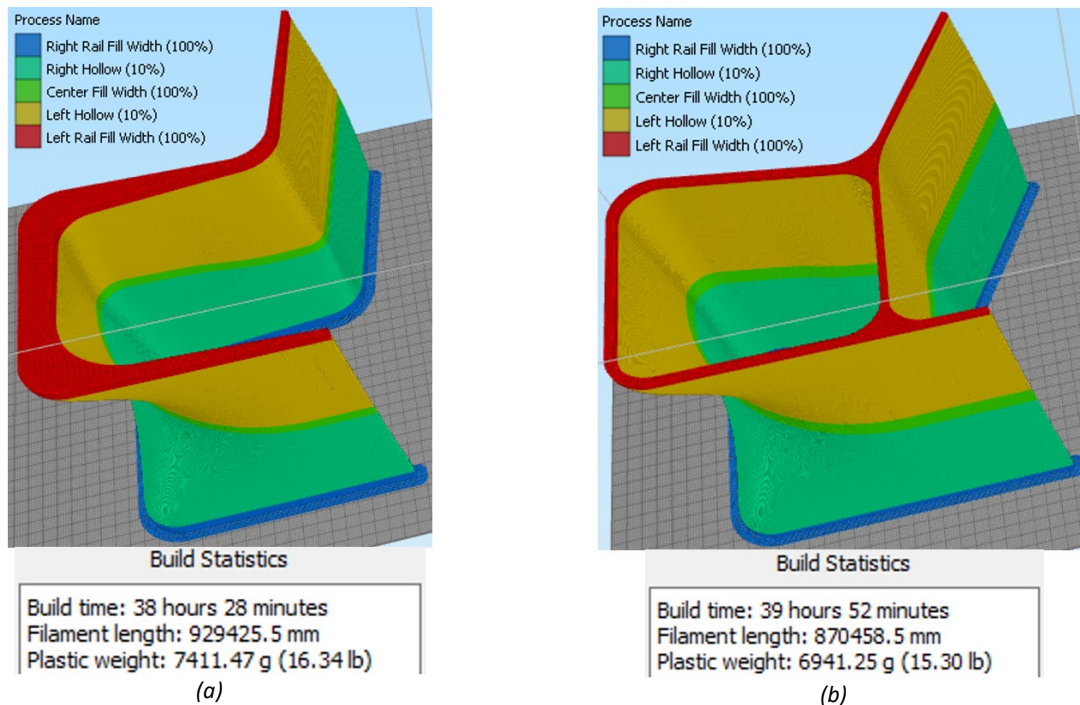


Figure 4.1: Images displaying Simplify3D's visual G-code print representation and estimated print time and material requirements for the cantilever chair (a) and the braced-cantilever chair (b) designs.

Although the braced-cantilever chair model uses nearly 0.5 kg less PLA compared to the cantilever chair model, its print time is over an hour longer. A deeper analysis reveals that the

average mass flow rate is 0.193 kg/h and 0.174 kg/h for the cantilever and braced-cantilever chair designs, respectively. The overall slower flow rate of the braced-cantilever chair is likely caused by interactions between the print parameters and the chair's geometrical differences. The cantilever chair has more layers consisting of 100% infill while the braced-cantilever chair has more perimeter lengths due to its brace. With the print parameters discussed in chapter 3.2.2, the print speed of 100% infills and perimeters were set to 80% and 50% of the defaulted print speed respectively. This results in the braced-cantilever chair having an overall lower flow rate compared to the cantilever chair design. Additionally, the internal perimeter existing on every print layer of the braced-cantilever model results in an additional travel movement where the hotend transfers to the internal perimeter after completing the external perimeter. These relative reductions in print speed cause the braced-cantilever chair to have a longer print time than the cantilever chair even though it requires less material. Regardless of the 3.64% increase in print time, the braced-cantilever chair design was chosen to be printed due to its lower material and fatigue requirements.

Approximately fifteen hours after commencing the print on the 3DP 300 printer, the process was aborted due to adhesion failure. This failure was estimated to occur 4 hours into the print. It became clear that factors other than print parameters must also be considered to successfully print large-scale objects. These factors include adhesion, warping, and filament storage. The following subchapters go through how each of these concerns were realized, the actions taken, and the results after implementation.

## **4.1 Adhesion**

It is common for desktop FFF printers to print PLA to bare glass or aluminum with good adhesion performance [62]. Originally, printing PLA directly onto the glass print bed was sufficient thanks to the precautions and print parameters discussed in chapter 3.2.1. However, the first attempt at printing the chair showed that additional adhesion strength is required for large-scale prints which approach the 3DP 300's dimensional build surface limits. Additionally, shortly after the chair print failed, glass chipping occurred in which several large chunks of glass roughly the size of an individual's thumb were pulled up from the build surface during removal of several large surface area parts. This chipping is believed to occur from the sudden release of shear stress during print removal and may become more probable as glass ages from heat cycling. Strong adhesion performance between glass and PLA have been shown to cause glass chipping in desktop



3D printers as well [63], with the probability rate being constantly debated amongst the 3D printing community.

Therefore, an experiment was designed and performed to determine an appropriate adhesive substance in which solved both the adhesive and chipping issues. The ideal adhesive would improve the adhesion between PLA and glass when the build surface is held at print temperature but provide little to no adhesion once the build surface cools to room temperature. This would both keep the chair adhered when printing and release the chair once cooled to prevent chipping.

#### **4.1.1 Adhesion Considerations**

There are many different methods used through the 3D printing community to improve adhesive performance for a variety of materials. Solutions such as blue painters' tape, Kapton tape, white glue stick, hairspray, and sugar water are popular solutions [7], [20], [83]. Due to the 3DP 300's build surface being fixed to the printer and relatively large, economic adhesion methods focusing on fast and easy application were desired. Therefore, three substances were tested for their PLA-glass adhesive performance, those being hairspray, sugar water, and salt water. The Aqua Net® Unscented Extra Super Hold hairspray [84] was chosen due to its preference throughout the 3D printing community [20], [83]; however, any hairspray containing both VA/Crotonates/Vinyl Neodecanoate Copolymer and Acrylates Copolymer should perform similarly [85]. Sugar water and salt water were considered primarily for their cheap value and easy accessibility with sugar water being another preference throughout the 3D printing community for PLA [83], [86], and salt water being displayed to have excellent holding and releasing properties in a document created by a 3D printing enthusiast [87]. For this experiment, Redpath® Sugar Ltd granulated sugar [88] and Windsor® Salt Ltd. iodized table salt [89] were used specifically due to their availability.

While application of hairspray is simply point and spray, that of salt water and sugar water were more complex. First, the concentrations of each substance were determined. Several test concentrations of sugar and saltwater were created using a 25 mL pipet, a gram scale, and tap water. These concentrations were then applied to the glass print bed while heated to 60 °C using a piece of paper towel by continuously wiping in 0 and 90° directions until all water had evaporated.

This process allowed for an even distribution while preventing the substances from drying in large droplets on the glass surface.

Sugar water was initially tested at 100 g/L as that was what had been previously used for desktop 3D printers in the department. 200 g/L was also attempted to see the effects of sugar concentration. When properly applied, the sugar water leaves behind a hard-rough coating that does not feel sticky when brushed lightly with your fingers. Both test results are illustrated in Figure 4.2. Although one is double the concentration of the other, there was no significant difference between the two coatings other than the time required before all water had evaporated. The 100 g/L concentration was chosen due to the additional time it provides when being applied evenly across the large build surface.

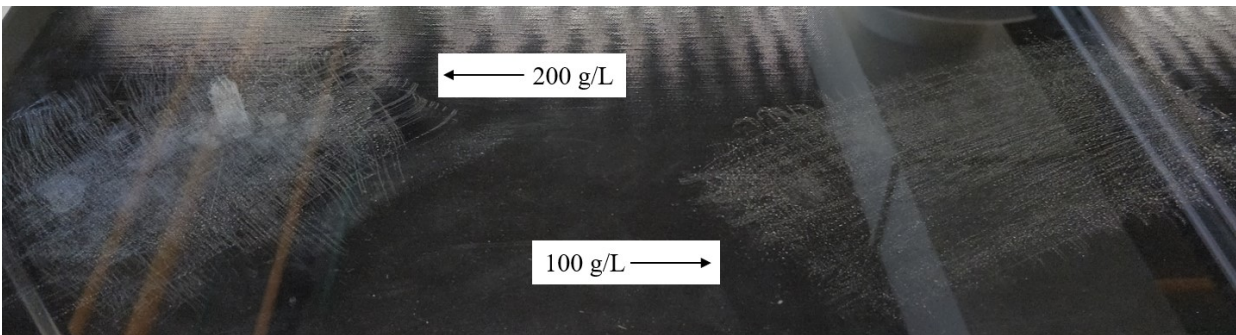


*Figure 4.2: Image displaying sugar water application tests using 200 g/L and 100 g/L concentrations.*

As described by [87], the salt water coating should leave a very fine mist of salt that is nearly invisible to the unaided eye. To obtain this coating, salt water was initially tested at 200 g/L but was sequentially lowered to 100, 60, 20, and 10 g/L. The results of these concentrations can be seen in Figure 4.3, from which the saltwater concentration of 10 g/L was deemed acceptable to use.

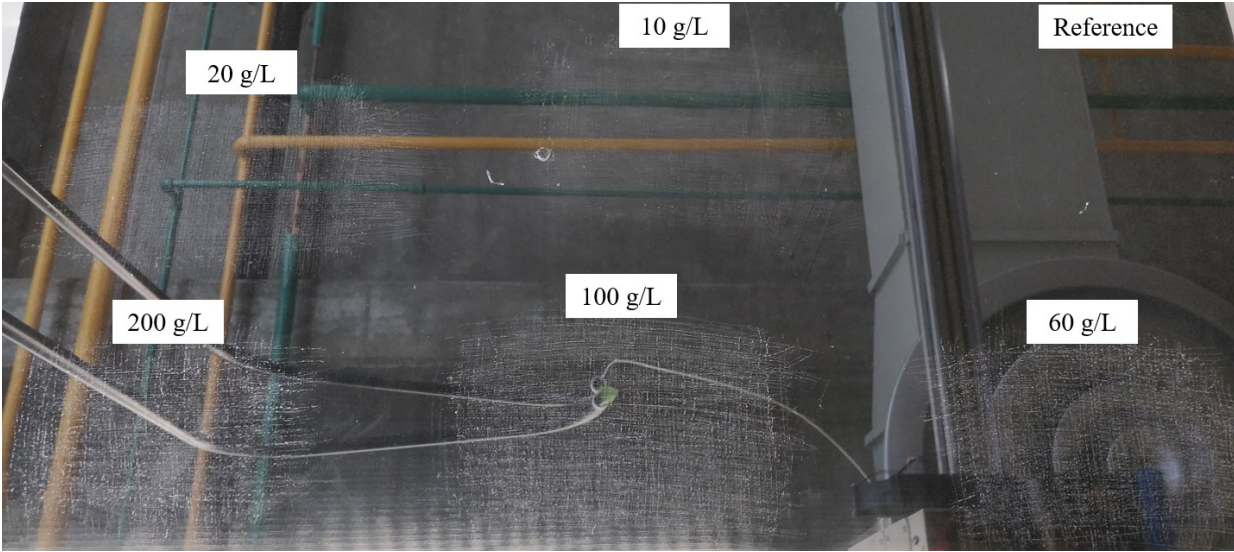


Figure 4.3: Image displaying saltwater application tests using 200 g/L, 100 g/L, 60 g/L, 20 g/L, and 10 g/L concentrations.

#### 4.1.2 Adhesion Experimental Design

To test the relative adhesive performance of each substance, a simple cantilever tower design was created. This design consists of printing a rectangular tower in which a rod is fed through two holes located at the top. This rod serves to hold calibration weights on its furthest end in which the maximum weight applied before the 3d printed part releases from the build surface was recorded.

All tower dimensions are illustrated in Figure 4.4, with orthogonal drawings displayed in Appendix B. The 25 mm base was chosen as it seemed appropriate when considering the typical size of objects printed and the amount of material that would be consumed. The 5 mm radii along the vertical edges were applied to reduce warpage, and the rod was placed 180 mm above the print bed to allow two calibration weights to hang in series. Thanks to the insignificant force magnitude being applied to the tower, it was printed with a single wall thickness of 1 mm to both minimize strains caused by warping and minimize print material.

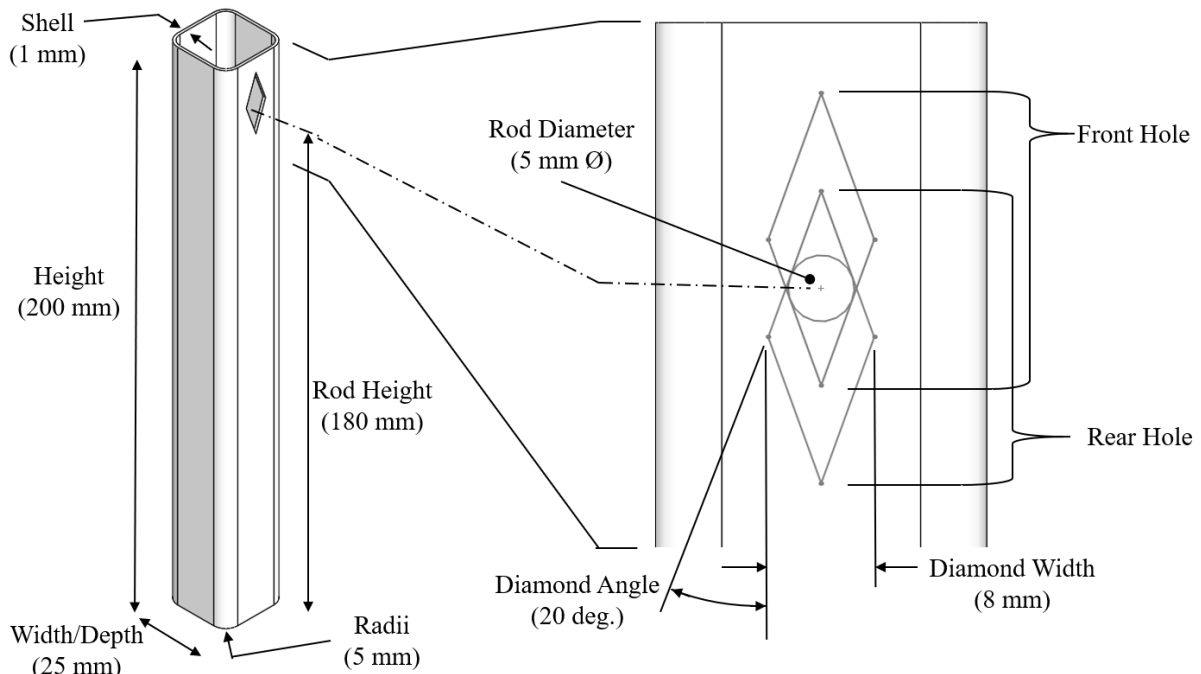


Figure 4.4: Annotated illustrations displaying the adhesion test tower dimensions and features.

An important feature of the tower design is the offset diamond holes seen in Figure 4.4 which allows the rod to be inserted into each tower without disturbing the print. This is possible due to the clearances achieved when inserting the rod at a downward angle. Adding the weights after the rod has been positioned then levels the rod horizontally due to the supporting surfaces on the two holes.

To avoid any potential build surface temperature inconsistencies, the towers were printed with the cooling fans disabled. This then presents the issue of warping due to inadequate cooling between each print layer. To avoid this, the towers were printed in sets of six, layer by layer, such that each tower layer was given a short time to cool naturally while the layer was sequentially completed on the other towers.

#### 4.1.3 Adhesion Experimental Procedure

Four tests were completed: one for clean glass, hairspray, sugar water, and salt water. Before each test, the glass build surface was thoroughly washed using tap water and a dish cloth. Additionally, the printer completed a mesh based auto leveling sequence while the print bed was heated to ensure each test had equivalent first layer squish. Just before starting the print, the adhesive layer was evenly applied to the print bed. In the case of the salt and sugar water, the chosen concentrations were sprayed over the surface using a herbicide sprayer before being

repeatedly wiped with a paper towel in a similar manner to the concentration tests completed in chapter 4.1.1.

Once prepared, six towers were printed at once with adequate distance between them as illustrated in Figure 4.5a. The ending G-code for the print had been altered such that the build surface temperature remained at 60 °C after the print was completed. At that point, the front three towers were each tested by inserting the rod and adding weight to the end in 50 g increments. This test is illustrated in Figure 4.5b, in which twenty seconds were allowed to pass between each incremental weight increase. Caution was taken to ensure each test placed the weights at equal distances from the tower. This was accomplished by placing tape on the pole to indicate how far the pole is set into the tower and the exact placement to hang the weights. As this is purely a relative test, the exact distance magnitude was not important. After the max weight for the first three towers were recorded, the heated build surface was disabled and allowed to cool to 25 °C before the process was repeated for the last three towers. This process was repeated for each adhesive being tested, including bare glass.

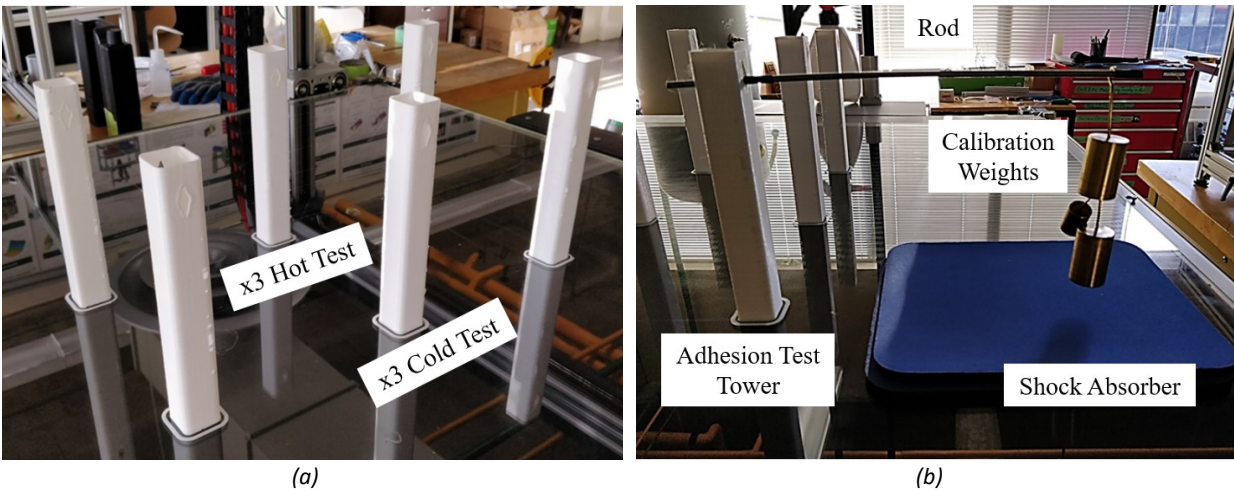


Figure 4.5: Images displaying the completed 6 adhesion test tower print (a) and an adhesion test tower undergoing the adhesion test procedure (b) for clean glass.

#### 4.1.4 Adhesion Results

The results can be seen the Table 4.1. From the data, Test 3's magnitude for glass would likely be much closer to the previous two tests due to the weights used on the Test 2 dropping and rattling on the glass close to the third test tower. This rattle likely released some of the part from the glass resulting in the considerably lower score of 150 g compared to the previous 600 g and 550 g. Also, many of the towers released from the print surface with a slight touch when the build

surface had cooled to 25 °C, typically occurring while positioning the pole on to the tower. While these towers were not fully released when the test procedure initiated, they required much less force than the 50 g weight and were therefore given a half score of 25 g. Those that remained adhered until the 50 g weight was placed were given the full score of 50 g while those that were fully released initially were given a score of 0.

*Table 4.1: Bed adhesion test results for glass, hairspray, sugar water, and salt water at 60 °C and 25 °C print bed temperatures.*

	<b>Glass</b>		<b>Hairspray</b>		<b>Sugar Water</b>		<b>Salt Water</b>	
	<b>60 °C</b>	<b>25 °C</b>	<b>60 °C</b>	<b>25 °C</b>	<b>60 °C</b>	<b>25 °C</b>	<b>60 °C</b>	<b>25 °C</b>
<b>Test 1:</b>	600 g	25 g	750 g	25 g	850 g	0 g	600 g	25 g
<b>Test 2:</b>	550 g	50 g	750 g	100 g	1050 g	25 g	900 g	25 g
<b>Test 3:</b>	150 g	25 g	750 g	0 g	900 g	25 g	450 g	50 g

The average weight magnitudes for each adhesive and their standard deviations are clearly shown in Figure 4.6, in which the standard deviations were determined using the STDEV.P function within Excel® [90]. From this we can see that all adhesives performed better than glass, even if Test 3 for glass was excluded. Hairspray performed well and had excellent repeatability, likely due to the ease in which an even layer can be applied from the compressed air can. Sugar water performed the best of the three with slight variation while salt water performed the worse due to its significant fluctuation. This variation is likely due to the difficulty in spreading an even layer of salt mist over the large build surface. While salt water did achieve 900 g score on Test 2, the specific conditions in which the salt must be applied is unpractical for the large build surface area. Not only did sugar water perform the best while the build surface was heated, it also performed the best once the build surface had cooled to room temperature. Sugar water had the most promising 25 °C print bed temperature results in that prints would release from the print bed freely while hairspray performed the worst by keeping them adhered the most.

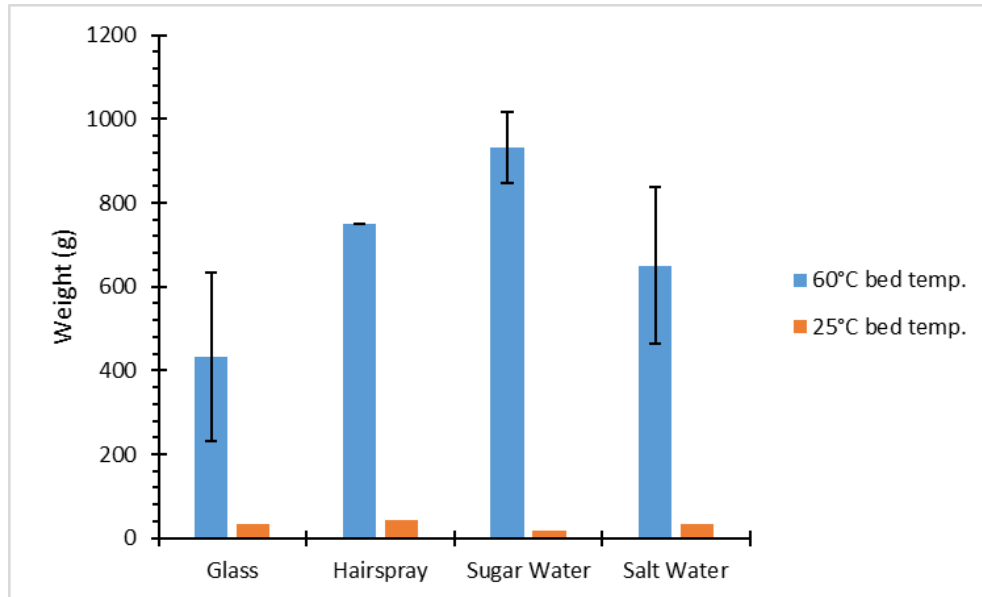


Figure 4.6: Bar graph displaying the adhesion test results for glass, hairspray, sugar water, and salt water at 60 °C and 25 °C print bed temperatures.

Of the three adhesives tested, sugar water was deemed the better choice for PLA prints on a glass surface. Sugar water was shown to outperform the others not only in its PLA print adhesive performance, but also its ability to release the print from the glass build surface when cooled to room temperature.

#### 4.1.5 Adhesion Implementation

Printing of the braced-cantilever chair on the 3DP 300 printer was attempted again, this time using sugar water to increase the adhesion performance between PLA and the glass build surface. Additionally, the brim was substantially increased to obtain greater surface contact. This time, the print completed successfully; however, the surface quality was far from ideal.

As seen in Figure 4.7, the brim struggled to hold the chair down during printing. In Figure 4.7a, The brim broke from the edge of the print allowing it to gradually warp upwards causing over-extruded layers. Similar over-extruded layers are seen in Figure 4.7b but instead of the brim breaking, it gradually lifted off the print surface. This layering pattern is seen all over the chair. Due to typical 3D printers operating blind, simply performing as the G-code directs them, the printer cannot adjust for smaller layer heights in instances where the print warps towards the nozzle. This causes the printer to extrude for the full layer height even if print's previous layer is pressed flush against the nozzle, therefore causing inconsistent layers on the print surface.



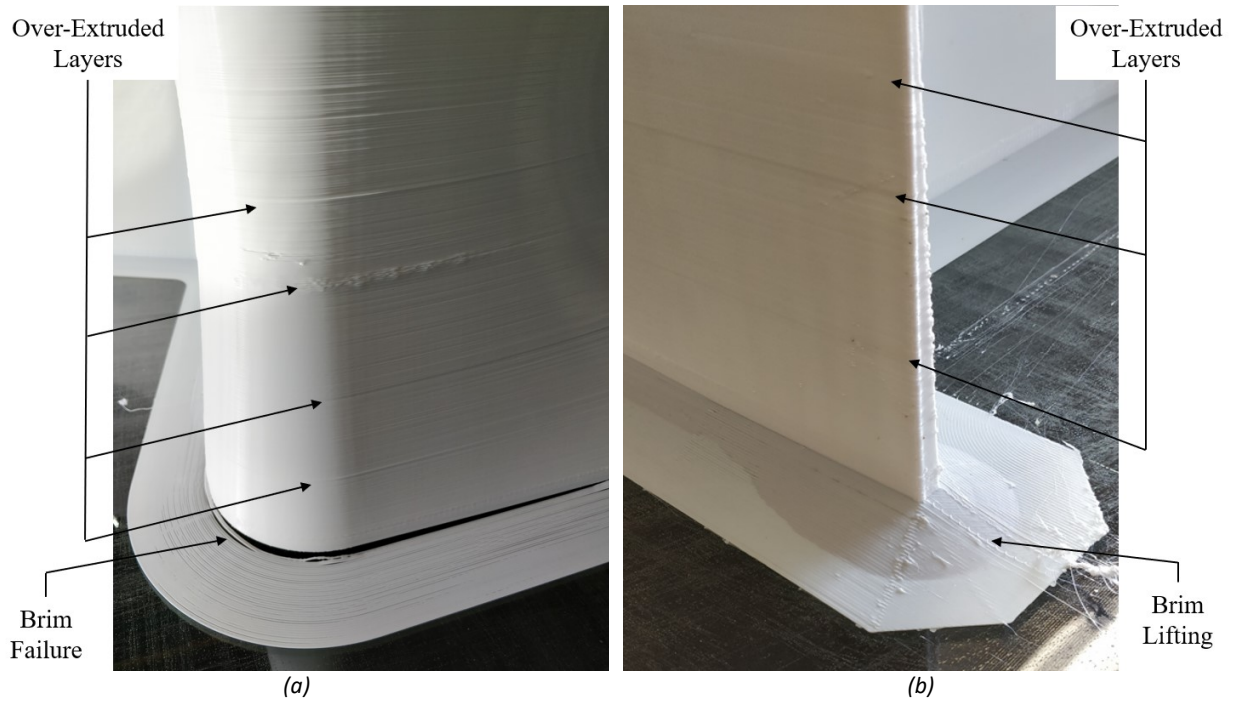


Figure 4.7: Annotated images of the braced-cantilever chair's adhesion performance with the use of sugar water and a large brim width with (a) displaying the front seating radius and (b) showing the rear floor lip.

Warping of the chair was considered before the print was commenced. To help prevent print failure in the instance where the chair was to warp, the secondary hotend was set to a temperature of 230 °C. This was done to reduce the physical impacts between the secondary nozzle and the print by allowing the nozzle to melt through the PLA. While this seemed to have worked, it left blobs on the part surface as shown in Figure 4.8. Blobbing is a common occurrence with extruder oozing, but in this case, it was caused by the second nozzle picking up molten PLA and depositing it whenever it crossed the chair layer's perimeter.



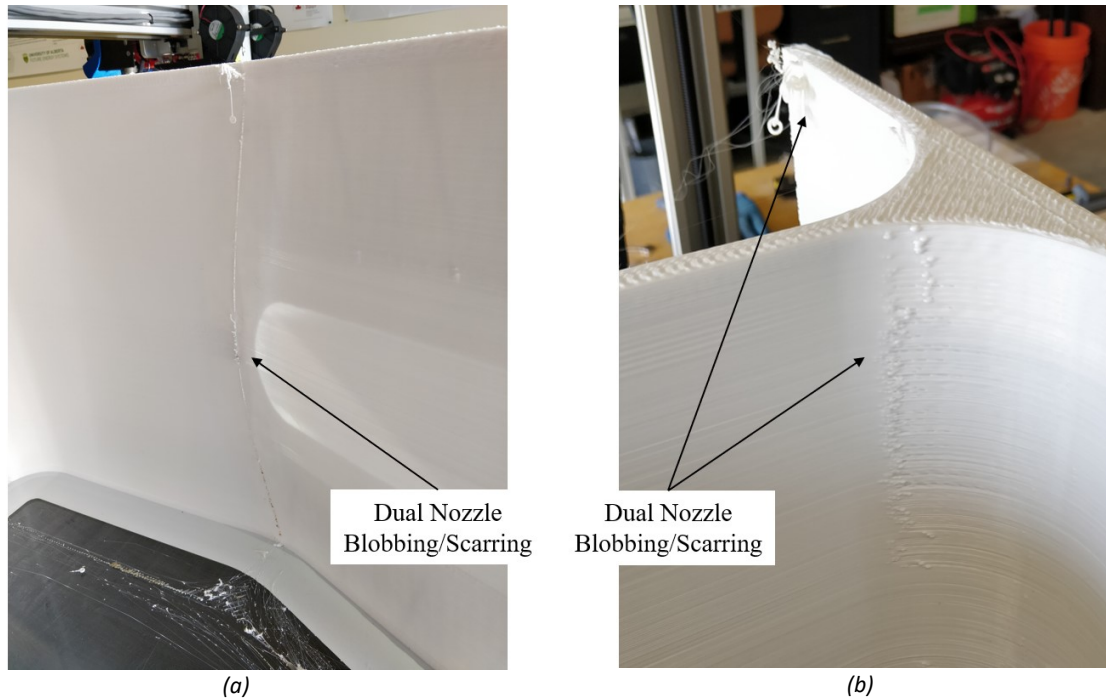
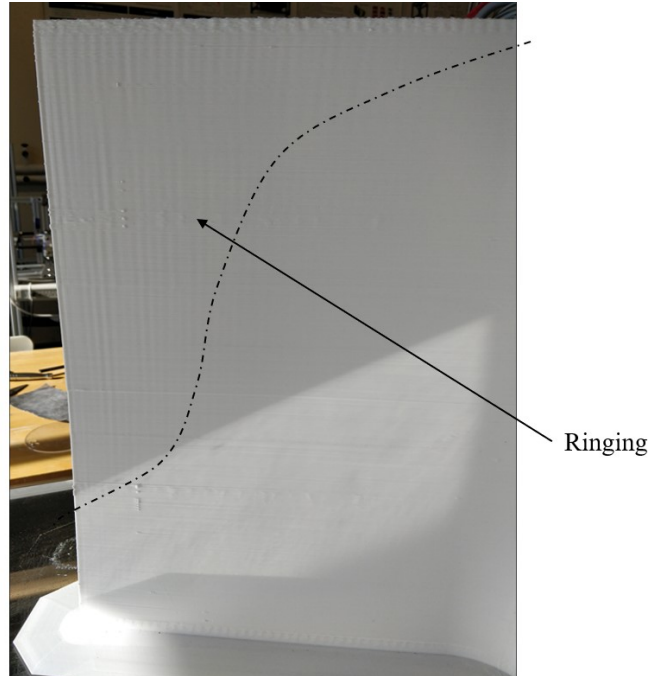


Figure 4.8: Annotated images of the blobbing effect caused by having the secondary hotend at 230 °C during printing of the braced-cantilever chair in which (a) is at the outer upper brace surface and (b) is at the inner lower brace surface.

The final print surface imperfection observed was severe ringing occurring on the back rest illustrated in Figure 4.9. As discussed in chapter 3.2.3, ringing is typically caused by acceleration induced vibrations in the frame and/or drive system. The ringing on the chair can be seen to start approximately where the first signs of warpage occurs and grows exponentially as the print becomes taller. This observation seems to suggest that the chair started oscillating with respect to the printer once the brim failed to keep the backrest secured against the build surface. The 3DP 300's frame visually oscillates upon its workbench during printing due to the forces involved in accelerating the relatively heavy HFE 300 extruders. However, ringing does not occur to this extent on prints that are securely held by the build surface. With the brim lifting and allowing movement, the backrest can oscillate out of sync with the printer thereby causing the observed ringing. It is unclear how much of the exponential ringing growth could be avoided with the absence of warpage. It is highly probable that ringing will still occur due the compromise in both frame and chair rigidity as the printing height increases. However, the overall effect is likely much lower when the chair is held securely throughout the print process and no forces are exerted directly by the nozzle.



*Figure 4.9: Annotated image of the ringing effect occurring on the front surface of the back rest during printing of the braced-cantilever chair.*

## 4.2 Warping

While the second attempt printed successfully, there exists severe warping issues that not only cause surface imperfections but also reduce print repeatability and reliability. Warping occurs due to similar reasons discussed in chapter 3.2.1, in which the layered thermoplastic introduces shear stress as it cools and shrinks. While a heated build surface ensures uniform temperatures on the first few layers, later layers are free to cool and will therefore create a temperature gradient. This un-uniform cooling creates internal stresses that cause the print to deform and curl upwards resulting in the effects seen previously with the chair print [91].

Common warp fixes use the brute force method in which adhesion is increased between the print and the build surface. These included methods discussed in chapters 3.2.1 and 4.1.1 such as using a heated build platform, brims, and adhesives. More direct warp fixes include printing within an enclosure [65], [92]. An enclosure helps by preventing ambient air currents from excessively cooling the print, maintaining a stable printing environment, and keeping warmth within the print proximity. For better results, a heated enclosure can be utilized [9], [93]. Having a heated enclosure allows the print environment to be maintained just below the glass transition

temperature of the print material. In doing this, the material cools just enough to solidify and is held there until the print is completed where it is then allowed to cool uniformly therefore limiting any internal stresses from distorting the print.

3D Platform does sell a compatible enclosure for the 3DP 300 printers. This enclosure is advertised to maintain an internal temperature of 40 °C with 80 °C being achievable when a forced air heater is included [94]. Due to economic limitations, an enclosure was created with inspiration from the 3DP enclosure. Other than retaining heat, several factors such as adaptability and accessibility were considered during its design.

#### **4.2.1 Enclosure Adaptability**

The 3DP 300 printer manual states that the environmental temperature should not exceed 32 °C [20]. Although an enclosure can be purchased through 3D Platform that is capable of 80 °C [94], it is unknown if parts of the printer must be replaced before it is capable of operating at those temperatures. Therefore, the enclosure was designed with the intention of fitting a heater later if it was required. Another potential modification includes an air purifying or vent system such that thermoplastics which generate harmful fumes could be printed safely. To avoid restrictions in future adaptability, the 3DP 300 printer enclosure was built from T-slot aluminum extrusions and twin-wall polycarbonate panels.

T-slot aluminum extrusions offer extensive design flexibility and customization at affordable prices without requiring manufacturing skillsets or complex machinery. These T-slot systems not only provide a variety of extrusion sizes for different strength requirements, but also include a vast library of compatible parts such as casters, hinges, brackets, linear motion methods, etc. Providers such as 80/20<sup>®</sup> Inc. [95] and McMaster-Carr<sup>®</sup> [96] provide CAD models of all their available extrusions and parts allowing anyone to virtually build their project and order the exact quantity of parts and extrusion lengths required. This allowed the design of multiple enclosure iterations such that the end design would fit the 3DP 300 with confidence and include the desired features. Specifically, 80/20's 15 series extrusions were used for the enclosure's design due to its appropriate strength and abundance of compatible parts.

Multi-walled polycarbonate panels are commonly used in greenhouses, sunroofs, and awnings due to their durability and translucency. These panels provide multiple benefits that make

them an obvious choice for the 3DP 300 enclosure. Their bulk use in industry and private sectors enable a few large sheets to be purchased at affordable prices in which they can easily be cut to shape using a utility knife. They are strong and light weight such that they can handle bumps and jabs while limiting the overall weight of the enclosure. Their hollow geometry presents insulative properties such that they can keep heat within the enclosure while being mechanically stable at temperatures up to 120 °C [97]. Lastly, they are transparent enough to spot when a print has gone awry, therefore allowing print checkups without breaking the insulative seal. Specifically, EcoFort Innovation Corp<sup>®</sup>'s [98] clear 8 mm thick twinwall polycarbonate sheets were used in the enclosure's design. These panels provided the additional benefit of fitting snugly within the 80/20's 15 series T-slot profile therefore reducing the need for additional fasteners.

#### ***4.2.2 Enclosure Accessibility***

The final enclosure iteration is shown in Figure 4.10, with orthogonal drawings displaying overall dimension seen in Appendix B. Due to the z-axis of the 3DP 300 printer raising, lowering, and traversing with the hotend, the bottom of the enclosure must be left open. Therefore, the sides are extended below the build surface to be level with the work bench in which the printer sits on. The sides were not lowered further due to the placement of the water cooling controls, filament sensors, and drawers; however, a workaround could be implemented later if required. Other than compatibility, accessibility was a big concern when designing the enclosure. Two different accessibility requirements were desired, one for quick build surface access for typical use and one for full printer access in situations where maintenance or part replacements are performed.

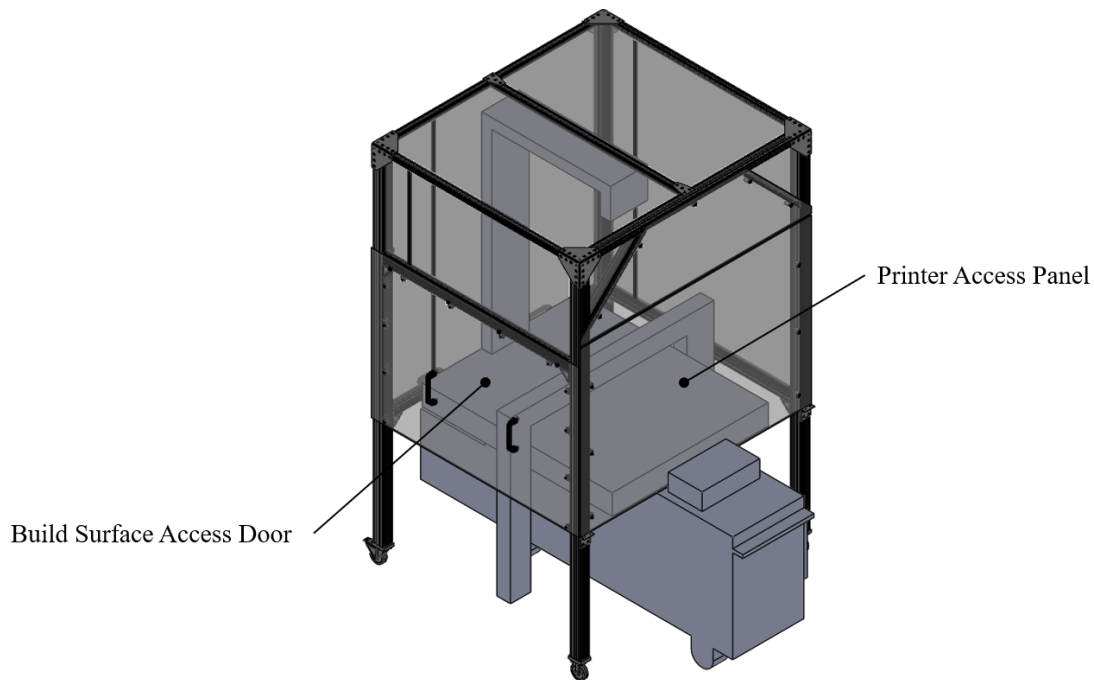


*Figure 4.10: Annotated illustration of the custom designed 3DP 300 enclosure's SOLIDWORKS CAD model.*

The enclosure features involved with the build surface access door are illustrated in Figure 4.11. This access door is meant for everyday use in which the user would prepare the build surface and remove the finished print. Three main factors were considered for its design; those being its un-limiting access, ease of access, and ability to seal. To provide the least restriction, the door was designed to span the entire width of the enclosure and reveal an opening that is 1.98 (6.5 ft) high from the ground. This grants most people the ability to comfortably enter the enclosure with minimal hassle. To allow the door to be easily removed and installed, four bolts spaced evenly along the header rail act as hanger pins. With corresponding holes along the top of the door panel, the lightweight twinwall polycarbonate panel door is easily lifted over the pins using the installed handles. Lastly, to ensure a seal is created along the enclosure frame, 12 magnet latches are installed around the inner frame perimeter. Once the door is hung over the pins, a slight press connects the metal plates installed on the door with the magnet catches installed on the frame. The magnets keep the door pressed firmly against the frame therefore limiting air from escaping the enclosure.

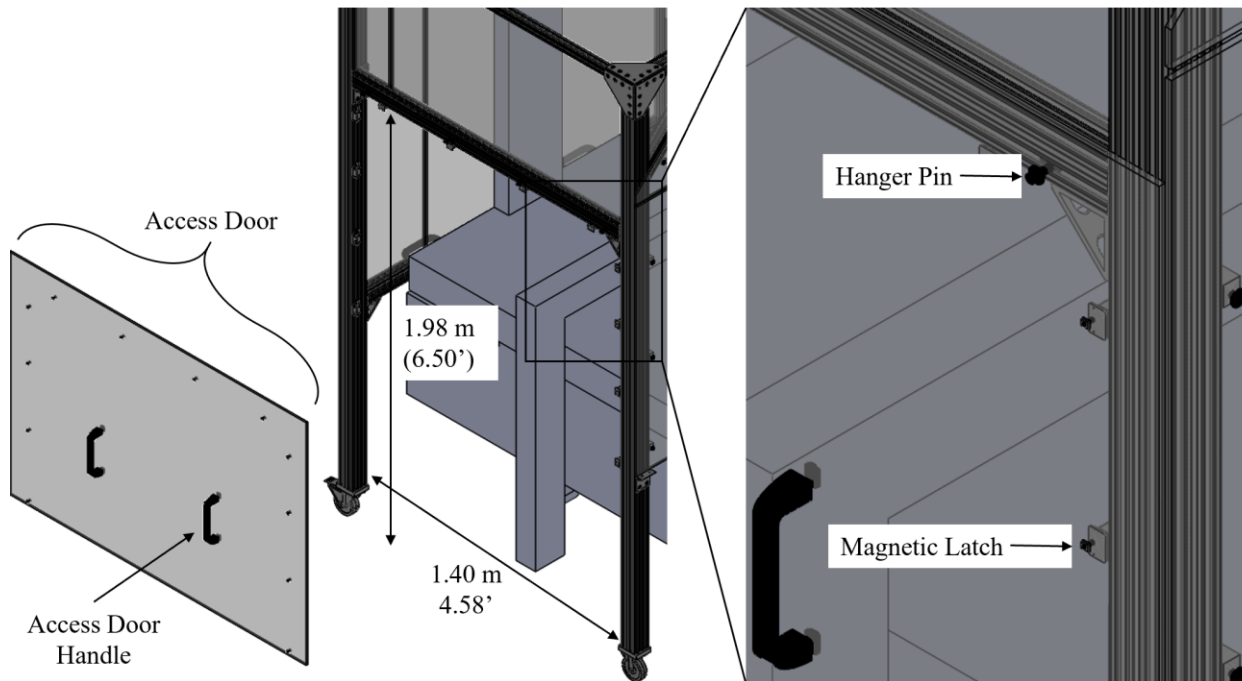


Figure 4.11: Annotated illustrations of the 3DP 300 printer's custom enclosure's build surface access door design.

The enclosure features involved with full printer access is illustrated in Figure 4.12. This access point is meant for printer repair or maintenance in which greater access is required than that which the build surface door can provide. Other than keeping the enclosure sealed, the primary factor was the ability to remove the enclosure from the printer within reasonable effort. This was enabled by having the front side of the enclosure frame fully open with 45° braces in the upper corners for structural support. With the front side consisting of only panels, the enclosure can be removed in two steps. First, the front panel is unbolted from the frame. These bolts help keep the panels flush against the enclosure frame to limit air leaks. The panel mounts in which the bolts screw into can be sunk back from the frame face if additional panel-frame force is required to hold an air seal. Once removed, the enclosure can then be pulled backwards using the handles at the rear. Unlike the workbench in which the printer sits on, the enclosure can be moved with precision due to the mixture of fixed and pivot casters with the pivot casters being at the rear closest to the handles.

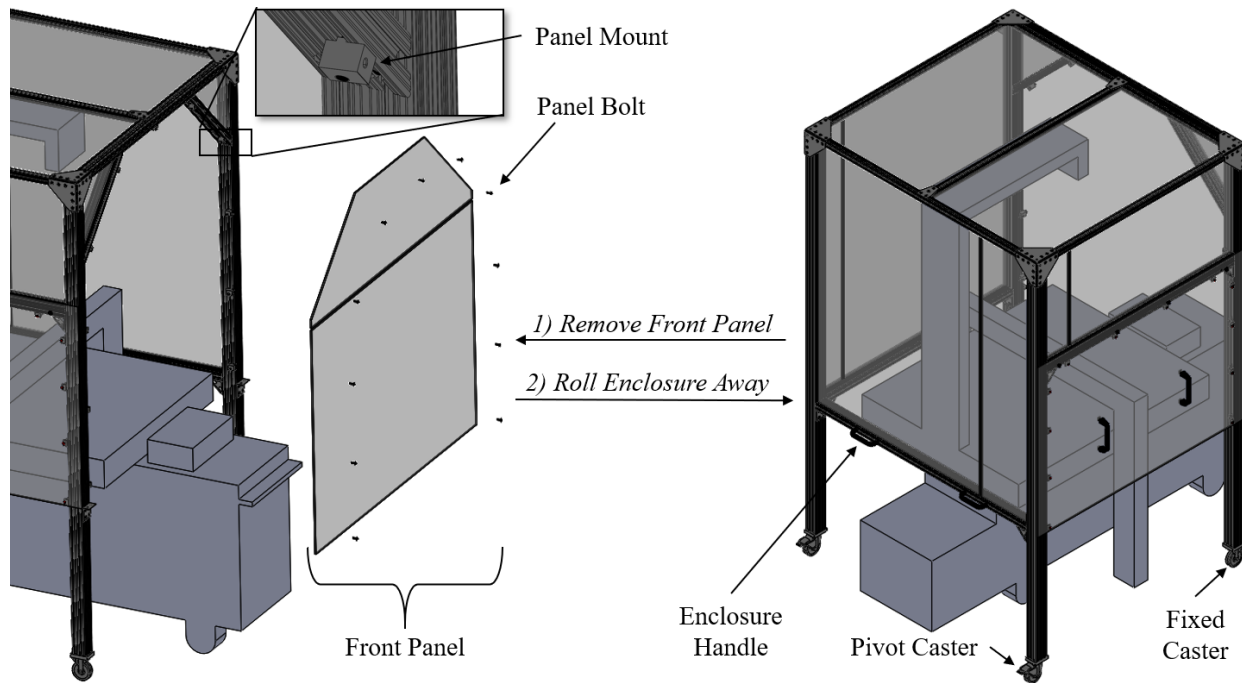


Figure 4.12: Annotated illustrations of the 3DP 300's custom enclosure's printer access design.

### 4.2.3 Enclosure Implementation

Thanks to the ability to fully design the 3DP 300 enclosure virtually before proceeding, the enclosure was completed without any issues using little more than a hex key set and a utility knife. The completed enclosure can be seen in Figure 4.13. A brief test showed that the enclosure air temperature rose from the ambient temperature of 23 °C to 31 °C after the print bed was left at 60 °C for 15 minutes. This differential is expected to increase when the HFE 300 hotend is active at 205 °C during PLA printing. Furthermore, the environment within the enclosure felt uncomfortably stagnant compared to the surrounding environment. This is promising as the still air means no outside drafts that would disrupt temperatures during the printing process.

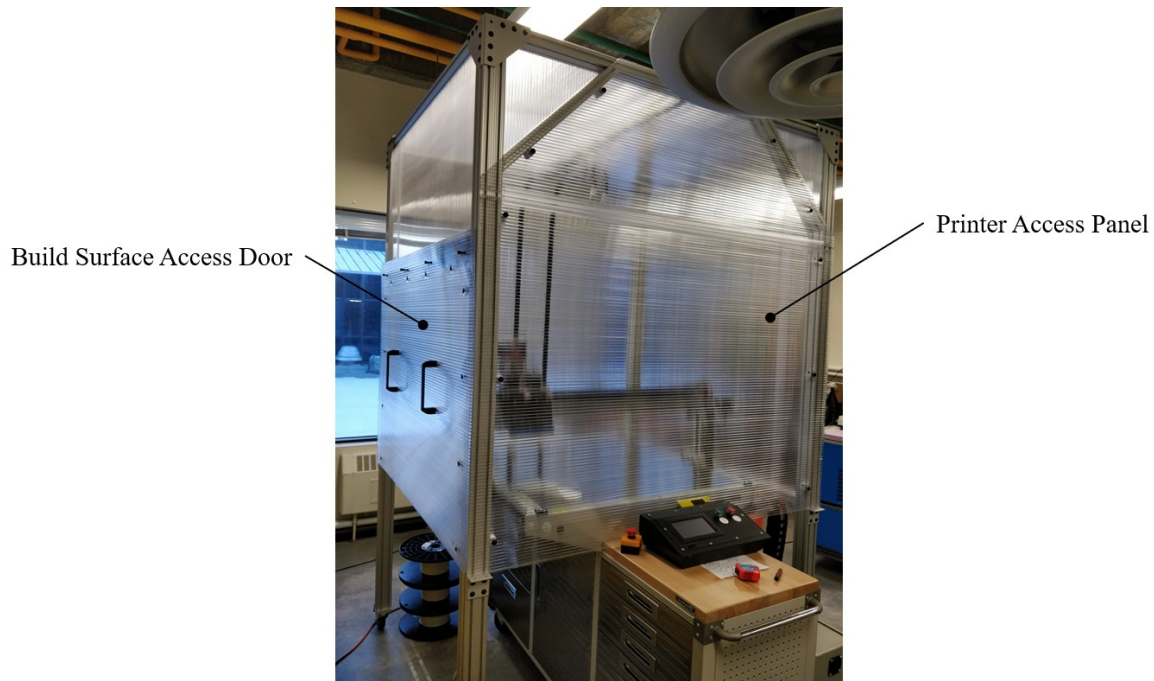


Figure 4.13: Annotated image of the custom built 3DP 300 enclosure.

Further testing could not be completed due to university procedures taken with regards to the COVID-19 pandemic. However, shortly after the enclosure was completed, a print caused the borosilicate glass build surface to crack into multiple pieces. While the glass sheet had several thumb-sized chips on its underside, these defects did not present any issues before the enclosure was situated. Other than a coincidence, it is hypothesized that the stable environment created by the enclosure increased the adhesion between the glass and the PLA. This increased adhesion then resulted in irregular shear strengths as the print cooled to enclosure temperatures. Considering that a scratch can reduce the strength of borosilicate glass by as much as 50% [99], this increased shear stress was likely too much for the damaged glass sheet to handle. Further tests will need to be completed to understand the effects the enclosure may have on an uncompromised borosilicate glass build surface and if a heated enclosure is necessary for both build surface health and quality warp-free prints.

### 4.3 Filament Storage

Since the purchase of the 3DP 300 printer over a year earlier, 10 kg spools of EcoTough PLA filament were placed on the designated rear rack exposed to the ambient environment. These 10 kg spools typically lasted 2-7 months depending on the prints requested throughout the university department. During the 3DP 300 enclosure conception, the PLA filament was found to



become brittle to the point of snapping when pulled off the spool. This brittle behavior then disappeared after a print had been completed, with no clear indication on what had initially caused it. This led into an investigation into filament degradation in which filament storage was discovered to be important for print appearance and strength.

Most, if not all, FFF filaments are hygroscopic meaning they absorb moisture from the ambient air [100], [101]. The rate, amount, and ability to absorb moisture in certain environments is unique for each material with highly hygroscopic filaments such as Nylon, PETG, PVA, and flexible thermoplastic polymers capable of becoming saturated within minutes or hours [100]–[102]. While also hygroscopic, PLA filaments are much less susceptible with saturation occurring in days or months [7], [101]. The water molecules absorbed by filaments then evaporate during the 3D printing extrusion process creating voids or air bubbles within the print. These voids significantly reduce the print's tensile strength and surface quality [100]–[104]. Chemical engineer and 3D print enthusiast [105] has stated that most plastics absorb 1% water by weight in open air and behave optimally during melt processes at 0.1-0.2% w/w. With pure PLA being shown to become saturated at 1% w/w within 4 to 15 days by [106], [107], it becomes clear that moisture absorption by PLA could become problematic if precautions are not taken.

In addition to printability, the presence of moisture in PLA also causes the rate of hydrolysis to increase. This process involves the breaking of polymer chains caused by the attachment of water molecules to polymer molecules [100], [103], and is the primary cause of PLA degradation [40], [48]. The tensile strength of PLA has been shown by [48] to be highly sensitive to hydrolysis degradation, with [106] showing a 33% reduction in dried PLA tensile strength after being submerged in water for 30 days. PLA degradation by hydrolysis therefore explains the common symptom of brittle PLA filament due to inadequate filament storage [101], [103], [108]. This brittleness has been further stated by [109] to commonly occur on the outer most filament roll layers due to exposure to the humid environment which would explain why the PLA filament was no longer brittle after the completion of a print.

Since air bubbles had never occurred in any prints completed on the 3DP 300 printer thus far, it is believed that the PLA filament was not continuously saturated. Instead, the accelerated degradation of the PLA filament is believed to be caused by unstable humidity levels. Not only is the 3DP 300 printer situated in an older building, but various experiments and machinery which

contain water utilize the same lab space. It is believed that oscillations in humidity created oscillations in PLA moisture levels. These oscillations may have allowed hydrolysis to progress periodically within the PLA filament. To prevent this issue from reducing the repeatability of prints, a storage solution was considered.

#### **4.3.1 Filament Storage**

The recommended humidity levels for filament storage is argued extensively throughout the 3D printing community; however, it is commonly agreed that relative humidity levels above 50% is too high for PLA [105], [108], [110]. Agreeable safe levels for PLA seem to be around 20% [101], [110], with 10-15% recommended as generically safe for all filament materials [103], [104]. PLA should last over a year with no noticeable degradation when stored correctly, but can become unusable in less than 2 months if left exposed to the environment [103].

The storage of FFF filament is simply any method in which prevents ambient humidity from being absorbed by the filament. Common recommendations include placing filament into airtight containers or resealable bags [7], [20], [101], [108], [111]. The use of rechargeable desiccant is also highly recommended to absorb any moisture seeping into the container/bag and keep the relative humidity low [100], [104], [105], [109], [111], [112]. While there are filament specific storage options available in the market [111], do it yourself (DIY) solutions are commonly used. These DIY solutions include humidity controlled storage bins [113] and direct feed dry boxes [114].

A DIY solution was required for the large 40 cm diameter, 16 cm width, 10 kg PLA rolls currently used by the 3DP 300 printer. Ideally, the storage solution would be airtight to keep stable humidity levels, be transparent to see filament levels and desiccant color, and fit one or two filament rolls without too much empty space. Finding a suitable container proved to be difficult; however, pet food containers appeared to be a valid solution. These airtight containers are built to keep dog, cat, and bird dry food fresh. Large size variants are typically thin tall containers with good depth for housing 45 lb. dog food bags. Not only could this hold a large filament spool, but they also commonly have wheels and large lids which would allow easy maneuvering and spool replacement. With a bit of DIY by printing a spool holding mechanism, creating a filament exit hole, installing a hygrometer, and layering the bottom with color changing rechargeable desiccant; this solution should work perfectly for the 3DP 300 printer. Additionally, a Bowden tube or PTFE

tube, could be run between the dry box and the HEF 300's extruder to reduce the moisture absorbed by the filament while inactive or during printing.

While the various items required to build the DIY 10 kg roll dry box were ordered, the items did not arrive before the university lockdown procedure was initiated due to safety concerns regarding the COVID-19 pandemic. This solution will be situated in the future but no pictures or experimental data proving its functionality is available at the time of writing this thesis.

#### **4.3.2 Filament Drying Options**

Due to the hydrolysis breakdown of PLA and potentially other plastics, care should be taken to store FFF filaments in consistent low humidity environments. However, there may come times where saturated filament needs to be dried, either to become suitable for storage or for increased printability of highly hygroscopic materials.

The two most common drying methods used throughout the 3D printing community are food dehydrators and convection ovens [100], [101], [105], [109]. While there are existing products available for small filament rolls [103], they are essentially food dehydrators with increased convince for use with filament spool. DIY solutions also exist [115] but a household oven is typically used instead. These drying methods operate the same way; by increasing the temperature of air such that the air's relative humidity drops and absorbs moisture from the filament. Therefore, the temperatures are set as high as possible to achieve the lowest relative humidity to both increase the moisture removal rate and amount. The only limitation is the glass transition temperature of the plastics being dried. If the glass transition temperature is reached or surpassed, the filament will deform and become incompatible with FFF 3D printing systems.

The oven or dehumidifier temperature required to dry PLA is unanimously recommended as 45 °C throughout the 3D printing community; however, the drying time is stated anywhere from 2 to 12 hours [100], [101], [109]. Using these unconventional sources can become risky, especially for PLA due to its relatively low glass transition temperature. The heat can be unstable or produce hotspots within the drying chamber causing momentary temperature spikes within the filament [100], [101]. Due to these risks, it is typically recommended to perform short incremental drying periods for rolls larger than 2 kg in size [101]. Additionally, repeated drying, excessive drying times, and temperatures above 50 °C have been known to increase PLA degradation [101], [112].

Vacuum drying is an intriguing option for drying filament. By reducing the ambient air pressure to around 3kPa absolute or 30 mbar, water will boil at ambient room temperatures [116]. This type of drying is used extensively in the food industry, in which 30-50 mbar pressures are typically used [117]. While some say heat is required to separate the water molecules from the polymer chains [103], others have stated that PLA dries well when left in a dry environment such as a dry box with desiccant [105], [118]. Vacuum drying of filament has been attempted by various 3D printing enthusiasts previously with mixed results. Individuals sharing poor results typically had weak vacuum pressures [118], or turn the vacuum pump off at desired pressures [119]. One 3D printing enthusiast has shared promising results for vacuum drying filament. They kept a vacuum pump running for 30 hours providing a consistently high vacuum and stated that the level of dryness obtained was greater than using an oven [120]. They stated that the moisture would be absorbed by the vacuum pump oil in which they would drain, freeze, and filter to remove the water and increase the lifespan of the oil. While the vacuum process appears slower than heat related drying methods, there is little to no risk in melting, deforming, or degrading the filament. This makes it an optimal drying method for the university laboratory where otherwise uninformed or unfamiliar individuals could use the drying system with little to no risk to their material.

To increase the drying rate of vacuum drying, heat could be introduced into the system to prevent temperatures from dropping during the endothermic evaporation process. Due to the vacuum environment, heat transmission is limited to conduction and radiation. For conduction heating, heat pads could be wrapped around the vacuum chamber. The disadvantage to conduction heating is that heat is transferred through surface contact therefore producing ununiform temperatures and limited heat transfer through insulative materials. As for radiant heating, there is infrared and microwave. Infrared heating could be accomplished by directing an infrared heater through a vacuum chamber surface consisting of an infrared transparent material. Radiant heating could also be applied from the vacuum chamber walls by coloring them black and applying heat through the exterior surface. The disadvantage to infrared radiant heating is similar to conduction in that the energy is absorbed by the impeding surfaces. For filament rolls, this means the outer layers are directly heated while the inner surfaces receive heat through its own conduction. The microwave radiant heating method is the most challenging to implement but also provides ideal heating. Microwaves could penetrate surfaces increasing water molecule temperatures directly. This has been attempted in the food industry in which drying times were reduced by over 120

times [117]. The disadvantage to this heating method is that any substances containing metal would cause problems.

A DIY vacuum drying system could be created for use with 10 kg filament rolls. Oil vacuum systems capable of achieving the vacuum pressures required for vacuum drying is commonly found online for economical prices. The difficulty lies in finding an economic solution for the large vacuum chamber required for the large-scale filament rolls. An option includes purchasing a heavy-duty stock pot and a thick acrylic plate for a lid. Further development on this subject had been halted due to university shutdown procedures taken due to safety concerns regarding the COVID-19 pandemic.

## CHAPTER 5. PRODUCT OPTIMIZATION

Other than surface imperfections, the chair's overall geometry printed successfully after print adhesion was increased with the use of sugar water. Several images of the printed chair presented next to a similar tube style chair are shown in Figure 5.1. When held in front of a bright light source, the 10% rectilinear infill can be seen between the Center Fill Width and Rail Fill Width sections. While the chair was not loaded to failure, it felt sturdy enough to hold up to the 124.74 kg (275 lb.) force defined in the FEA analysis. Desktop printer parts containing low infill percentages typically crackle when under load; however, a 77.11 kg (170 lb.) individual was able to sit, bounce, and lean on the chair without a sound.



*Figure 5.1: Images of the successfully printed PLA braced-cantilever chair alongside a visually similar tube style chair.*

Once print repeatability is obtained by utilizing the enclosure and filament storage system discussed in the previous chapter, there are several areas in which should be further studied.

Subjects such as printer scale, print parameters, and print material could be optimized for strength, speed, and/or surface quality. While there exists many studies comparing print parameters and specifications with print strength, most are completed on smaller scale desktop FFF printers. The general trend concluded from these studies is expected to be similar for large-scale FFF printers; however, quantitative results cannot be compared due to the unique mechanical properties produced by each 3D printer [54], [121]. Additional studies utilizing a large-scale FFF printer would need to be completed to confirm trends and obtain quantitative results.

## **5.1 Effects of Printer Scale**

The primary benefit of increasing printer scale is reduced print times. By utilizing larger extrusion widths and layer heights at similar print speeds, the flow rate is increased therefore allowing the print to be completed faster. There are two limiting factors for increasing flow rates, hotend size and nozzle size. The hotend size becomes a limiting factor due to its finite ability to achieve high flow rates. As discussed in chapter 3.2.2, larger hotends allow adequate heat transfer time to sufficiently melt the thermoplastic during higher material feed rates. Once the hotend becomes capable of high flow rates, a large nozzle diameter is required to enable larger extrusion widths and layer heights. While higher flow rates could be achieved through faster print speeds, this can negatively affect the bonding between extrusions resulting in reduced tensile strength [55]. Higher print speeds can also cause print surface issues like those described in chapter 3.2.3. When considering these concerns, it is safest to increase nozzle size over print speed when increased flow rates are desired.

Although most sources seem to unify nozzle diameter and extrusion width, the print parameters listed in Table 3.1 that were used in the creation of the braced-cantilever chair show the extrusion width being 120% of the nozzle diameter. This increased width is recommended by Simplify3D to account for thermoplastic expanding when exiting the nozzle [122]. While no literature was found discussing the relationship between extrusion width and nozzle diameter, this additional width is presumed to increase transverse extrusion adhesion due to the additional horizontal flow or spread as illustrated between Figure 5.2a and Figure 5.2b. An extrusion width to nozzle diameter ratio ( $W/D$ ) of 1.2 is assumed to increase horizontal plastic flow enough to significantly increase surface contact with adjacent extrusions while not being excessive to the

point of causing upward flow as illustrated in Figure 5.2c. Since the extrusion width is directly proportional to the nozzle diameter, larger nozzles are required to obtain larger extrusion widths.

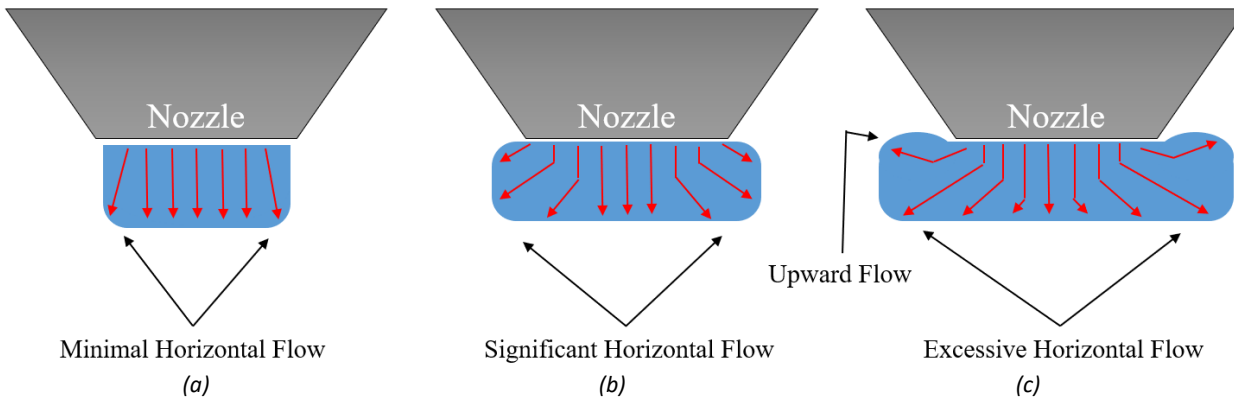


Figure 5.2: Annotated illustration displaying the approximate flow distribution of extruded filament when the extrusion width is equal to (a), larger than (b), and excessively larger than (c), the nozzle diameter.

Layer height can then be increased proportionally to the extrusion width. While increasing the layer height independently can increase the flow rate, the maximum layer height is limited by the extrusion width. As the extrusion width to layer height ratio ( $W/H$ ) increases from 1, the extrusion cross-sectional geometry transforms from circular to rectangular [123]. This effect is illustrated in Figure 5.3. As the ( $W/H$ ) ratio increases, so does the bonding surfaces between the extrusions thereby reducing the print's porosity [55], [123], [124]. For this reason, an ( $W/H$ ) ratio of 1.2 or lower typically result in bonding too weak to be useful [57], [123].



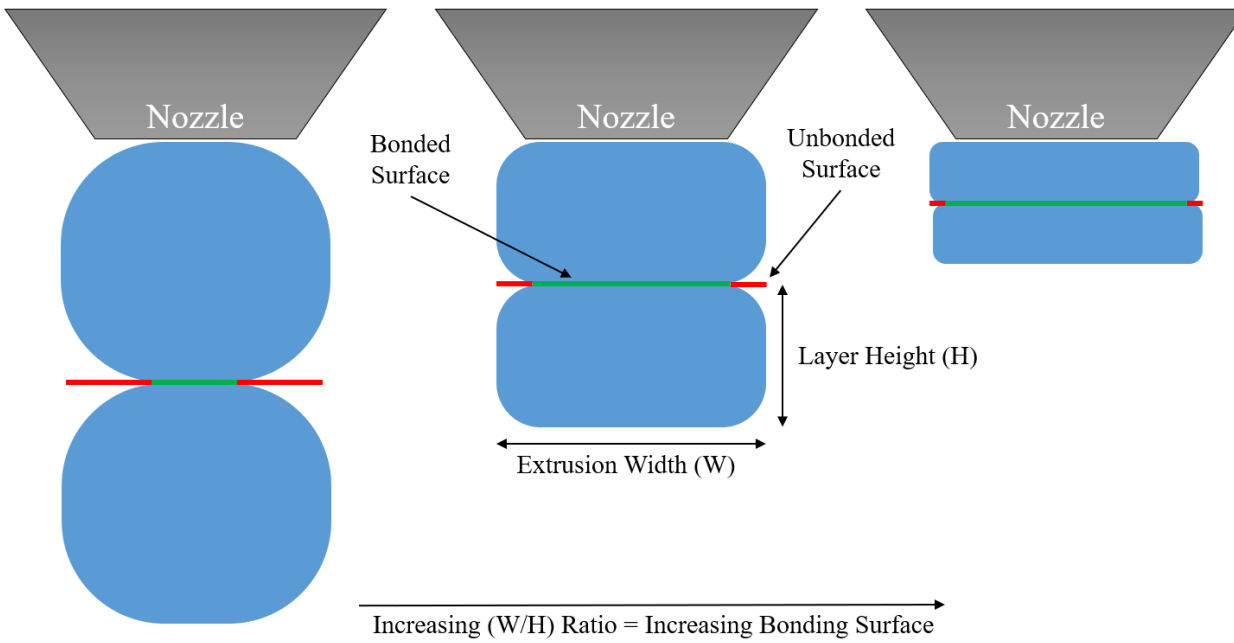


Figure 5.3: Annotated illustration displaying the effect extrusion width to layer height ratios ( $W/H$ ) have on bonding surfaces.

The increased bonding area of larger ( $W/H$ ) ratios significantly affect the mechanical properties of 3D printed parts. Larger ( $W/H$ ) ratios have been shown to increase flexural strength [52], [123], [125], and tensile strength in the normal [37], [124], [125], and transverse directions [55]. While larger ( $W/H$ ) ratios have been shown to reduce tensile strength in the longitudinal direction [52], the limiting tensile strength in 3D printed objects is commonly in the normal direction in which higher ( $W/H$ ) ratios are shown to be beneficial [35]–[37], [53], [55]. These sources seem to agree with [123] in that using an ( $W/H$ ) ratio less than 2 can be done for low-duty prints, 2-4 for functional and economic prints, and 4+ for mechanically critical prints. This is because these mechanical properties increase logarithmically with respect to the ( $W/H$ ) ratio and thereby require exceedingly long print times when print speed is held constant. However, a higher ( $W/H$ ) ratio is not always beneficial for a print's mechanical properties. The capabilities and stability of the FFF 3D printer can limit the lowest beneficial layer height. Exceeding that minimum layer height limit can result in reduced mechanical performance [123], [124], [126]. There are also mechanical properties that benefit from relatively low ( $W/H$ ) ratios such as fatigue [34] and impact strength [52].

The volumetric flow rate of a 3D printer can be determined by simply multiplying the extrusion width, layer height, and print speed [127]. The equation can be further modified by

incorporating the nozzle diameter, extrusion width to nozzle diameter ratio, and extrusion width to layer height ratio, resulting in the following equation:

$$Q = WHV = W \frac{W}{\left(\frac{W}{H}\right)} V = \frac{W^2 V}{\left(\frac{W}{H}\right)} = \frac{\left[D \left(\frac{W}{D}\right)\right]^2 V}{\left(\frac{W}{H}\right)} \quad (5.1)$$

where

$Q$	=	volumetric flow rate [mm <sup>3</sup> /s]
$W$	=	extrusion width [mm]
$H$	=	layer height [mm]
$V$	=	print speed [mm/s]
$(W/H)$	=	extrusion width to layer height ratio
$D$	=	nozzle diameter [mm]
$(W/D)$	=	extrusion width to nozzle diameter ratio

To fully utilize an FFF 3D printer's potential for large-scale objects, the nozzle diameter, print speed, and  $(W/H)$  ratio should be selected to maximum volumetric flow rate of the hotend. In the case study of using the 3DP 300 printer equipped with HFE 300 hotends, the maximum stated volumetric flow rate for PLA was stated in chapter 3.2.2 as 68.38 mm<sup>3</sup>/s. This leaves three unknowns when the  $(W/D)$  ratio is held constant at 1.2. When considering the availability of nozzle diameter sizes and desirable  $(W/H)$  ratios, it seems more appropriate to rearrange equation (5.1) to solve for print speed resulting in the following equation:

$$V = \frac{Q \left(\frac{W}{H}\right)}{\left[D \left(\frac{W}{D}\right)\right]^2} \quad (5.2)$$

where

$V$	=	print speed [mm/s]
$Q$	=	volumetric flow rate [mm <sup>3</sup> /s]
$(W/H)$	=	extrusion width to layer height ratio
$D$	=	nozzle diameter [mm]
$(W/D)$	=	extrusion width to nozzle diameter ratio

Plotting this equation with regards to varying nozzle diameters at  $(W/H)$  ratios of 2, 4, and 6 results in the graph shown in Figure 5.4. From this graph, it can be seen that larger nozzle diameters are required if print speeds are reduced while holding the  $(W/H)$  ratio constant. Additionally, print speeds or nozzle diameters must increase to achieve higher  $(W/H)$  ratios.

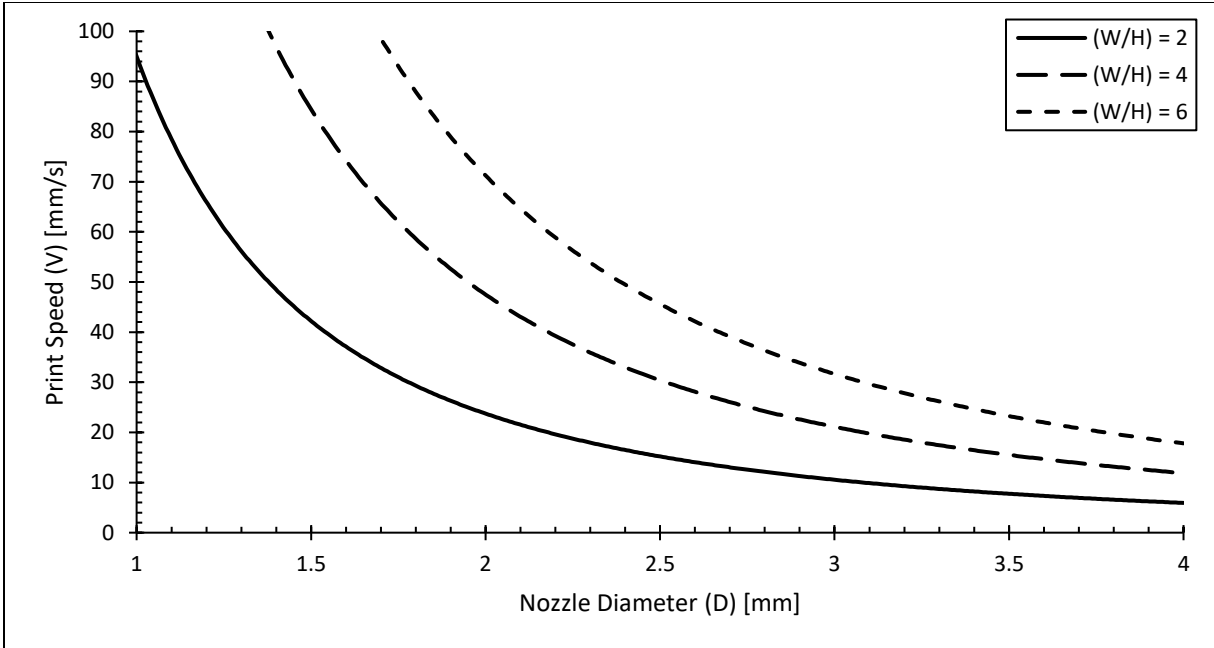


Figure 5.4: Line graph displaying the relationship between nozzle diameter ( $D$ ), extrusion width to layer height ratio ( $W/H$ ), and print velocity ( $V$ ) when the volumetric flow rate ( $Q$ ) and extrusion width to nozzle diameter ratio ( $W/D$ ) is kept constant at  $68.38 \text{ mm}^3/\text{s}$  and  $1.2$  respectively.

In the case study of using the 3DP 300 printer equipped with HFE 300 hotends, a ( $W/H$ ) ratio of 2.4 was used at a default print speed of 100 mm/s. An observation was made during initial test prints that having the perimeter print speed defined at 50% of the default print speed, or 50 mm/s, resulted in cleaner print surfaces with more uniform layers and less ringing. To optimize the volumetric flow rate of the HFE 300 hotend, choosing a larger nozzle that lowers the default print speed to levels that can be kept constant throughout the printing process could reduce print times and produce better quality prints. Furthermore, larger nozzle diameters allow the ability to reach higher ( $W/H$ ) ratios therefore increasing various mechanical properties such as tensile strength. An analysis of the resulting print speeds and layer heights for various nozzle diameters and ( $W/H$ ) ratios are shown in Table 5.1. From the table it can be seen that a nozzle diameter of 1.0 mm is relatively restrictive. Increasing the ( $W/H$ ) ratio would result in impractical print speeds while reducing print speeds would result in impractical ( $W/H$ ) ratios. Using a nozzle size of 2.0 mm offers more flexibility with ( $W/H$ ) ratios of 2, 4, and 6 resulting in reasonable print speeds. A nozzle diameter of 3.0 mm could also be useful for obtaining high ( $W/H$ ) ratios prints while keeping the print velocity below 50 mm/s.

Table 5.1: Comparing print speeds (V), layer heights (H), and Simplify3D's estimated print times (T) and PLA mass consumptions (M) for printing the braced-cantilever chair at various nozzle diameters (D) and extrusion width to layer height ratios (W/H) with a volumetric flow rate (Q) of 68.38 mm<sup>3</sup>/s, extrusion width to nozzle diameter ratio (W/D) of 1.2, and no brim.

	D: 1.0 mm	D: 2 mm	D: 3 mm
<b>W/H: 2</b>	V: 94.97 mm/s H: 0.60 mm T: 23h 50m M: 6.920 kg	V: 23.74 mm/s H: 1.20 mm T: 31h 06m M: 9.242 kg	V: 10.55 mm/s H: 1.80 mm T: 33h 07m M: 9.901 kg
<b>W/H: 4</b>	V: 189.94 mm/s H: 0.30 mm T: 25h 05m M: 6.912 kg	V: 47.49 mm/s H: 0.60 mm T: 31h 55m M: 9.255 kg	V: 21.10 mm/s H: 0.90 mm T: 33h 45m M: 9.899 kg
<b>W/H: 6</b>	V: 284.92 mm/s H: 0.20 mm T: 26h 20m M: 6.918 kg	V: 71.23 mm/s H: 0.40 mm T: 32h 47m M: 9.254 kg	V: 31.65 mm/s H: 0.60 mm T: 34h 28m M: 9.902 kg

The affect nozzle sizes and (W/H) ratios have on Simplify3D's estimated print time and material consumption for the braced-cantilever chair is also shown in Table 5.1. The behavior when considering larger (W/H) ratios with constant nozzle diameters is as expected. The material consumption does not significantly change, and the print time increases slightly due to the additional layers required to complete the print. Every layer has a short period of time in which material is not extruded through travel movements and retractions. By increasing the number of print layers, the total time of non-extrusion events increases thereby increasing total print time.

Table 5.1 also shows a significant increase in material consumption and print time with larger nozzle sizes. This is caused by the interaction between the printer scale, print properties, and print geometry. As illustrated in Figure 5.5, excessively extruded shell widths contribute to the additional material consumption. For reasons discussed in chapter 3.2.2, the extrusion width is locked to a static value. This causes Simplify3D to perform multiple full extrusion widths until the desired shell width of 2.0 mm is either reached or surpassed. In the case for the 1 mm nozzle with an extrusion width of 1.2 mm shown in Figure 5.5a, two passes are required to reach a total shell width of 2.4 mm. The 2.0 mm nozzle shown in Figure 5.5b also performs two passes for a total

shell width of 4.8 mm. This additional pass is likely generated due to the curvature of the print surface and the increased layer height of the larger nozzle resulting in a total horizontal width greater than 2.4 mm. Lastly, the 3.0 mm nozzle shown in Figure 5.5c will do a single pass for a total shell width of 3.6 mm. The way infill generation interacts between print geometry and nozzle size also contributes to the increased material consumption with increasing nozzle diameter. Simplify3D generates rectangular infill as a continuous extrusion by extruding up the inner shell wall to avoid retracting after every infill line. This results in the excess extrusions illustrated in Figure 5.5a and Figure 5.5b that function to adhere the shell to the infill. When the space is too small for infill to be generated at the defined extrusion widths, Simplify3D will instead perform a gap fill where the space is treated as 100% infill. While both the infill and shell generation within Simplify3D can be adjusted to avoid or reduce the additional material consumption, this shows that the print geometry and print properties should be heavily considered with respect to the printer scale being utilized.

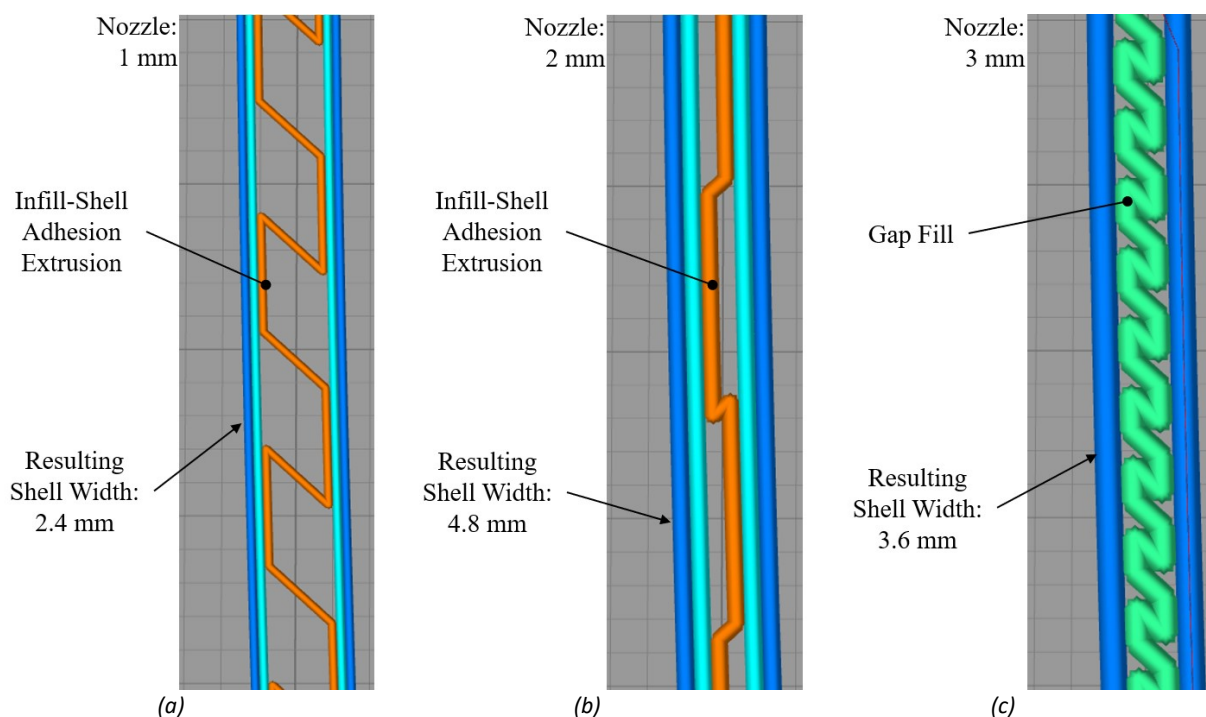


Figure 5.5: Annotated images comparing Simplify3D's 10% rectilinear infill and 2.0 mm shell when a nozzle size of 1.0 mm (a), 2 mm (b), and 3 mm (c) is defined with a (W/H) ratio of 4 at a braced-cantilever chair print layer 27 mm from the build surface.

An issue with increasing print scale is the reduced surface finish caused by the large layer heights. 3D Platform has shown that automotive high filler primers and gel coats can be used to produce a smooth finish on 3D prints [128]. They also stated that this technique could work for

their 6 mm nozzle 3D printers. Other techniques such as automotive body filler, tetrahydrofuran, dichloromethane, and ethyl acetate has been stated to produce high quality surface finishes on 3D printed PLA parts [129]. In addition to surface treatments, print parameters could be adjusted to achieve better surface quality at larger scales. An example of this is Simplify3D's "Combine Infill Every \_" print parameter. By setting this \_ value to 2, the printer will complete two shell layers before printing the infill at double the default layer height. When setting the layer height to 0.3 mm with a 1 mm nozzle, 1.2 mm extrusion width, the print will have an W/H ratio of 4 on the print surfaces and 2 internally therefore obtaining a better surface finish with reasonable print times. Various surface treatment processes, print parameters, and printer scales would need to be studied to obtain a balance between fast print times, acceptable mechanical properties, and suitable surface qualities.

## 5.2 Effects of Print Parameters

As discussed in chapter 2.3, 3D printing produces anisotropic prints with regards to their tensile strength with their magnitudes declining through the longitudinal, transverse, and normal directions, respectively [35], [36]. The longitudinal extrusion direction is also optimal for other mechanical properties such as flexural strength and impact strength [52]. While simple prints could be orientated such that stress primarily exists in the longitudinal extrusion direction, complex prints are more involved. Infill and shell print parameters must be varied to optimize strength/material distribution.

For prints that endure a bending moment, such as the bends in which form the cantilever and braced-cantilever chair designs, an infill density below 100% is likely optimal. This would place most of the material in the shell where the stress is greatest and reduce material in the center where the neutral axis lies. The infill used for the braced-cantilever chair was rectilinear in which alternated 90° every layer such that the strength benefits of the longitudinal extrusion direction merged with the transverse direction. An infill geometry that may perform better would be the honeycomb pattern. This geometry has been shown to outperform rectilinear in tensile strength and elastic modulus [38], [130], and provide its strength more uniformly along its planar directions due to its hexagonal pattern [38]. The disadvantage with this infill type is that it consumes more print time due to the additional decelerations and accelerations required. The divergence in print

times was shown by [121] to be quite significant with 45% honeycomb infill being equivalent to 100% rectilinear.

Other than geometry, infill density can also be adjusted for better mechanical performance. By increasing the density, the porosity of the print reduces thereby increasing tensile strength [55], [130], elastic modulus [130], fatigue performance [34], and impact strength [121]. However, the rate in which various mechanical properties increase with respect to infill density varies. While the elastic modulus has been shown by [130] to increase significantly between 20% and 50% densities for both honeycomb and rectilinear infills when compared to their respective 100% density performance, tensile strength behaves more meagerly. In addition, [121] has shown tensile strength of honeycomb infill to level off at 60% density before increasing nearly 50% upon reaching 100% infill density in which the infill geometry defaulted to rectilinear. The data obtained from both these sources agree with [38] in that infill densities below 100% result in lower tensile strength to mass ratios therefore resulting in less efficient material usage. When this is considered, the use of 100% infill layers within the braced-cantilever chair design appears optimal compared to establishing a uniform infill density for structural support.

While infill and shell print parameters can be adjusted for strength/material optimization in directions aligned with the build plate, little can be done about the limiting strength in the normal direction. The effect this has on the performance of a print can be reduced through either print orientation, in which print layers are stacked in the direction of minimal stress, or adjusting print parameters that improve layer-to-layer bonding. Raising the nozzle temperature can increase layer bonding through better layer fusion [54], [126], [131], [132]. This effect also occurs when cooling fans are disabled due to the extended molten state time allowing extrusions to spread into smaller crevices therefore reducing voids within the print. Omitting forced convection cooling also increases tensile strength in the longitudinal extrusion direction due to the extended cooling time, allowing PLA to become more crystalline [53], [132]. However, higher nozzle temperature and/or disabled cooling may result in increased warping and dimensional inaccuracy if each layer is not given enough time to solidify before the proceeding layer is printed.

### **5.3 Effects of Print Material**

Obviously, print material heavily impacts the mechanical performance of 3D printed objects. Even similar materials created by different brands can exhibit different mechanical

properties and print characteristics [54], [123]. What might not be obvious is that different filament colors of the same brand and material can also behave differently and produce prints with unique mechanical properties [54], [121]. Of common PLA filament colors, natural filaments typically produce better performing prints under similar print parameters due to the lack of pigment restricting flow thereby reducing voids and increasing layer bonding [123], [131]. However, PLA containing color pigments have been shown by [131] to obtain higher degrees of crystallinity with natural filaments being nearly amorphous with less than 1% crystallinity and white being the highest with over 5% crystallinity. They also showed that the crystallinity of white PLA can be increased to nearly 14% when a nozzle temperature of 210 °C was used. However, increasing it further to 215 °C reverted crystallinity back below 6% while still improving tensile strength therefore showing that extrusion bonding is more significant than material strength in 3D printed objects.

The mechanical performance of 3D printed objects can be further increased through post processing. As discussed earlier, increasing nozzle temperature or disabling cooling can increase the crystallinity of 3D prints by allowing additional cooling time above the material's glass transition temperature. However, aggressive cooling may be required in situations where warping is a concern, thereby producing prints that are nearly amorphous. This is where annealing can be beneficial in which the print is placed in an environment held at temperatures just above the material's glass transition temperature to allow molecular chains to align thereby increasing its crystallinity. Using this method, [132] has shown that annealing PLA at 85 °C increased its crystallinity to ~24% thereby increasing flexural strength by 17%. Another method of post processing is radiation treatment in which the aim is to increase cross-linking thereby increasing bonding strength between extrusions. This process was shown by [133] to work with PLA in which the tensile strength in the transverse extrusion direction was increased from 42% to 72% of the longitudinal tensile strength with the longitudinal direction being unchanged. Specifically, they subjected PLA containing 10% by weight of triallylisocyanurate (TAIC) to 50 kGy gamma radiation and ambient temperatures of 60 °C. The increased strength caused by cross-linking between extrusions should work in the weaker normal direction of prints as well, thereby reducing the anisotropic characteristics of 3D printed objects. This process could potentially revolutionize the field of 3D printing in industrial applications where strength is important.



Lastly, mechanical or economic benefits could be had through the utilization of fibers and fillers. With PLA being a common polymer for 3D printing composites [1], natural wood fibers/fillers such as cellulose and lignin are commonly used to preserve the environmental characteristics discussed in chapter 2.3.3. These wood derivatives are cheap, environmentally friendly, plentiful, and have the potential to increase the mechanical strength of PLA prints [134], [135]. Different forms of cellulose are commonly used with PLA to improve its mechanical properties. A few examples include the use of cellulose nanofibers to improve PLA's tensile strength and elastic modulus by 60% and 30%, respectively [136], and the use of macrocrystalline cellulose to improve PLA's elastic modulus by 7% [137]. Lignin is also of interest due to it being a waste material in wood related industries and is therefore very economical. While using lignin to increase PLA's mechanical properties has proved difficult [138], its use as a filler to reduce material cost could prove beneficial in large-scale 3D printing where strength is often overachieved.

## CHAPTER 6. CONCLUSION

In this thesis, an industrial application of large-scale FFF 3D printing of a cantilever chair was completed as a case study to understand the challenges involved with using large-scale FFF printers. The chair was designed in SOLIDWORKS in which easy variability and complex geometry were emphasized to take advantage of 3D printing's ability for mass customization and economic complexity. The use of PLA as the 3D printing material further highlighted the ability to create fully sustainable, recyclable, and biodegradable products. After minimizing mass using SOLIDWORKS FEA, 3D printing the cantilever chair with a brace addition was decided to reduce material consumption and avoid fatigue failure complications.

The characteristics of large-scale FFF 3D printers and their implications with slicer settings were discussed. The large glass build surface resulted in significant temperature gradients and fluctuations in which cooling fan settings and adhesion additions were adjusted with regards to print adhesion. The large hotend resulted in significant oozing and reduced feed rate to flow rate responsiveness in which slicer settings that modify retractions, travel movements, flow rates, and accelerations were tuned. Additionally, the stiffness of the printer frame, clearances in the mechanical system, accelerations, and print speed were considered due to the large translating mass causing dimensional inaccuracies in the form of ringing.

After the slicer settings in Silmplify3D were adjusted for the 3DP 300 printer, the braced-cantilever chair was produced. While successful, several issues involving adhesion, warping, and filament degradation were encountered. The adhesion capabilities between PLA and glass was found too weak for larger prints and removing cooled prints damaged the glass surface. An experiment was conducted to determine an easily applicable and economical adhesive substance that would provide good adhesion while the build surface was heated and release the print once cooled to room temperature. Through this experiment, sugar/water solution was found to perform better than clean glass, salt/water solution, and hairspray for PLA in both desired circumstances. To solve the warping issue, an enclosure was designed and built from T-slot aluminum extrusions and twinwall polycarbonate panels to provide insulative properties and easily allow future modifications. While no experimentation was produced to verify its functionality, it is assumed to work due to the previously damaged glass build surface severely cracking during a print shortly after installation. A solution for filament degradation was also determined using an air-tight plastic

pet food container and desiccant to maintain a consistent low-humidity environment. The effect of the enclosure and filament storage solutions were not determined due to university shutdown procedures initiated for safety during the COVID-19 pandemic.

Lastly, the effects print scale, print parameters, and print material have on mechanical, visual, and economic-based optimization were reviewed from sources using desktop-scale FFF printers. The volumetric flow rate limitations of hotends and nozzle diameters, and the relationships between nozzle diameters, extrusion widths, and layer heights were discussed. The geometrical effects of the extrusion width to nozzle diameter and extrusion width to layer height ratios were illustrated and the effect the extrusion width to layer height ratio has on a print's mechanical properties were reviewed. An equation relating volumetric flow rate to nozzle diameter, print speed, extrusion width to nozzle diameter ratio, and extrusion width to layer height ratio was then created and used to present optimal nozzle diameter, extrusion width to layer height ratio, and print speed combinations for 3D Platform's HFE 300 hotend. These combinations of increasing nozzle diameter with constant volumetric flow rates and extrusion width to layer height ratio were then applied to the braced-cantilever chair case study by observing Simplify3D's estimated print time and material consumption. From this, it was discovered that larger nozzle sizes could result in significant increases in material consumption and print time due to print parameter settings and print geometry. The affect print parameters have on the mechanical properties of FFF objects were further reviewed with respect to parameters such as infill density, infill geometry, nozzle temperature, and cooling parameters. From this review, it was revealed that forced cooling and low nozzle temperatures typically effects the mechanical properties of prints negatively through diminished layer bonding. Lastly, the effect of print material color, print post-processing treatments, and wood-based inclusions were reviewed. Significant discoveries include the superior bonding ability of natural PLA, the post-processing radiation treatment to reduce anisotropic tensile strength behavior, and the use of cellulose nanofibers to increase PLA's tensile strength and elastic modulus. Once print repeatability is achieved through the adhesion, warping, and filament degradation solutions, further analysis should be conducted to verify general hypotheses and conclusions made by these sources that have used smaller FFF printers. Examples of such future works includes using a large-scale FFF printer capable of high print repeatability to measure the effects of extrusion width to layer height ratios on print tensile strength and elastic modulus. Additionally, a study attempting to confirm the theory that directly changing nozzle

diameter while keeping the extrusion width to layer height ratio constant does not provide any significant enhancements to a large-scale print's mechanical properties.

## References

- [1] T. D. Ngo, A. Kashani, G. Imbalzano, K. T. Q. Nguyen, and D. Hui, “Additive Manufacturing (3D Printing): A Review of Materials, Methods, Applications and Challenges,” *Compos. Part B Eng.*, vol. 143, pp. 172–196, 2018.
- [2] R. Bogue, “3D printing: The Dawn of a New Era in Manufacturing?,” *Assem. Autom.*, vol. 33, no. 4, pp. 307–311, 2013.
- [3] T. Campbell, C. Williams, O. Ivanova, and B. Garrett, “Could 3D Printing Change the World? Technologies, Potential, and Implications of Additive Manufacturing,” 2011.
- [4] B. Berman, “3-D printing: The New Industrial Revolution,” *Bus. Horiz.*, vol. 55, pp. 155–162, 2012.
- [5] C. Weller, R. Kleer, and F. T. Piller, “Economic Implications of 3D Printing: Market Structure Models in Light of Additive Manufacturing Revisited,” *Int. J. Prod. Econ.*, vol. 164, pp. 43–56, 2015.
- [6] Brett *et al.*, “Making Sense of 3-D Printing: Creating a Map of Additive Manufacturing Products and Services,” *Addit. Manuf.*, vol. 1–4, pp. 64–76, 2014.
- [7] L. W. Kloski and N. Kloski, *Make: Getting Started with 3D Printing*. Maker Media Inc., 2016.
- [8] M. Petch, “3D Printing Community Responds to COVID-19 and Coronavirus Resources,” *3D Printing Industry*, 2020. [Online]. Available: <https://3dprintingindustry.com/news/3d-printing-community-responds-to-covid-19-and-coronavirus-resources-169143/>. [Accessed: 01-Jul-2020].
- [9] J. W. Stansbury and M. J. Idacavage, “3D Printing with Polymers: Challenges Among Expanding Options and Opportunities,” *Dent. Mater.*, vol. 32, no. 1, pp. 54–64, 2016.
- [10] S. Curran *et al.*, “Big Area Additive Manufacturing and Hardware - in - the - Loop for Rapid Vehicle Powertrain Prototyping : A Case Study on the Development of a 3 - D - Printed Shelby Cobra,” in *SAE 2016 World Congress and Exhibition*, 2016, pp. 1–11.

- [11] L. Love, *3D Printed Shelby Cobra*. OSTI.GOV, 2015.
- [12] BigRep, “BigRep.” [Online]. Available: <https://bigrep.com/>.
- [13] Modix Modular Technologies LTD, “Modix.” [Online]. Available: <https://www.modix3d.com/>.
- [14] Cosine Additive Inc., “Cosine.” [Online]. Available: <https://www.cosineadditive.com/>.
- [15] BLB Industries, “BLB.” [Online]. Available: <https://blbindustries.se/>.
- [16] 3D Platform, “3D Platform.” [Online]. Available: <https://www.3dplatform.com/>.
- [17] C. Naramore, “3D Printing Seating With BLB Industries,” *BLB Industries*, 2019. [Online]. Available: <https://3dprinting.com/company/blb-industries/3d-printing-seating-with-blb-industries/>. [Accessed: 28-Jul-2020].
- [18] Top 3D Shop, “Consumer-Oriented and Professional Large Format 3D Printers,” *Top 3D Shop*. [Online]. Available: <https://top3dshop.com/blog/large-format-3d-printers>. [Accessed: 29-Jul-2020].
- [19] S. Rogers, “This Innovative 3D-Printed Electric Car is Made of Just 57 Parts,” *Dornob.com*. [Online]. Available: <https://dornob.com/this-innovative-3d-printed-electric-car-is-made-of-just-57-parts/>. [Accessed: 28-Jul-2020].
- [20] 3D Platform, “Workseries User Manual 200, 300 & 400 Series,” vol. C. 3D Platform, 2017.
- [21] 3D Platform, “Work Series Additive Manufacturing System,” vol. 4. 3D Platform, 2018.
- [22] The Editors of Encyclopaedia Britannica, “Ladder-back Chair,” *Encyclopaedia Britannica*, 2006. [Online]. Available: <https://www.britannica.com/topic/ladder-back-chair>. [Accessed: 19-Jul-2019].
- [23] B. Franken, C. Loose, N. Baier, S. Kim, and C. Widjaja, “Voronoi Chair,” *Franken/Architekten GMBH*, 2011. [Online]. Available: <http://www.franken-architekten.de/index.php?pagetype=projectdetail&lang=en&cat=3&param=cat&param2=1175&param3=0&>. [Accessed: 19-Jul-2019].

- [24] T. Vogelgsang, “Law, Design, and Market Value: Lessons from the Cantilever Chair, 1929-1936,” *Enterp. Soc.*, vol. 18, no. 3, pp. 536–565, 2017.
- [25] Wikipedia Contributors, “Cantilever Chair,” *Wikipedia, The Free Encyclopedia*, 2018. [Online]. Available: [https://en.wikipedia.org/wiki/Cantilever\\_chair](https://en.wikipedia.org/wiki/Cantilever_chair). [Accessed: 22-Feb-2019].
- [26] A. White, “Classic Chairs Made Simple,” *Ana White*, 2011. [Online]. Available: <https://ana-white.com/woodworking-projects/classic-chairs-made-simple>. [Accessed: 19-Jul-2019].
- [27] W. Pokojski and P. Pokojaska, “Voronoi Diagrams – Inventor, Method, Applications,” *Polish Cartogr. Rev.*, vol. 50, no. 3, pp. 141–150, 2018.
- [28] Chippwalters, “Voronoi Chair Tutorial,” *MoI*, 2015. [Online]. Available: <http://moi3d.com/forum/lmessages.php?webtag=MOI&msg=7596.8>. [Accessed: 19-Jul-2019].
- [29] Plastic le Meg, “Panton Chair, a Timeless Classic,” *Plastics le Mag*, 2015. [Online]. Available: <http://plastics-themag.com/Panton-chair-a-timeless-classic>. [Accessed: 19-Jul-2019].
- [30] CCSS, “Mies van der Rohe MR10 Cantilever Chairs, 1960s,” CCSS. [Online]. Available: <https://ccss.shop/products/mies-van-der-rohe-mr10-cantilever-chairs-1960s>. [Accessed: 19-Jul-2019].
- [31] Vitra, “Panton Chair,” *smow.com*. [Online]. Available: <https://www.smow.com/en/manufacturers/vitra/chairs/panton-chairs/panton-chair-tangerine.html>. [Accessed: 15-Jun-2020].
- [32] Dassault Systèmes SolidWorks Corporation, “SOLIDWORKS.” [Online]. Available: <https://www.solidworks.com/>.
- [33] Brezlin, “Chair Design Guidelines,” *Brezlin*. [Online]. Available: <http://www.brezlin.com/design/chairguidelines.html>. [Accessed: 10-Feb-2019].
- [34] R. Jerez-Mesa, J. A. Travieso-Rodriguez, J. Llumà-Fuentes, G. Gomez-Gras, and D. Puig,

- “Fatigue Lifespan Study of PLA Parts Obtained by Additive Manufacturing,” *Procedia Manuf.*, vol. 13, pp. 872–879, 2017.
- [35] Y. Song, Y. Li, W. Song, K. Yee, K.-Y. Lee, and V. L. Tagarielli, “Measurements of the Mechanical Response of Unidirectional 3D-Printed PLA,” *Mater. Des.*, vol. 123, pp. 154–164, 2017.
- [36] J. M. Chacón, M. A. Caminero, E. García-Plaza, and P. J. Núñez, “Additive Manufacturing of PLA Structures Using Fused Deposition Modelling: Effect of Process Parameters on Mechanical Properties and Their Optimal Selection,” *Mater. Des.*, vol. 124, pp. 143–157, 2017.
- [37] T. Yao, Z. Deng, K. Zhang, and S. Li, “A Method to Predict the Ultimate Tensile Strength of 3D Printing Polylactic Acid (PLA) Materials with Different Printing Orientations,” *Compos. Part B Eng.*, vol. 163, pp. 393–402, 2019.
- [38] D. Farbman and C. McCoy, “Materials Testing of 3D Printed ABS and PLA Samples to Guide Mechanical Design,” in *International Manufacturing Science and Engineering Conference*, 2016.
- [39] BIFMA, “ANSI/BIFMA X5.1 Office Chairs.” 2017.
- [40] S. Farah, D. G. Anderson, and R. Langer, “Physical and Mechanical Properties of PLA, and Their Functions in Widespread Applications — A Comprehensive Review,” *Adv. Drug Deliv. Rev.*, vol. 107, pp. 367–392, 2016.
- [41] J. Lunt, “Large-Scale Production, Properties and Commercial Applications of Poly Lactic Acid Polymers,” *Polym. Degrad. Stab.*, vol. 59, no. 1–3, pp. 145–152, 1998.
- [42] E. T. H. Vink, K. R. Rábago, D. A. Glassner, and P. R. Gruber, “Applications of Life Cycle Assessment to NatureWorks™ Polylactide (PLA) Production,” *Polym. Degrad. Stab.*, vol. 80, no. 3, pp. 403–419, 2003.
- [43] V. Peinado, P. Castell, L. García, and A. Fernández, “Effect of Extrusion on the Mechanical and Rheological Properties of a Reinforced Poly(Lactic Acid): Reprocessing and Recycling of Biobased Materials,” *Materials (Basel)*, vol. 8, no. 10, pp. 7106–7117, 2015.



- [44] I. Anderson, “Mechanical Properties of Specimens 3D Printed with Virgin and Recycled Polylactic Acid,” *3D Print. Addit. Manuf.*, vol. 4, no. 2, pp. 110–115, 2017.
- [45] A. Lanzotti, M. Martorelli, S. Maietta, S. Gerbino, F. Penta, and A. Gloria, “A Comparison Between Mechanical Properties of Specimens 3D Printed with Virgin and Recycled PLA,” *Procedia CIRP*, vol. 79, pp. 143–146, 2019.
- [46] X. G. Zhao, K. J. Hwang, D. Lee, T. Kim, and N. Kim, “Enhanced Mechanical Properties of Self-Polymerized Polydopamine-Coated Recycled PLA Filament Used in 3D Printing,” *Appl. Surf. Sci.*, vol. 441, pp. 381–387, 2018.
- [47] J. J. Shen, “Comparative Life Cycle Assessment of Polylactic acid (PLA) and Polyethylene Terephthalate (PET),” pp. 1–16, 2011.
- [48] X. Zhang, U. P. Wyss, D. Pichora, and M. F. A. Goosen, “An Investigation of Poly(Lactic Acid) Degradation,” *J. Bioact. Compat. Polym.*, vol. 9, no. 1, pp. 80–100, 1994.
- [49] G. L. Siparsky, K. J. Voorhees, and F. Miao, “Hydrolysis of Polylactic Acid (PLA) and Polycaprolactone (PCL) in Aqueous Acetonitrile Solutions: Autocatalysis,” *J. Environ. Polym. Degrad.*, vol. 6, no. 1, pp. 31–41, 1998.
- [50] M. A. Paul, C. Delcourt, M. Alexandre, P. Degée, F. Monteverde, and P. Dubois, “Polylactide/Montmorillonite Nanocomposites: Study of the Hydrolytic Degradation,” *Polym. Degrad. Stab.*, vol. 87, no. 3, pp. 535–542, 2005.
- [51] Filaments.ca, “Introducing EcoTough™ PLA 3D Filament - Naturally Safe , Naturally Strong !,” *Filaments.ca*, 2018. [Online]. Available: <https://filaments.ca/blogs/news/introducing-ecotough-pla-3d-filament-naturally-safe-naturally-strong>. [Accessed: 09-May-2020].
- [52] X. Liu, M. Zhang, S. Li, L. Si, J. Peng, and Y. Hu, “Mechanical Property Parametric Appraisal of Fused Deposition Modeling Parts Based on the Gray Taguchi Method,” *Int. J. Adv. Manuf. Technol.*, vol. 89, pp. 2387–2397, 2017.
- [53] C. Y. Lee and C. Y. Liu, “The Influence of Forced-Air Cooling on a 3D Printed PLA Part Manufactured by Fused Filament Fabrication,” *Addit. Manuf.*, vol. 25, pp. 196–203, 2019.

- [54] B. M. Tymrak, M. Kreiger, and J. M. Pearce, “Mechanical Properties of Components Fabricated with Open-Source 3-D Printers under Realistic Environmental Conditions,” *Mater. Des.*, vol. 58, pp. 242–246, 2014.
- [55] H. Li, T. Wang, J. Sun, and Z. Yu, “The Effect of Process Parameters in Fused Deposition Modelling on Bonding Degree and Mechanical Properties,” *Rapid Prototyp. J.*, vol. 24, no. 1, pp. 80–92, 2018.
- [56] MakeItFrom.com, “Polyactic Acid (PLA, Polyactide),” *MakeItFrom.com*, 2018. [Online]. Available: <https://www.makeitfrom.com/material-properties/Polylactic-Acid-PLA-Polylactide>. [Accessed: 22-Feb-2019].
- [57] B. Evans, *Practical 3D Printers: [The Science and Art of 3D Printing ; Calibrate, Modify, and Create Amazing Things with Your 3D Printer]*. Manning, Paul, 2012.
- [58] Simplify3D, “Simplify3D.” [Online]. Available: <https://www.simplify3d.com/>.
- [59] Ultimaker BV, “Ultimaker Cura.” [Online]. Available: <https://ultimaker.com/software/ultimaker-cura>.
- [60] A. Q., “13 Best 3D Printing Slicer Software FDM Domination,” *inov3D*, 2019. [Online]. Available: <https://www.inov3d.net/3d-printing-slicer-software-download/>. [Accessed: 01-Jun-2020].
- [61] 3D Platform Representative, “Word of Mouth.” 3D Platform, 2018.
- [62] S. L. Messimer, A. E. Patterson, N. Muna, A. P. Deshpande, and T. Rocha Pereira, “Characterization and Processing Behavior of Heated Aluminum-Polycarbonate Composite Build Plates for the FDM Additive Manufacturing Process,” *J. Manuf. Mater. Process.*, vol. 2, no. 1, 2018.
- [63] M. Spoerk, J. Gonzalez-Gutierrez, J. Sapkota, S. Schuschnigg, and C. Holzer, “Effect of the Printing Bed Temperature on the Adhesion of Parts Produced by Fused Filament Fabrication,” *Plast. Rubber Compos.*, vol. 47, no. 1, pp. 17–24, 2018.
- [64] M. Kujawa, “The Influence of First Layer Parameters on Adhesion Between the 3D

- Printer's Glass Bed and ABS," no. September, 2017.
- [65] Ultimaker BV, "How to Fix Warping," *Ultimaker*, 2020. [Online]. Available: <https://ultimaker.com/en/resources/19537-how-to-fix-warping>. [Accessed: 20-Jul-2019].
- [66] W. Puchot, "E-Mail." Voxel Factory, 2020.
- [67] E. Tyson, "What is a 3D Printing Raft, Brim or Skirt - Why and How to Use Them," *rigid.ink*. [Online]. Available: <https://rigid.ink/blogs/news/3d-printed-raft-brim-skirt>. [Accessed: 20-Jul-2019].
- [68] Simplify3D, "Rafts, Skirts and Brims!," *Simplify3D*, 2019. [Online]. Available: <https://www.simplify3d.com/support/articles/rafts-skirts-and-brims/>. [Accessed: 20-Jul-2019].
- [69] A. Chavan, "3D Printing Raft , Brim and Skirt – All You Need to Know," *All3DP*, 2019. [Online]. Available: <https://all3dp.com/2/3d-printing-raft-brim-and-skirt-all-you-need-to-know/>. [Accessed: 20-Jul-2019].
- [70] SPOOL3D, "E3DV6 HotEnd Metal Parts Only - 1.75mm Universal." [Online]. Available: <https://spool3d.ca/e3dv6-hotend-metal-parts-only-1-75mm-universal/>. [Accessed: 03-Jun-2020].
- [71] E3D-Online, "Volcano HotEnd," *E3D-Online*. [Online]. Available: <https://e3d-online.com/volcano-hotend>. [Accessed: 03-Jun-2020].
- [72] Ultimaker BV, "How to Fix Stringing," *Ultimaker*, 2020. [Online]. Available: <https://support.ultimaker.com/hc/en-us/articles/360012016280-How-to-fix-stringing>. [Accessed: 03-Jun-2020].
- [73] B. Obudho, "3D Printing Stringing: 5 Easy Ways to Prevent It," *All3DP*, 2020. [Online]. Available: <https://all3dp.com/2/3d-print-stringing-easy-ways-to-prevent-it/>. [Accessed: 03-Jun-2020].
- [74] Simplify3D, "Stringing or Oozing," *Simplify3D*, 2020. [Online]. Available: <https://www.simplify3d.com/support/print-quality-troubleshooting/stringing-or-oozing/>.

[Accessed: 03-Jun-2020].

- [75] H. Kondo, “3D Printing: Ghosting / Ringing - 3 Easy Fixes,” *All3DP*, 2019. [Online]. Available: <https://all3dp.com/2/3d-printer-ringing-easy-fixes/>. [Accessed: 04-Jun-2020].
- [76] Simplify3D, “Vibrations and Ringing,” *Simplify3D*, 2020. [Online]. Available: <https://www.simplify3d.com/support/print-quality-troubleshooting/vibrations-and-ringing/>. [Accessed: 04-Jun-2020].
- [77] E. Rice, “StepSERVO Closed Loop Improves 3D Printing,” *Applied Motion Products, Inc.*, 2016. [Online]. Available: <https://www.applied-motion.com/news/2016/01/stepservo™-closed-loop-improves-3d-printing>. [Accessed: 04-Jun-2020].
- [78] S. J. Grunewald, “3D Platform Releases Faster and More Accurate SurePrint Servo Technology Upgrade Package,” *3DPrint.com*, 2016. [Online]. Available: <https://3dprint.com/116355/3d-platform-sureprint-upgrade/>. [Accessed: 04-Jun-2020].
- [79] I. Rockford, “3D Platform Advances Large Format 3D Printing Capabilities with SurPrint Servo Technology,” *Additive Manufacturing*, 2016. [Online]. Available: <http://additivemanufacturing.com/2016/01/23/3d-platform-advances-large-format-3d-printing-capabilities-with-sureprint-servo-technology/>. [Accessed: 04-Jun-2020].
- [80] M. Matisons, “3D Platform Brings Industry New Standards through SurePrint Servo Technology,” *3DPrint.com*, 2015. [Online]. Available: <https://3dprint.com/97760/3d-platform-sureprint-servo/>. [Accessed: 04-Jun-2020].
- [81] 3D Platform, “Mechatronics In Large Format 3D Printing,” *3D Platform*, 2014. [Online]. Available: <https://www.3dplatform.com/Blog/2019/July/Mechatronics-In-Large-Format-3D-Printing>. [Accessed: 04-Jun-2020].
- [82] 3D Platform, “3DP Workbench User Manual.” 3D Platform, 2016.
- [83] Palmdelta and \_unregistered, “What’s the Best Hairspray for Helping the First Layer on a Glass Bed?,” *Reddit Inc.*, 2017. [Online]. Available: [https://www.reddit.com/r/3Dprinting/comments/60bej1/whats\\_the\\_best\\_hairspray\\_for\\_helping\\_the\\_first/](https://www.reddit.com/r/3Dprinting/comments/60bej1/whats_the_best_hairspray_for_helping_the_first/). [Accessed: 19-Jul-2019].

- [84] Lornamead, “AquaNet.” [Online]. Available: <https://www.lornameadna.com/index.php/aquanet/>.
- [85] tesseract, “How do we Use Hairspray Successfully?,” *robo*, 2014. [Online]. Available: <http://community.robo3d.com/index.php?threads/how-do-we-use-hairspray-successfully.2365/>. [Accessed: 19-Jul-2019].
- [86] Lazerlord10, “Bed Adhesion Goals. Who Needs Rafts, Anyway?,” *Reddit Inc.*, 2017. [Online]. Available: [https://www.reddit.com/r/3Dprinting/comments/606emz/bed\\_adhesion\\_goals\\_who\\_needs\\_rafts\\_anyway/](https://www.reddit.com/r/3Dprinting/comments/606emz/bed_adhesion_goals_who_needs_rafts_anyway/). [Accessed: 10-May-2020].
- [87] G. Keteleer, “Treating the Glass Build-Plate of a 3D-Printer with Salt Water Improves Bonding of PLA-Prints.” 2015.
- [88] Redpath Sugar LTD., “Special Fine Granulated Sugar,” *Redpath Sugar*. [Online]. Available: <https://www.redpathsugar.com/products/granulated-white-sugar>. [Accessed: 29-Jul-2020].
- [89] Windsor Salt LTD., “Widsor Table Salt - Iodized,” *Windsor Salt*. [Online]. Available: <https://windsorsalt.com/product/table-salt-and-household-salt/>. [Accessed: 29-Jul-2020].
- [90] Microsoft, “Microsoft Excel.” [Online]. Available: <https://www.microsoft.com/en-ca/microsoft-365/excel>.
- [91] M. S. Alsoufi and A. E. Elsayed, “Warping Deformation of Desktop 3D Printed Parts Manufactured by Open Source Fused Deposition Modeling (FDM) System,” *Int. J. Mech. Mechatronics Eng.*, vol. 17, no. 4, pp. 7–16, 2017.
- [92] L. Kivela, “3D Print Warping: 10 Easy Fixes for PLA, PETG & ABS,” *All3DP*, 2020. [Online]. Available: <https://all3dp.com/2/3d-print-warping-what-it-is-how-to-fix-it/>. [Accessed: 06-Jun-2020].
- [93] Simplify3D, “Warping,” *Simplify3D*, 2020. [Online]. Available: <https://www.simplify3d.com/support/print-quality-troubleshooting/warping/>. [Accessed: 07-Jun-2020].

- [94] 3D Platform, *3D Platform's New Environmental Enclosures*. 2017.
- [95] 80/20 Inc., "80/20 Inc." [Online]. Available: <https://8020.net/>.
- [96] McMaster-Carr, "McMaster-Carr." [Online]. Available: <https://www.mcmaster.com/>.
- [97] EcoFort Innovation Corp., "Installation Guide." EcoFort Innovation Corp., Calgary, 2020.
- [98] EcoFort Innovation Corp., "EcoFort." [Online]. Available: <https://www.ecofort.ca/>.
- [99] J. J. Swab, S. R. Thies, J. C. Wright, J. A. Schoenstein, and P. J. Patel, "Influence of Surface Scratches on the Flexure Strength of Soda-Lime Silicate and Borosilicate Glass," *Exp. Mech.*, vol. 53, no. 1, pp. 91–96, 2013.
- [100] H. Kondo, "How to Dry Filament: PLA, ABS, & Nylon," *All3DP*, 2020. [Online]. Available: <https://all3dp.com/2/how-to-dry-filament-pla-abs-and-nylon/>. [Accessed: 11-Jun-2020].
- [101] M. Tyson, "Starters Guide to Moisture, Drying and Filament Storage," *3D Printing Solutions*, 2018. [Online]. Available: <https://www.3dprintingsolutions.com.au/User-Guides/starters-guide-to-moisture-drying-and-filament-storage>. [Accessed: 11-Jun-2020].
- [102] I. T. Garces, S. Aslanzadeh, Y. Boluk, and C. Ayranci, "Effect of Moisture on Shape Memory Polyurethane Polymers for Extrusion-Based Additive Manufacturing," *Materials (Basel)*, vol. 12, no. 244, 2019.
- [103] Filament2Print, "Humidity: The Great Enemy of the Filaments for 3D Printing," *Filament2Print*, 2018. [Online]. Available: [https://filament2print.com/gb/blog/45\\_humidity-problems-3d-filaments.html](https://filament2print.com/gb/blog/45_humidity-problems-3d-filaments.html). [Accessed: 11-Jun-2020].
- [104] pinshape inc., "3D Filament Storage - Top 5 Tips!," *pinshape inc.*, 2016. [Online]. Available: <https://pinshape.com/blog/top-3d-filament-storage-tips/>. [Accessed: 11-Jun-2020].
- [105] R. Carlyle, "Can Aged PLA be Refurbished?," *Stack Exchange*, 2016. [Online]. Available: <https://3dprinting.stackexchange.com/questions/1404/can-aged-pla-be-refurbished>.

[Accessed: 11-Jun-2020].

- [106] G. H. Yew, A. M. Mohd Yusof, Z. A. Mohd Ishak, and U. S. Ishiaku, “Water Absorption and Enzymatic Degradation of Poly(Lactic Acid)/Rice Starch Composites,” *Polym. Degrad. Stab.*, vol. 90, no. 3, pp. 488–500, 2005.
- [107] H. Wang, X. Sun, and P. Seib, “Strengthening Blends of Poly(Lactic Acid) and Starch with Methylenediphenyl Diisocyanate,” *J. Appl. Polym. Sci.*, vol. 82, no. 7, pp. 1761–1767, 2001.
- [108] Ultimaker BV, “How to Store Material,” *Ultimaker*, 2020. [Online]. Available: <https://support.ultimaker.com/hc/en-us/articles/360012101319>. [Accessed: 11-Jun-2020].
- [109] ECO, “How To Fix PLA Filament Getting Brittle,” *ECO*, 2019. [Online]. Available: <https://ecoreprap.com/pla-filament-brittle/>. [Accessed: 12-Jun-2020].
- [110] Garyg, “Humidity Range for Filament Storage.,” *3D Hubs B.V.*, 2018. [Online]. Available: <https://www.3dhubs.com/talk/t/humidity-range-for-filament-storage/8131/4>. [Accessed: 11-Jun-2020].
- [111] C. Schmied, “3D Printer Filament Storage: 8 Safe Ways to Store Filament,” *All3DP*, 2018. [Online]. Available: <https://all3dp.com/2/filament-spool-8-ways-to-safely-store-your-filament/>. [Accessed: 11-Jun-2020].
- [112] Tom, “5 Ways to Ruin Your Filament (And How to Fit It)!,” *Tom’s 3D*, 2017. [Online]. Available: <https://toms3d.org/2017/09/25/5-ways-to-ruin-your-filament/>. [Accessed: 11-Jun-2020].
- [113] E. Conrad and K. Petrea, “Peltier Dehumidifier for 3D Printer Filament,” *Hackster.io*, 2018. [Online]. Available: <https://www.hackster.io/iot14/peltier-dehumidifier-for-3d-printer-filament-flabf7>. [Accessed: 11-Jun-2020].
- [114] Kameya, “Filament Storage Box DIY,” *MaerkerBot Thingiverse*, 2016. [Online]. Available: <https://www.thingiverse.com/thing:1372828>. [Accessed: 11-Jun-2020].
- [115] Akshay.gupta.904108, “Filament Dehumidifier,” *instructables*, 2018. [Online]. Available: <https://www.instructables.com/id/Filament-Dehumidifier/>. [Accessed: 11-Jun-2020].

- [116] Y. A. Cengel and M. A. Boles, *Thermodynamics An Engineering Approach*, 8th ed. McGraw-Hill Education, 2015.
- [117] A. E. Drouzas, E. Tsami, and G. D. Saravacos, “Microwave/Vacuum Drying of Model Fruit Gels,” *J. Food Eng.*, vol. 39, no. 2, pp. 117–122, 1999.
- [118] CNC Kitchen, *Vacuum vs Dehydrator! What’s the Best Way to Dry Filament?* 2020.
- [119] Design Prototype Test, *Is Vacuum Filament Drying Best the Best Technique?* 2019.
- [120] zemlin, “Drying Flament Under Vacuum,” *Raise3D*, 2018. [Online]. Available: <https://forum.raise3d.com/viewtopic.php?f=7&t=9757&sid=4f583318cfe9c7e702cc04a8434a4ee1>. [Accessed: 16-Jun-2020].
- [121] K. L. Alvarez C., R. F. Lagos C., and M. Aizpun, “Investigating the Influence of Infill Percentage on the Mechanical Properties of Fused Deposition Modelled ABS Parts,” *Ing. e Investig.*, vol. 36, no. 3, pp. 110–116, 2016.
- [122] billyd, “Auto vs Manual Extrusion Width,” *Simplify3D*, 2015. [Online]. Available: <https://forum.simplify3d.com/viewtopic.php?t=2232#:~:text=For best print results%2C it,a 1.00 mm nozzle%2C etc.> [Accessed: 30-Jul-2020].
- [123] V. E. Kuznetsov, A. N. Solonin, O. D. Urzhumtsev, R. Schilling, and A. G. Tavitov, “Strength of PLA Components Fabricated with Fused Deposition Technology Using a Desktop 3D Printer as a Function of Geometrical Parameters of the Process,” *Polymers (Basel)*, vol. 10, no. 3, 2018.
- [124] H. A. Habeeb, M. R. Alkahari, F. R. Ramli, R. Hasan, and S. Maidin, “Strength and Porosity of Additively Manufactured PLA Using a Low Cost 3D Printing,” in *Proceedings of Mechanical Engineering Research Day 2016*, 2016, pp. 69–70.
- [125] Babagowda, R. S. Kadadevara Math, R. Goutham, and K. R. Srinivas Prasad, “Study of Effects on Mechanical Properties of PLA Filament which is Blended with Recycled PLA Materials,” *IOP Conf. Ser. Mater. Sci. Eng.*, vol. 310, no. 1, 2018.
- [126] J. Torres, M. Cole, A. Owji, Z. DeMastry, and A. P. Gordon, “An Approach for Mechanical



- Property Optimization of Fused Deposition Modeling with Polylactic Acid via Design of Experiments,” *Rapid Prototyp. J.*, vol. 22, no. 2, pp. 387–404, 2016.
- [127] PrintIt Industries LLC., “Print Speed Calculator,” *PrintIt Industries*. [Online]. Available: <https://www.printitindustries.com/pages/print-speed-calculator>. [Accessed: 05-Aug-2020].
- [128] 3D Platform, “3D Print Post Processing Saves Thousands,” *3D Platform*, 2017. [Online]. Available: <https://www.3dplatform.com/Blog/2017/June/3D-Print-Post-Processing-Saves-Thousands>. [Accessed: 20-Jun-2020].
- [129] K. J. Hauger, “3D Printing Finishing Techniques.” 2015.
- [130] M. Fernandez-Vicente, W. Calle, S. Ferrandiz, and A. Conejero, “Effect of Infill Parameters on Tensile Mechanical Behavior in Desktop 3D Printing,” *3D Print. Addit. Manuf.*, vol. 3, no. 3, pp. 183–192, 2016.
- [131] A. Ben and W. Joshua, “The Effects of PLA Color on Material Properties of 3-D Printed Components,” *Addit. Manuf.*, vol. 8, pp. 110–116, 2015.
- [132] R. A. Wach, P. Wolszczak, and A. Adamus-Wlodarczyk, “Enhancement of Mechanical Properties of FDM-PLA Parts via Thermal Annealing,” *Macromol. Mater. Eng.*, vol. 303, no. 9, pp. 1–9, 2018.
- [133] S. Shaffer, K. Yang, J. Vargas, M. A. Di Prima, and W. Voit, “On Reducing Anisotropy in 3D Printed Polymers via Ionizing Radiation,” *Polymer (Guildf.)*, vol. 55, no. 23, pp. 5969–5979, 2014.
- [134] F. H. M. Graichen *et al.*, “Yes, We Can Make Money out of Lignin and other Bio-Based Resources,” *Ind. Crops Prod.*, vol. 106, pp. 74–85, 2017.
- [135] W. Xu, X. Wang, N. Sandler, S. Willför, and C. Xu, “Three-Dimensional Printing of Wood-Derived Biopolymers: A Review Focused on Biomedical Applications,” *ACS Sustain. Chem. Eng.*, vol. 6, no. 5, pp. 5663–5680, 2018.
- [136] J. Dong *et al.*, “The Influence of Grafted Cellulose Nanofibers and Postextrusion Annealing Treatment on Selected Properties of Poly(Lactic Acid) Filaments for 3D Printing,” *J. Polym.*

*Sci. Part B Polym. Phys.*, vol. 55, no. 11, pp. 847–855, 2017.

- [137] C. A. Murphy and M. N. Collins, “Microcrystalline Cellulose Reinforced Polylactic Acid Biocomposite Filaments for 3D Printing,” *Polym. Compos.*, vol. 39, no. 4, pp. 1311–1320, 2018.
- [138] E. Gkartzou, E. P. Koumoulos, and C. A. Charitidis, “Production and 3D Printing Processing of Bio-Based Thermoplastic Filament,” *Manuf. Rev.*, vol. 4, p. 1, 2017.

## Appendix A: FEA Iteration Data

The following two tables show the variable magnitudes used for each iterative FEA completed. Table A-1 shows that of the cantilever chair while Table A-2 shows that of the braced-cantilever chair. The highlighted values indicate the parameters that were changed from the previous iteration, while the row contained within double underlines show the final parameter values selected.

Table A-1: FEA Iteration Data for Cantilever Chair

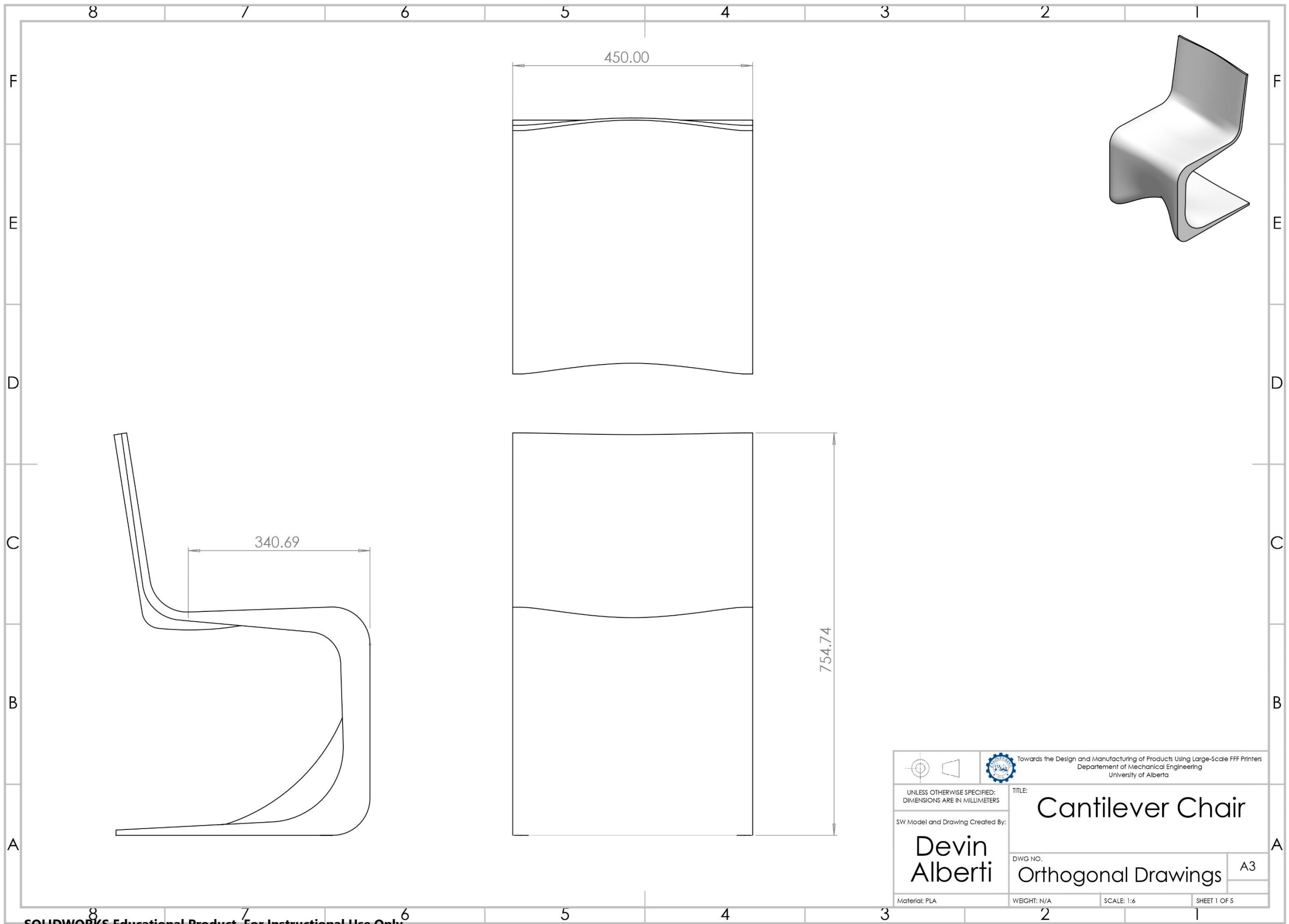
FFF Defined Strength Parameters (mm)			Load Bearing Parameters (mm)													Results		Peak Stress Location
Shell Width	Rail Fill Width	Center Fill Width	Rail Width	CT	RT1	RT2	RT3	RT4	RT5	RT6	RT7	RT8	RR1	RR2	RR3	Min FoS	Volume (mm <sup>3</sup> )	
2	25	15	10	4	10	35	60	60	60	15	15	10	140	110	70	2.8	5 387 969	At internal center fill width edge of RR3.
2	25	15	5	4	10	30	55	55	50	15	15	10	140	110	70	2.5	5 068 954	At internal rail fill width edge of RR1.
2	25	15	5	4	10	25	50	50	45	15	15	10	140	110	70	2.0	4 859 364	At internal rail fill width edge of RR1.
3	25	15	5	4	10	25	50	50	45	15	15	10	140	110	70	2.5	5 832 891	At internal rail fill width edge of RR1.
3	25	15	5	4	10	20	45	45	35	10	10	10	140	110	70	1.8	5 419 208	At internal rail fill width edge of RR2.
2	35	15	5	4	10	25	50	50	45	15	15	10	140	110	70	2.8	5 669 042	At internal rail fill width edge of RR1.
2	35	15	5	4	10	20	45	45	40	15	15	10	140	110	70	2.2	5 401 532	At internal rail fill width edge of RR1.
2	35	15	5	4	10	15	40	40	35	15	10	10	140	110	70	1.8	5 014 457	At internal rail fill width edge of RR1.
3	35	15	5	4	10	15	40	40	35	15	10	10	140	110	70	2.0	5 887 068	At Roller/Slider boundary, realistic FoS estimated at 2.5.
2	20	15	5	4	10	25	50	50	45	15	15	10	140	110	70	1.8	4 452 434	At internal rail fill width edge of RR1.
2	20	15	5	4	10	25	50	55	45	15	15	10	140	110	70	1.3	4 498 792	At internal center fill width of RR3.
2	20	20	5	4	10	25	50	55	45	15	15	10	140	110	70	2.1	4 490 573	At internal rail fill width edge of RR3.
2	20	20	3	4	10	25	50	55	45	15	15	10	140	110	70	2.0	4 496 800	At internal rail fill width edge of RR3.
2	20	20	10	4	10	25	50	55	45	15	15	10	140	110	70	2.1	4 459 581	At Roller/Slider boundary, realistic FoS estimated at 2.3.
2	20	20	15	4	10	25	50	55	45	15	15	10	140	110	70	2.1	4 433 958	At Roller/Slider boundary, realistic FoS estimated at 2.2.

Table A-2: FEA Iteration Data for Braced-Cantilever Chair

FFF Defined Strength Parameters (mm)			Addition Parameter (mm)	Load Bearing Parameters (mm)													Results		Peak Stress Location
Shell Width	Rail Fill Width	Center Fill Width	Brace Width	Rail Width	CT	RT1	RT2	RT3	RT4	RT5	RT6	RT7	RT8	RR1	RR2	RR3	Min FoS	Volume (mm <sup>3</sup> )	
2	20	20	15	15	4	15	15	15	15	15	15	15	15	55	55	55	1.6	4 472 585	At CT of RR2.
2	20	20	15	15	4	15	15	15	15	15	15	15	15	65	65	65	1.5	4 609 751	At CT of seating indent.
2	15	25	15	10	4	15	15	15	15	15	15	15	15	65	65	65	1.7	4 352 873	At CT of RR2.
2	10	25	15	5	4	15	15	15	15	15	15	15	15	65	65	65	1.7	4 054 036	At CT of RR2.
2	10	30	15	5	4	15	15	15	15	15	15	15	15	65	65	65	2	4 079 060	At CT of RR2.
2	10	30	15	5	4	10	15	15	15	15	15	10	10	60	60	75	1.9	3 984 970	At CT of seating indent.
2	10	30	10	5	4	10	15	15	15	15	15	10	10	60	60	75	2.8	3 880 056	At CT of RR2.
Test for susceptibility for the brace design to deform excessively at RR2 and the brace joints that would cause the chair to fold. Compare to thicker 15 mm brace width.																			
2	10	30	10	5	4	10	15	15	15	15	15	10	10	60	60	75	2.4	-	(lean force @ 40 lb) At CT of RR2.
2	10	30	10	5	4	10	15	15	15	15	15	10	10	60	60	75	2.5	-	(lean force @ 80 lb) At CT of RR2.
2	10	30	10	5	4	10	15	15	15	15	15	10	10	60	60	75	1.8	-	(weight force @ 350 lb) At CT of RR2.
2	10	30	10	5	4	10	15	15	15	15	15	10	10	60	60	75	1.5	-	(weight force @ 425 lb) At CT of RR2.
2	10	30	15	5	4	10	15	15	15	15	15	10	10	60	60	75	1.9	-	At CT of RR2.
2	10	30	15	5	4	10	15	15	15	15	15	10	10	60	60	75	2	-	(back force @ 40 lb) At CT of seating indent.
2	10	30	15	5	4	10	15	15	15	15	15	10	10	60	60	75	1.7	-	(back force @ 80 lb) At CT of seating indent.
2	10	30	15	5	4	10	15	15	15	15	15	10	10	60	60	75	1.6	-	(weight force @ 350 lbf) At CT of RR2.
2	10	30	15	5	4	10	15	15	15	15	15	10	10	60	60	75	1.3	-	(weight force @ 425 lbf) At CT of RR2.
No excessive deflections were observed.																			

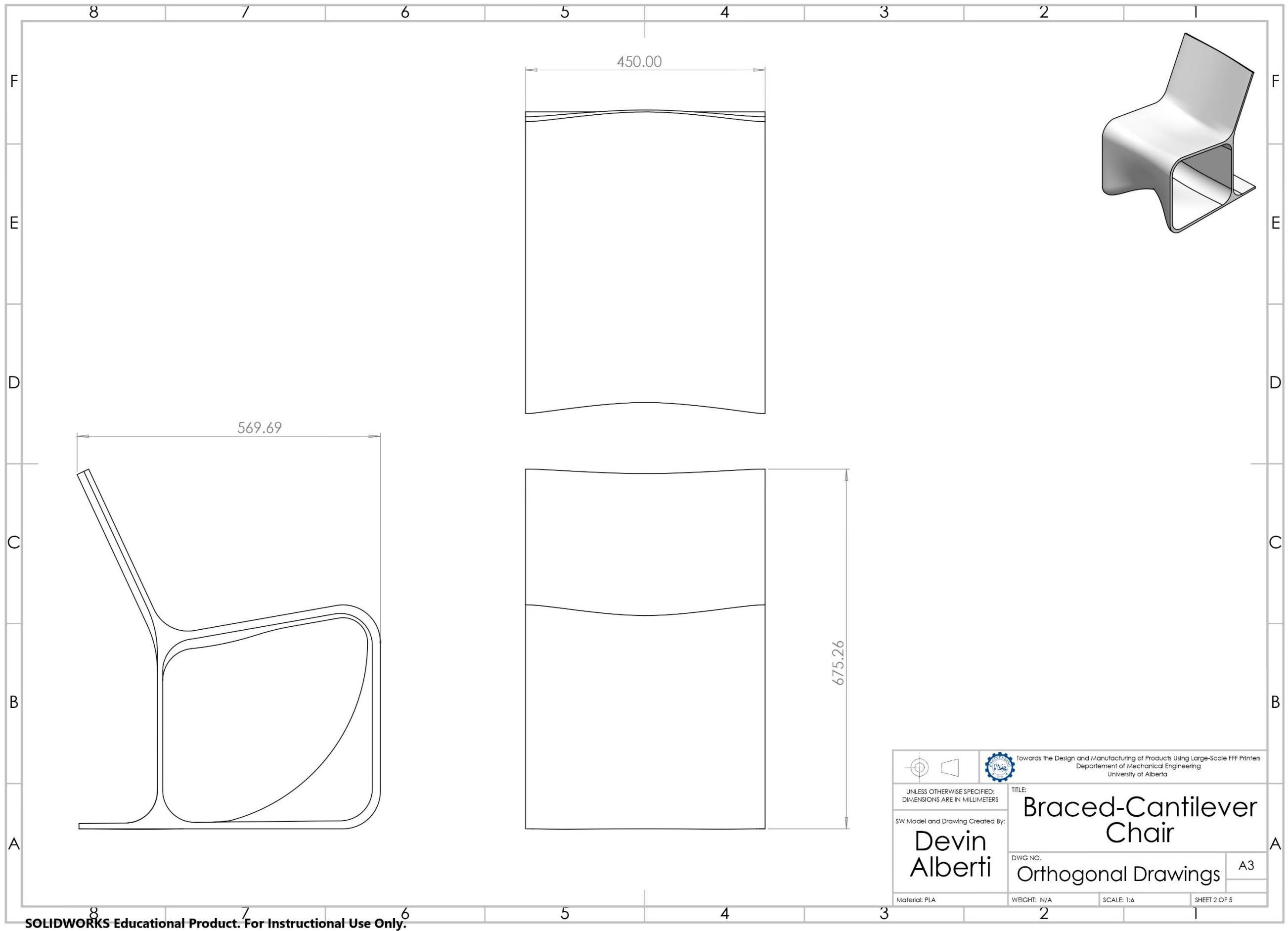
## **Appendix B: Orthogonal Drawings**

The following SOLIDWORKS drawings contain orthogonal drawings displaying overall dimension of the cantilever chair, braced-cantilever chair, adhesion test tower, and custom 3DP 300 enclosure.



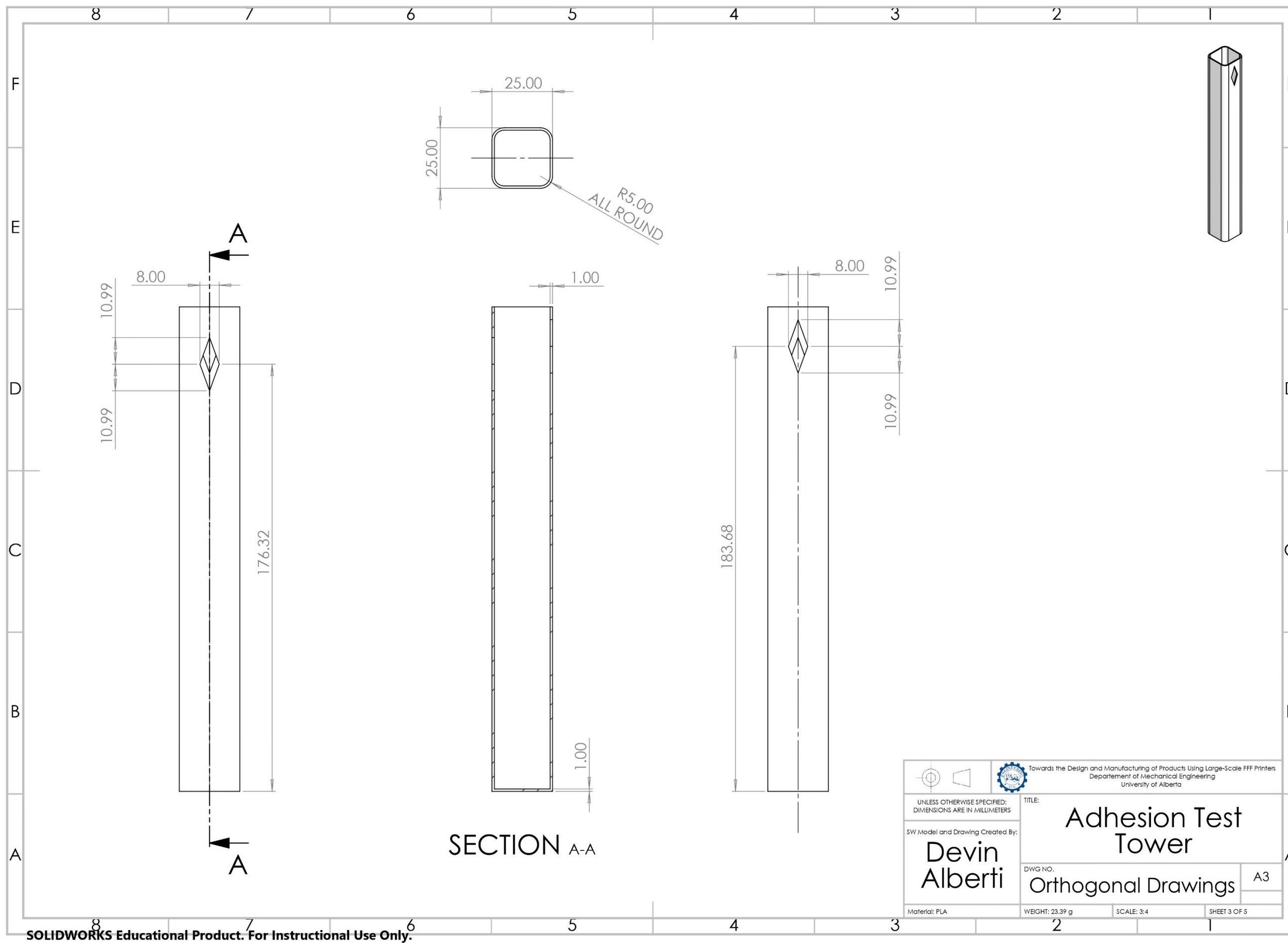
SOLIDWORKS Educational Product. For Instructional Use Only.

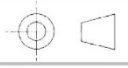
 Towards the Design and Manufacturing of Products Using Large-Scale FFF Printers Department of Mechanical Engineering University of Alberta	
TITLE: Cantilever Chair	
DWG NO. Orthogonal Drawings	
SHEET 1 OF 5	
Material: PLA	
WEIGHT: N/A	
SCALE: 1:6	

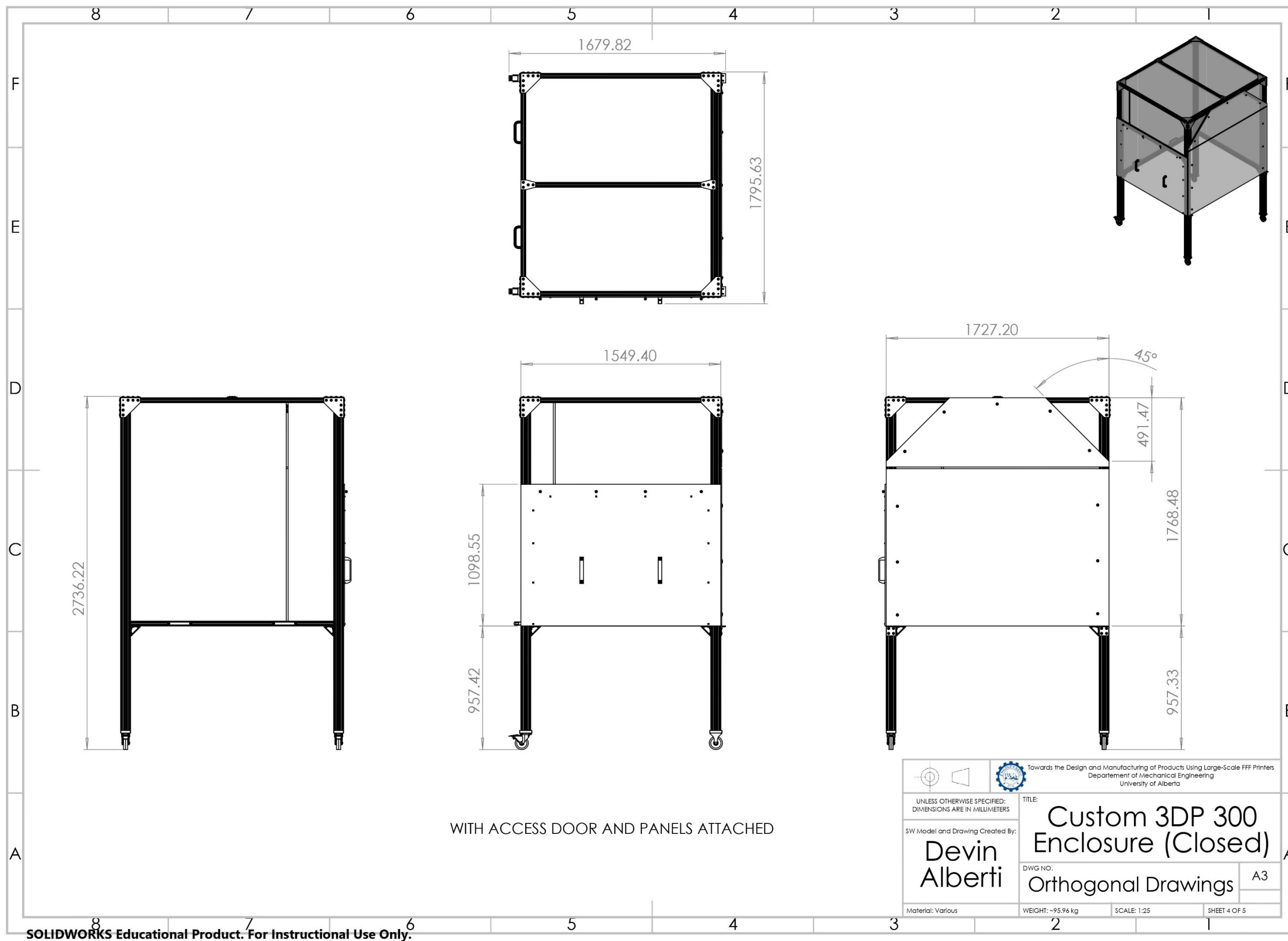


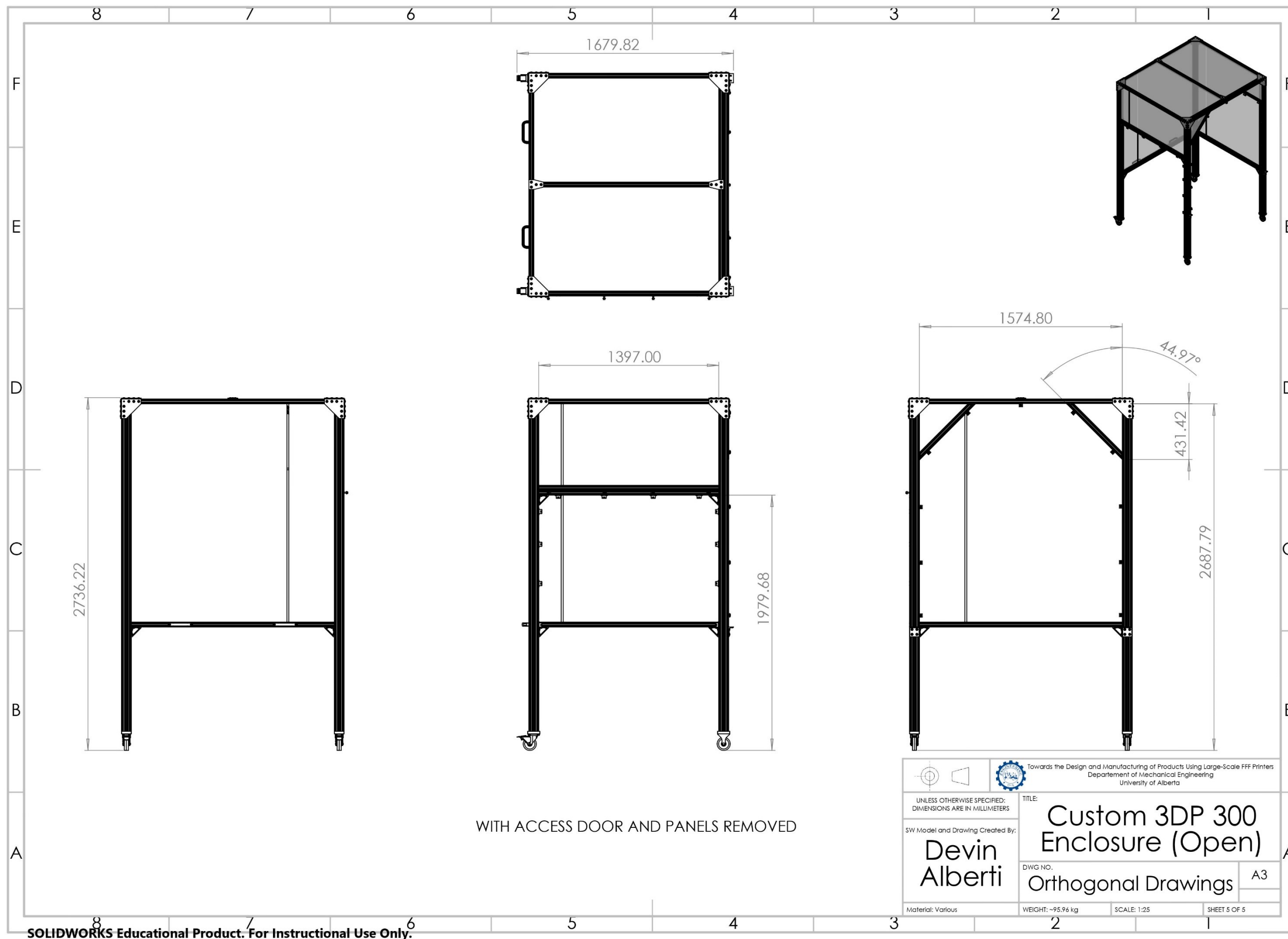
SOLIDWORKS Educational Product. For Instructional Use Only.





 Towards the Design and Manufacturing of Products Using Large-Scale FFF Printers Department of Mechanical Engineering University of Alberta	
UNLESS OTHERWISE SPECIFIED: DIMENSIONS ARE IN MILLIMETERS	
TITLE: <b>Adhesion Test Tower</b>	
SW Model and Drawing Created By: <b>Devin Alberti</b>	
DWG NO. <b>Orthogonal Drawings</b>	
A3	
Material: PLA	WEIGHT: 23.39 g
SCALE: 3:4	SHEET 3 OF 5



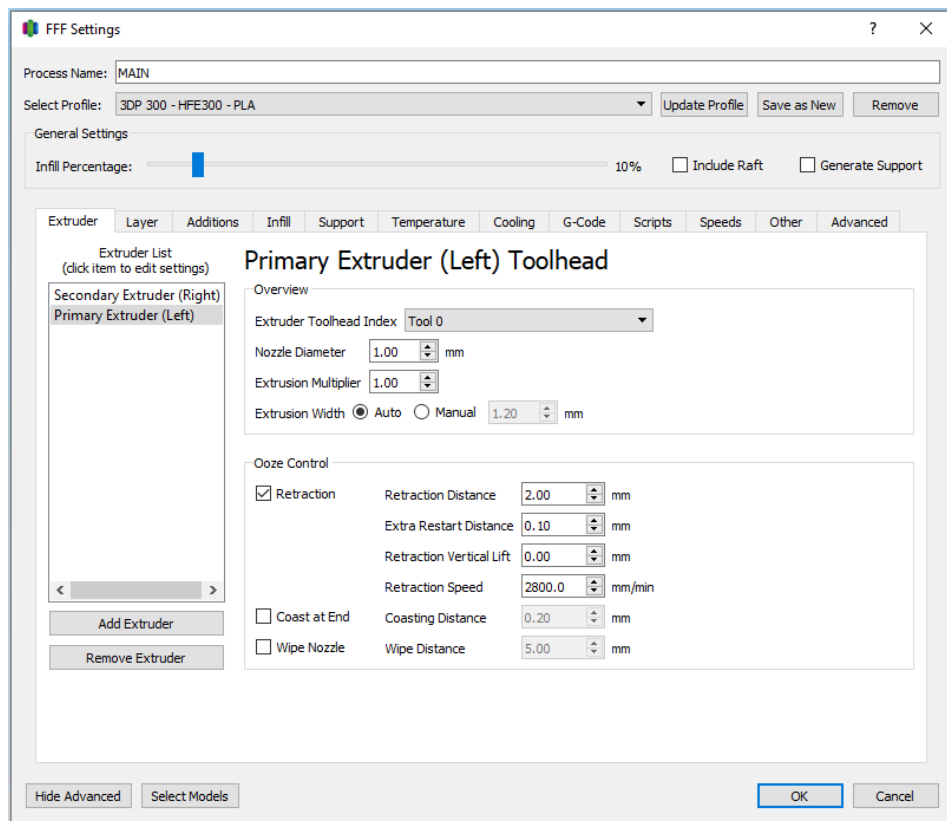


SOLIDWORKS Educational Product. For Instructional Use Only.

 Towards the Design and Manufacturing of Products Using Large-Scale FFF Printers Department of Mechanical Engineering University of Alberta	
TITLE: Custom 3DP 300 Enclosure (Open)	
UNLESS OTHERWISE SPECIFIED: DIMENSIONS ARE IN MILLIMETERS	DWG NO. Orthogonal Drawings
SW Model and Drawing Created By: <b>Devin Alberti</b>	A3
Material: Various	WEIGHT: ~95.96 kg
SCALE: 1:25	SHEET 5 OF 5

## Appendix C: Print Parameters

The following figures display all print parameters within Simplify3D 4.1.2 defined for a 3DP 300-2E7C2-A3300-100 printer. Note that several settings located under the Layer, Additions, and Infill tabs are print specific such as Top Solid Layers, Bottom Solid Layers, Outline/Perimeter Shells, Skirt Outlines, Interior Fill Percentage, and potentially others. For the chair specifically, all parameters shown were held constant with modifications to the Additions > Skirt Outlines for adhesion, Infill > Interior Fill Percentage for solid fill sections, and Advanced > Start/Stop Print at Height for the various print section Processes that make up the chair.



FFF Settings

Process Name: MAIN

Select Profile: 3DP 300 - HFE300 - PLA Update Profile Save as New Remove

General Settings

Infill Percentage: 10% ☐ Include Raft ☐ Generate Support

Extruder Layer Additions Infill Support Temperature Cooling G-Code Scripts Speeds Other Advanced

Layer Settings

Primary Extruder: Primary Extruder (Left)

Primary Layer Height: 0.5000 mm

Top Solid Layers: 4

Bottom Solid Layers: 4

Outline/Perimeter Shells: 2

Outline Direction: ☐ Inside-Out ☒ Outside-In

☐ Print islands sequentially without optimization

☐ Single outline corkscrew printing mode (vase mode)

First Layer Settings

First Layer Height: 100 %

First Layer Width: 100 %

First Layer Speed: 50 %

Start Points

☐ Use random start points for all perimeters

☒ Optimize start points for fastest printing speed

☐ Choose start point closest to specific location

X: 1000.0 Y: 500.0 mm

Hide Advanced Select Models OK Cancel

FFF Settings

Process Name: MAIN

Select Profile: 3DP 300 - HFE300 - PLA Update Profile Save as New Remove

General Settings

Infill Percentage: 10% ☐ Include Raft ☐ Generate Support

Extruder Layer Additions Infill Support Temperature Cooling G-Code Scripts Speeds Other Advanced

☒ Use Skirt/Brim

Skirt Extruder: Primary Extruder (Left)

Skirt Layers: 1

Skirt Offset from Part: 0.00 mm

Skirt Outlines: 10

☐ Use Prime Pillar

Prime Pillar Extruder: All Extruders

Pillar Width: 12.00 mm

Pillar Location: North-West

Speed Multiplier: 100 %

☐ Use Raft

Raft Extruder: Secondary Extruder (Right)

Raft Top Layers: 3

Raft Base Layers: 1

Raft Offset from Part: 3.00 mm

Separation Distance: 0.10 mm

Raft Top Infill: 100 %

Above Raft Speed: 30 %

☐ Use Ooze Shield

Ooze Shield Extruder: All Extruders

Offset from Part: 2.00 mm

Ooze Shield Outlines: 1

Sidewall Shape: Waterfall

Sidewall Angle Change: 30 deg

Speed Multiplier: 100 %

Hide Advanced Select Models OK Cancel

FFF Settings

?

×

Process Name: MAIN

Select Profile: 3DP 300 - HFE300 - PLA

Update Profile

Save as New

Remove

General Settings

Infill Percentage: 10%

☐ Include Raft

☐ Generate Support

Extruder

Layer

Additions

Infill

Support

Temperature

Cooling

G-Code

Scripts

Speeds

Other

Advanced

General

Infill Extruder: Primary Extruder (Left)

Internal Fill Pattern: Rectilinear

External Fill Pattern: Rectilinear

Interior Fill Percentage: 10 %

Outline Overlap: 8 %

Infill Extrusion Width: 100 %

Minimum Infill Length: 4.00 mm

Combine Infill Every: 1 layers

☐ Include solid diaphragm every 20 layers

Internal Infill Angle Offsets

0 deg

45

-45

Add Angle

Remove Angle

☐ Print every infill angle on each layer

External Infill Angle Offsets

0 deg

45

-45

Add Angle

Remove Angle

Hide Advanced

Select Models

OK

Cancel

FFF Settings

?

×

Process Name: MAIN

Select Profile: 3DP 300 - HFE300 - PLA

Update Profile

Save as New

Remove

General Settings

Infill Percentage: 10%

☐ Include Raft

☐ Generate Support

Extruder

Layer

Additions

Infill

Support

Temperature

Cooling

G-Code

Scripts

Speeds

Other

Advanced

Temperature Controller List  
(click item to edit settings)

Heated Bed

Secondary Extruder (Right)

Primary Extruder (Left)

Add Temperature Controller

Remove Temperature Controller

Heated Bed Temperature

Overview

Temperature Identifier: T2

Temperature Controller Type: ☐ Extruder ☒ Heated build platform

Relay Temperature Between Each: ☒ Layer ☒ Loop

☒ Wait for temperature controller to stabilize before beginning build

Per-Layer Temperature Setpoints

Layer	Temperature
1	60

Add Setpoint

Remove Setpoint

Layer Number: 1

Temperature: 200 °C

Hide Advanced

Select Models

OK

Cancel

FFF Settings

?

×

Process Name: MAIN

Select Profile: 3DP 300 - HFE300 - PLA

Update Profile

Save as New

Remove

General Settings

Infill Percentage: 10%

☐ Include Raft
 ☐ Generate Support

Extruder

Layer

Additions

Infill

Support

Temperature

Cooling

G-Code

Scripts

Speeds

Other

Advanced

Temperature Controller List

(click item to edit settings)

Heated Bed

Secondary Extruder (Right)

Primary Extruder (Left)

Add Temperature Controller

Remove Temperature Controller

Primary Extruder (Left) Temperature

Overview

Temperature Identifier: T0

Temperature Controller Type: Extruder

Heated build platform

Relay Temperature Between Each: Layer

Loop

☒ Wait for temperature controller to stabilize before beginning build

Per-Layer Temperature Setpoints

Layer	Temperature
1	205

Add Setpoint

Remove Setpoint

Layer Number: 1

Temperature: 200 °C

Hide Advanced

Select Models

OK

Cancel

FFF Settings

?

×

Process Name: MAIN

Select Profile: 3DP 300 - HFE300 - PLA

Update Profile

Save as New

Remove

General Settings

Infill Percentage: 10%

☐ Include Raft
 ☐ Generate Support

Extruder

Layer

Additions

Infill

Support

Temperature

Cooling

G-Code

Scripts

Speeds

Other

Advanced

Per-Layer Fan Controls

Layer	Fan Speed
1	0
3	5
10	10
20	20
40	40
80	60

Add Setpoint

Remove Setpoint

Layer Number: 1

Fan Speed: 60 %

Fan Options

☐ Blip fan to full power when increasing from idle

Fan Overrides

☐ Increase fan speed for layers below 30.0 sec
 

Maximum cooling fan speed 100 %

☐ Bridging fan speed override 100 %

Hide Advanced

Select Models

OK

Cancel

FFF Settings

Process Name:

Select Profile:

General Settings

Infill Percentage:  ☐ Include Raft ☐ Generate Support

Extruder Layer Additions Infill Support Temperature Cooling **G-Code** Scripts Speeds Other Advanced

G-Code Options

- ☒ 5D firmware (include E-dimension)
- ☐ Relative extrusion distances
- ☒ Allow zeroing of extrusion distances (i.e. G92 E0)
- ☐ Use independent extruder axes
- ☒ Include M101/M102/M103 commands
- ☒ Firmware supports "sticky" parameters
- ☐ Apply toolhead offsets to G-Code coordinates

Global G-Code Offsets

	X-Axis	Y-Axis	Z-Axis
Offset	<input type="text" value="0.00"/> mm	<input type="text" value="0.00"/> mm	<input type="text" value="0.00"/> mm

☒ Update Machine Definition

Machine type:

	X-Axis	Y-Axis	Z-Axis
Build volume	<input type="text" value="1000.0"/> mm	<input type="text" value="1000.0"/> mm	<input type="text" value="700.0"/> mm
Origin offset	<input type="text" value="0.0"/> mm	<input type="text" value="0.0"/> mm	<input type="text" value="0.0"/> mm
Homing dir	<input type="text" value="Min"/>	<input type="text" value="Min"/>	<input type="text" value="Min"/>
Flip build table axis	<input type="checkbox"/> X	<input checked="" type="checkbox"/> Y	<input type="checkbox"/> Z
Toolhead offsets	<input type="text" value="Tool 0"/> X <input type="text" value="0.00"/> Y <input type="text" value="0.00"/>		

☐ Update Firmware Configuration

Firmware type:

GPX profile:

Baud rate:  bits/sec

FFF Settings

Process Name:

Select Profile:

General Settings

Infill Percentage:  ☐ Include Raft ☐ Generate Support

Extruder Layer Additions Infill Support Temperature Cooling **G-Code** **Scripts** Speeds Other Advanced

Starting Script Layer Change Script Retraction Script Tool Change Script Ending Script

Starting Script

```

M581 E0 S0 T2 C1;
M582 T2;
G28;
G92 E0;

```

reactivate trigger 2 (filament alarm)  
check trigger 2 (filament alarm)  
home printer  
set current filament position to 0

Post Processing

Export file format:

☐ Add celebration at end of build (for .x3g files only)

Additional terminal commands for post processing



FFF Settings

?

×

Process Name: MAIN

Select Profile: 3DP 300 - HFE300 - PLA

Update Profile

Save as New

Remove

General Settings

Infill Percentage: 10%

☐ Include Raft
 ☐ Generate Support

Extruder

Layer

Additions

Infill

Support

Temperature

Cooling

G-Code

Scripts

Speeds

Other

Advanced

Starting Script

Layer Change Script

Retraction Script

Tool Change Script

Ending Script

M106 S1.0;

G10;

M104 S0;

M140 S0;

G0 X0 Y0;

M300;

M117 Print Complete;

M107;

turn fan to 100%

retract filament

turn heaters to 0

turn bed to 0

rapid move to X and Y home.

make beep sound

show message

turn off fan

Post Processing

Export file format: Standard G-Code (.gcode)

☐ Add celebration at end of build (for .x3g files only)
 

Looney Toons

Additional terminal commands for post processing

Hide Advanced

Select Models

OK

Cancel

FFF Settings

?

×

Process Name: MAIN

Select Profile: 3DP 300 - HFE300 - PLA

Update Profile

Save as New

Remove

General Settings

Infill Percentage: 10%

☐ Include Raft
 ☐ Generate Support

Extruder

Layer

Additions

Infill

Support

Temperature

Cooling

G-Code

Scripts

Speeds

Other

Advanced

Speeds

Default Printing Speed 6000.0 mm/min

Outline Underspeed 50 %

Solid Infill Underspeed 80 %

Support Structure Underspeed 75 %

X/Y Axis Movement Speed 9200.0 mm/min

Z Axis Movement Speed 1002.0 mm/min

Speed Overrides

☐ Adjust printing speed for layers below 20.0 sec
 

Allow speed reductions down to 30 %

Hide Advanced

Select Models

OK

Cancel

FFF Settings

Process Name:

Select Profile:

General Settings

Infill Percentage:  ☐ Include Raft ☐ Generate Support

Extruder Layer Additions Infill Support Temperature Cooling G-Code Scripts Speeds Other **Advanced**

Bridging

Unsupported area threshold  sq mm

Extra inflation distance  mm

Bridging extrusion multiplier  %

Bridging speed multiplier  %

☐ Use fixed bridging infill angle  deg

☐ Apply bridging settings to perimeters

Dimensional Adjustments

Horizontal size compensation  mm

Filament Properties

Filament Toolhead Index

Filament diameter  mm

Filament price  price/kg

Filament density  grams/cm<sup>3</sup>

Tool Change Retraction

Tool change retraction distance  mm

Tool change extra restart distance  mm

Tool change retraction speed  mm/min

FFF Settings

Process Name:

Select Profile:

General Settings

Infill Percentage:  ☐ Include Raft ☐ Generate Support

Extruder Layer Additions Infill Support Temperature Cooling G-Code Scripts Speeds Other **Advanced**

Layer Modifications

☐ Start printing at height  mm

☐ Stop printing at height  mm

Thin Wall Behavior

External Thin Wall Type

Internal Thin Wall Type

Allowed perimeter overlap  %

Single Extrusions

Minimum Extrusion Length  mm

Minimum Printing Width  %

Maximum Printing Width  %

Endpoint Extension Distance  mm

Ooze Control Behavior

☐ Only retract when crossing open spaces

☐ Force retraction between layers

☒ Minimum travel for retraction  mm

☐ Perform retraction during wipe movement

☐ Only wipe extruder for outer-most perimeters

Movement Behavior

☒ Avoid crossing outline for travel movements

Maximum allowed detour factor

Slicing Behavior

Non-manifold segments: ☐ Discard ☒ Heal

☐ Merge all outlines into a single solid model